Quantum consistent force field calculation of vibronic bandshapes and adiabatic potential energy surfaces for the 1Lb-1La electronic manifold of indole

by James Thomas Vivian

A thesis submitted in partial fulfillment of the requirements for the degree of Master of Science in Chemistry

Montana State University

Abstract:
Vibronic bandshapes and adiabatic potential energy surfaces for the 1Lb(S1) and 1La (S2) electronic states of indole, are computed within the harmonic, Born-Oppenheimer,,and Condon approximations by the Quantum Consistent Force Field (QCFF) semiempirical method. Franck-Condon factors are calculated utilizing the recursion relations of Doktorov, Malkin, and Man'ko which incorporate the effects of surface displacements, frequency shifts, and Duschinsky rotation and therefore provide FC factors which are exact within the harmonic approximation. In order to accurately calculate spectral bandshapes, the QCFF method has been modified to incorporate a difference-density scaling procedure based on the 260 ntn band of benzene, and the scale factor is transferred directly to indole. Results for adiabatic potential surfaces for indole predict an avoided crossing of the Lb and La surfaces in the region of the La equilibrium molecular geometry. A semi-quantitative picture of the photophysics of the 1Lb 1La electronic manifold is developed in which the La state dynamics are interpreted in terms of a diabatic picture for the electronic potential energy surfaces. The diabatic potential surfaces are produced in an approximate way in which the configuration interaction eigenvectors are "frozen" at their values at the Ly equilibrium molecular geometry. The validity of the diabatic prescription is evidenced by the spectral bandwidth computed within the "frozen CI" method. A Landau-Zener curve crossing model is briefly explored in order to rationalize the absence of La fluorescence in jet-cooled indole.

QUANTUM CONSISTENT FORCE FIELD CALCULATION OF VIBRONIC BANDSHAPES AND ADIABATIC POTENTIAL ENERGY SURFACES FOR THE ^1L_b- ^1L_a ELECTRONIC MANIFOLD OF INDOLE

by

James Thomas Vivian

A thesis submitted in partial fulfillment

of the requirements for the degree

of

Master of Science

in

Chemistry

MONTANA STATE UNIVERSITY

Bozeman, Montana

August, 1993

APPROVAL

of a thesis submitted by

James Thomas Vivian

This thesis has been read by each member of the thesis committee and has been found to be satisfactory regarding content, English usage, format, citations, bibliographic style, and consistency, and is ready for submission to the College of Graduate Studies.

Sept 7, 1993
Date

Patrick R Callis
Chairperson, Graduate Committee

Approval for the Major Department

David M Dooley
Date

Sept 7, 1993
Head, Major Department

Approval for the College of Graduate Studies

10/30/93
Date

R L Bowen
Graduate Dean

STATEMENT OF PERMISSION TO USE

In presenting this thesis in partial fulfillment of the requirements for a master's degree at Montana State University, I agree that the Library shall make it available to borrowers under rules of the Library.

If I have indicated my intention to copyright this thesis by including a copyright notice page, copying is allowable only for scholarly purposes, consistent with "fair use" as prescribed in the U.S. Copyright Law. Requests for permission for extended quotation from or reproduction of this thesis in whole or in parts may be granted only by the copyright holder.

Signature James T. Vivian

Date 25 OCTOBER, 1993.

In memory of Derek Hersey, climber extraordinaire and indoctrinated Fun Hog.

ACKNOWLEDGMENTS

I wish to thank Professor Patrik R. Callis for his guidance, support, and friendship during the course of this work. In addition to the resonance which we shared in research, PRC served as mentor, cultural hero, and a model of scientific and personal integrity which remains inspirational. I also wish to thank Professor Lee Spangler for his continual guidance, support, and encouragement which contributed significantly to my scientific development. Mr. Pedro Muiño deserves many thanks for his unfailing assistance in various computational matters, providing copies of his unpublished experimental results, and for very enjoyable interaction within the group. I wish also to thank Dr. David M. Sammeth, Ms. Sonja Siewert, and Ms. Jacqueline Fonnesbeck for many useful discussions ranging from experimental issues to methyl-rotor structure to Dancing Lessons from the Gods. As my colleagues and contemporaries, their contribution was significant. A special acknowledgment is extended to my climbing partner, Tim Davenport, who provided support to this work through the commodity of friendship and flexibility when work took priority over cragging. Jill Haniuk and her amazing daughter, Kelly, deserve considerable thanks for patience and encouragement during the later stages of this work. Professor John H. Frederick (University of Nevada, Reno) is gratefully acknowledged for assistance and providing resources for the production of the final draft of this thesis (nearly 900 miles from Bozeman!). Finally, I wish to thank my parents, Jim and Donna Vivian, and Gene and Emily Meyer, for their consistent support and belief that this is the right path, as well as for emphasizing that the choice between climbing or doing science is not a good choice to make -- that it is better to pursue both. This work was supported by the Department of Chemistry and Biochemistry, Montana State University, and by a grant (to PRC) from the National Institutes of Health.

TABLE OF CONTENTS

TABLE OF CONTENTS - Continued

TABLE OF CONTENTS - Continued

TABLE OF CONTENTS - Continued

LIST OF TABLES

LIST OF TABLES-Continued

LIST OF FIGURES

ABSTRACT

Vibronic bandshapes and adiabatic potential energy surfaces for the ^1L_b (S_1) and ^1L_a (S_2) electronic states of indole are computed within the harmonic, Born-Oppenheimer,,and Condon approximations by the Quantum Consistent Force Field (QCFF) semiempirical method. Franck-Condon factors are calculated utilizing the recursion relations of Doktorov, Malkin, and Man'ko which incorporate the effects of surface displacements, frequency shifts, and Duschinsky rotation and therefore provide FC factors which are exact within the harmonic approximation. In order to accurately calculate spectral bandshapes, the QCFF method has been modified to incorporate a difference-density scaling procedure based on the 260 nm band of benzene, and the scale factor is transferred directly to indole. Results for adiabatic potential surfaces for indole predict an avoided crossing of the L_b and L_a surfaces in the region of the L_a equilibrium molecular geometry. A semi-quantitative picture of the photophysics of the ^1L_b ^1L_a electronic manifold is developed in which the L_a state dynamics are interpreted in terms of a diabatic picture for the electronic potential energy surfaces. The diabatic potential surfaces are produced in an approximate way in which the configuration interaction eigenvectors are "frozen" at their values at the L_b equilibrium molecular geometry. The validity of the diabatic prescription is evidenced by the spectral bandwidth computed within the "frozen CI" method. A Landau-Zener curve crossing model is briefly explored in order to rationalize the absence of L_a fluorescence in jet-cooled indole.

CHAPTER 1

INTRODUCTION

Indole Chromophore Photophysics

The indole chromophore is responsible for the low energy UV absorption near ~280 nm of the amino acid tryptophan. The absorption and emission for this band are relatively strong (f~ 10^{-1}-10^{-2}) in both vapor and solution and the details of these photophysical processes depend very sensitively on the environment of the chromophore. For this reason, indole and tryptophan photophysics provide a unique and potentially powerful key towards the understanding of the structure, local environment, and dynamics within proteins.

One persistent problem in unraveling the details of the photophysics of indole is the existence of two quasi-degenerate electronic states which both contribute to the 280 nm absorption band. These states, the first two excited singlet states S_1 and S_2, are labeled ^1L_b and ^1L_a, respectively (1), in gas phase, with the ^1L_b being the lower of the two. It is believed that a detailed understanding of these two electronic states, which are responsible for ~90 percent of all protein UV absorption, is necessary in order to develop a knowledge and understanding of the much broader issue of protein structure and dynamics.

For these reasons, the indole chromophore has been the subject of intense experimental investigation (2-20), the focus of which relates to elucidation of the nature of the ^1L_a and ^1L_b electronic states and their photophysical behavior. Recently, polarized two-photon fluorescence excitation (PTPFE) experiments on jet-cooled indole (5,9), 3-methylindole (6,19), 5-methylindole (5), indole+water and indole+methanol van der Waals complexes (19,20) have helped to solidify existing assignments of L_b transitions in the gas phase absorption (excitation) spectrum of isolated indole. On the

other hand, the increased detail offered by jet-cooling techniques and polarization resolution has served to uncover new phenomena which have called into question previously existing experimental assignments and provided experimental features for which no suitable framework exists for their interpretation.

The most important and compelling example of this is in regard to the assignment of the L_a band origin for indole in both gas phase and solution experiments. While the L_b band origin is well established as occurring at ~35,200 cm^{-1} (284 nm), the L_a origin assignment remains an open question. At least two assignments have been proposed for the L_a origin, both of which raise considerable questions regarding the nature of the L_b-L_a electronic manifold. Strickland, et al. (18) performed vapor phase (~38 ^{0}C) absorption of indole coupled with absorption experiments of indole in hexane and perfluorinated hexane solution and assigned the L_a band origin to ~1450 cm^{-1} (11) to the blue of the L_b origin on the basis of differential solvent-induced red shifts of the transitions observed for indole vapor.

In a beautiful series of experiments, Callis and co-workers (4-6,9) performed PTPFE in efforts to clearly identify the first L_a character transitions of indole. Their assignment, based on the different response of L_b and L_a transitions to circular and linearly polarized photons (one-color, two-photon polarization ratio), proposes a "split" L_a origin comprised of two fairly strong transitions observed at 455 and 480 cm^{-1} to the blue of the L_b band origin. The argument for this origin assignment hinges on the premise that these transitions are not simply L_b vibrations whose oscillator strength and intensity are derived from Herzberg-Teller vibronic coupling to the L_a state and thus behave as false origins, depending upon the nearness of the L_a state (5,6).

Whether the 455 and 480 cm^{-1} indole transitions are truly the L_a origin or Herzberg-Teller induced false origins one fact is perfectly clear: the two-photon polarization ratios for these transitions unambiguously display L_a character (5,6,9). The difficulty in the

present context is one which pervades all of the more recent, high resolution experiments on the indoles and that is a need for a better theoretical understanding of the L_b-L_a electronic manifold in order to provide a framework for interpretation of these experiments and to cast away the level of speculation which has previously been necessary to attempt to answer questions regarding the L_a origin.

From a theoretical perspective, indole presents considerable challenges and several unique problems which make it less than amenable to a comprehensive, accurate, and definitive treatment. First, the relative size of the molecule (16 atoms, 10 π electrons) makes ab-initio treatments difficult and computationally expensive (21-23,27), and there are a sufficiently large number of degrees of freedom (42 vibrational modes) to make a comprehensive treatment in terms of wavepacket dynamics (28-31) an unlikely prospect. Further, since most of the issues of interest are concerned with excited states, the demands and challenges to theory are amplified exponentially.

The central issue and desired goal should be a detailed knowledge of the electronic structure of the L_b and L_a excited states, since all desired properties follow from this. Although the picture of electronic structure will be, by necessity, only an approximate one, a suitable theory for indole photophysics is one in which the (approximate) electronic structure of these two states is sufficiently accurate to provide for the calculation of spectral bandshapes which are at least in qualitative (and at best, semi-quantitative) agreement with experiment.

To date, no calculations of the indole UV-absorption spectrum have been performed. While there have been reasonably accurate normal coordinate treatments, based on semi-empirical force fields (32,98), these treatments have been restricted to consideration of the ground state potential surface and therefore cannot be used reliably for bandshape calculations of UV-VIS spectra. Ab-initio treatments for indole have been performed as well (25-27), but these have been restricted either to the ground electronic state (25,26)

or are prohibitively expensive for excited states (27), thus making a normal-coordinate treatment within the ab-initio approach an impossibility.

The most comprehensive theoretical treatment of indole, to date, has been that of Callis (33), utilizing a spectroscopically calibrated semiempirical molecular orbital method. This method, which is a special spectroscopic parameterization of the intermediate neglect of differential overlap + configuration interaction method (INDO/S-CI), provides for the calculation of transition energies, oscillator strengths, polarizations, state dipoles, and two-photon properties, as well as bond orders, transition densities, and CI eigenvectors. Unfortunately, it does not predict excited-state equilibrium molecular geometries very accurately, nor is it possible to obtain normal modes of vibration from INDO/S-CI. Although this study does define a significant contribution in the theoretical domain and in many aspects a tour-de-force within the framework of INDO, it leaves open the need for spectral bandshape calculations for indole which are necessary at this stage to get a handle on the L_a origin questions which remain.

Further, it should be noted that in one very important respect the vibrational assignment of the L_a transitions is still in its infancy. Although a reasonably comprehensive vibrational assignment of L_b transitions is now available (12), the persisting uncertainty in the L_a origin identification makes impossible the assignment of individual L_a transitions, as evidenced by two-photon polarization ratios, to vibrations within the L_a electronic state. It is the purpose of this work to provide a theoretical picture of the spectroscopy of isolated indole and to attempt an explanation of the elusive L_a origin.

Statement of the Problem

This work will address the problems of calculation of vibronic bandshapes and potential energy surfaces for indole within the Born-Oppenheimer, harmonic, and

Condon approximations. At interest here is the clear identification of the existence of the L_a origin, examination of the possibility of Herzberg-Teller vibronic coupling of L_b vibrations to the L_a electronic state, and a detailed, quantitative picture of the L_b-L_a electronic manifold in terms of Born-Oppenheimer adiabatic potential energy surfaces.

We are interested here in the full potential energy surfaces, in addition to the minimum positions on the respective surfaces for the ground and first two excited singlet states of indole. The reason for this is that the full surfaces are required in order to identify possible avoided crossings of the L_b and L_a electronic states. While the avoided crossings can be identified, in principle, through examination of the nature of the eigenvectors for the excited state electronic wavefunctions, a more detailed picture is provided by the surfaces themselves.

In addition, we wish to establish from this work the magnitude of the interaction between the L_b and L_a electronic states. Although we carry out all calculations of potential energy surfaces within the Born-Oppenheimer adiabatic approximation, without nuclear kinetic energy coupling terms, we are nonetheless able to pose the following question: "Is the Born-Oppenheimer adiabatic picture sufficient to predict accurate spectral bandshapes for isolated indole or is the nature of the excited state potential surfaces better described in terms of a diabatic picture?"

Theoretical Approach

Our approach to the problems outlined above is to perform calculations of spectral bandshapes and potential energy surfaces within the framework of semiempirical molecular orbital theory. In terms of level of theory, the semiempirical approach is a reasonably modest one, representing a significant improvement over standard Hückel MO theory in that the resonance and Coulomb integrals are explicitly incorporated into the formalism, but remaining well outside the essentially "exact" (and computationally

expensive) prescription of ab-initio theories.

We have chosen to employ the Quantum Consistent Force Field (QCFF) method of Warshel, et al. (34-37) as the source of our semiempirical quantum chemical calculations. The reasons for this choice are multi-fold. In the first place, QCFF can be regarded on a theoretical level as essentially a Pariser-Parr-Pople (PPP) Hamiltonian which includes configuration interaction (CI) for singly excited configurations in order to provide excited state properties. A central feature to the QCFF method is the adaptation of empirically derived analytic forms for the core, Coulomb, and resonance integrals, and constitutes an approximate approach which is flexible and efficient enough to provide many of the quantum-mechanical properties of interest with reasonable accuracy and without the exhaustive computational efforts required by more high-end ab-initio theories.

A second and perhaps more attractive feature of QCFF is in regard to the form of the molecular potential energy surface, which is provided for all electronic states as an explicit function of the 3N-Cartesian coordinates of the nuclei comprising the molecule. This has considerable advantages over a representation in internal coordinates (which are provided as well by QCFF) both in terms of out-right convenience in dealing with the excited state potentials but in terms of the normal modes of vibration.

QCFF provides, in canonical form, for the calculation of molecular geometries, bond orders, total molecular energy, configuration interaction excitation energies, CI eigenvectors, transition dipoles, oscillator strengths, and normal modes of vibration (eigenvectors and frequencies). As such, QCFF is a particularly useful package in that it incorporates a great deal of the properties of interest into one convenient and reasonably efficient suite of codes.

In our work with QCFF, we have introduced several modifications to the routines in order to carry out the calculation of spectral bandshapes and potential surfaces. For the most part, these modifications are either trivial adjustments of the QCFF in terms of

procedure or extensions of existing calculations within the code. The overall integrity of the QCFF method has been preserved in terms of parameterization and the functional forms of the model potentials and empirical integrals employed. These modifications are documented in detail in the chapter on Computational Methods (Chapter Three) of this thesis. The modified version of QCFF is designated as QCFFBOZE in order to distinguish our version from the canonical form which is commonly in use.

QCFF thus provides the ingredients -- normal modes of vibration and excitation energies -- necessary for the calculation of spectral bandshapes and potential energy surfaces. The spectral bandshape calculations require the evaluation of Franck-Condon factors, which govern the relative transition intensities for the electronic states at the limit of zero Kelvin. The zero Kelvin "stick" spectrum FC factors have essentially no width -- they represent infinitely narrow resonances -- which is appropriate for identifying the frequencies and relative intensities of the center of the bands but is nonphysical since it fails to account even for the effects of lifetime (Heisenberg) broadening of the transitions. The broadening is handled phenomenologically in our calculations through the application of Gaussian broadening factors to the zero Kelvin "stick" transitions.

The formalism for the calculation of Franck-Condon factors is described in detail in Chapter Two, and details of the algorithm implemented for the evaluation of the FC overlap integrals are discussed in Chapter Three. It suffices here to state that we utilize the recursion relations of Doktorov, et al. (39,40), to carry out the evaluation of the FC factors. This method has the advantage of being exact within the harmonic approximation in that it incorporates the effects of normal coordinate displacements, frequency shifts, and Duschinsky rotation (41), in addition to being reasonably straightforward to implement.

Potential energy surface calculations are carried out in a straightforward manner within the QCFFBOZE framework. The exception to this is the development of a "frozen

configuration interaction" technique which ultimately provides a direct method to approximate the limit of diabatic potential energy surfaces. The implications of this frozen CI method for the calculated spectral bandshapes provides a particularly insightful piece of information regarding the L_a electronic state of indole and constitutes one of the more important results of this work.

Lastly, with regard to the underlying philosophy for the calculations undertaken in this work, our approach is first and foremost a semiempirical one throughout. Our overriding goal is to make connection with experiment rather than to develop new theoretical methods. The main thread throughout is one of flexibility, coupled with direct input from experimental data, in order to develop a comprehensive and accurate characterization of the L_b-L_a electronic manifold. To that end, we have endeavored to elevate the methods which were developed in the course of this work to a status which is not simply that of a fitting procedure. Noteworthy is the fact that we have not empirically adjusted the computed normal coordinate displacements and vibrational frequencies in order to fit spectral bandshapes to agree with experiments -- the only input from experiment at the level of the bandshape calculations is in the form of the spectral bandwidth, oscillator strength ratio for the L_b and L_a states, and the L_a origin energy displacement. In order to accomplish this, the introduction of a difference-density scaling factor was developed within the QCFF formalism (this is, in fact, the definitive feature of QCFFBOZE) in order to globally adjust the bond length changes upon electronic excitation and therefore adjust the normal coordinate displacements without having to appeal to the experimental relative intensities to accomplish this (except for benzene, the calibration molecule). The difference-density scaling method was developed such that QCFFBOZE is able to correctly predict the B_{2u}<--A_{1g} (L_b) absorption spectrum for benzene. However, this method of difference-density scaling appears to have some transferability between molecules, since we apply directly to indole the scaling parameter

which was determined for benzene.

Despite the relatively modest level of theory employed in this work, we are able to obtain reasonably good results for indole in terms of computed spectral bandshapes and potential energy surfaces which strongly reflect what is observed in gas phase experiments. Modest it is: we utilize, through QCFFBOZE, only a CI singles description for the excited states, and all calculations are carried out at the harmonic level of approximation. Even the frozen CI method for approximating a diabatic description of the potential energy surfaces is remarkably simple in terms of approach but provides a very useful picture of the breakdown of the Born-Oppenheimer approximation without having to recast the molecular Hamiltonian to incorporate nuclear kinetic energy couplings. In these respects, the calculations described in this thesis met with considerable success and provide the theoretical framework which is necessary for understanding the interesting and challenging aspects of indole photophysics which have previously eluded explanation.

Thesis Outline

In this thesis it is demonstrated that a previously proposed avoided crossing of the L_b (S_1) and L_a (S_2) electronic surfaces based on the results of fluorescence excitation experiments on jet-cooled indole and methylindoles (5,6,9) is predicted at the CI singles level of semiempirical MO theory near the region of the L_a potential surface minimum. It is shown that an adequate description of the L_b-L_a electronic manifold in indole is provided by an effectively diabatic picture for these two states, and that breakdown of the Condon approximation in the region of the L_b-L_a avoided crossing region (ACR) is strongly evidenced. The picture which emerges in terms of calculated spectral bandshapes is that in which the diabatic prescription for the surfaces correctly predicts the L_a bandwidth and band maximum, providing strong evidence for curve-crossing by L_a

vibrations near the avoided crossing region.

The outline of this thesis is as follows. This Introduction chapter serves to briefly outline the relevant photophysical problems observed in indole and to provide a qualitative introduction to the theoretical techniques employed in this work, as well as to emphasize the problems at hand. Chapter Two, Theoretical Foundations, outlines in considerable detail the underlying assumptions, formalism, and concepts which provide the framework in which this work was carried out. In particular, the form of the Franck-Condon integral recursion relations is presented there, along with the jet-cooled versions of these expressions. Chapter Three, Computational Methods, focuses on the modifications to the QCFF method which were necessary to achieve accurate results for indole, as well as a detailed description of the difference-density scaling procedure which is unique to this work. Chapter Four, Results and Discussion, presents our preliminary results with QCFF for our test-case molecule, benzene, and the extension of the QCFFBOZE difference-density scaling procedure to indole. These results provide the basis for the Franck-Condon factors which are then utilized to examine the vibrational assignment of indole, for calculation of spectral bandshapes, and for the excited state potential energy surfaces. All results are presented and discussed in Chapter Four, along with a discussion which attempts to cast the results into the proper perspective in terms of experiment. In addition, a qualitative argument is presented to attempt to rationalize the experimental results for the methylindoles in light of the calculated results for isolated indole.

Finally, Chapter Five provides a summary and analysis of the collective results and presents a brief outline of suggestions for the logical extensions of the work contained in this thesis which appear promising. This outline or proposal for further work is provided in order to point out some of the areas in this study which appear to warrant further examination and to suggest potential improvements of the methods developed in this

work which could provide further insight into the details of the L_b-L_a electronic manifold of indole.

CHAPTER 2

THEORETICAL FOUNDATIONS

Molecular Hamiltonians and The Born-Oppenheimer Approximation

The Hamiltonian for a molecule comprised of N electrons and K nuclei can be written (in atomic units, e = hbar = m_e = 1)

$$H = T_e + T_n + V_{ee} + V_{nn} + V_{en}$$

$$H = -\frac{1}{2}\sum_{i}^{N}\nabla_i^2 - \sum_{\alpha}^{K}\frac{1}{2M_\alpha}\nabla_\alpha^2 + \frac{1}{2}\sum_{i>j}^{N}\frac{1}{|\mathbf{x}_i - \mathbf{x}_j|} + \frac{1}{2}\sum_{\alpha>\beta}^{K}\frac{Z_\alpha Z_\beta}{|\mathbf{q}_\alpha - \mathbf{q}_\beta|} - \frac{1}{2}\sum_{i,\alpha}^{N,K}\frac{Z_\alpha}{|\mathbf{x}_i - \mathbf{q}_\alpha|}$$

where $\mathbf{x}$ and $\mathbf{q}$ denote electronic and nuclear coordinates, respectively, Z_α represents nuclear charge in multiples of the electron charge, and M_α represents nuclear mass in multiples of the electron mass. The first two terms in the Hamiltonian are the kinetic energy operators of the electrons (nuclei), the second two terms represent the potential energies of electron-electron (nuclear-nuclear) repulsion, and the last term is the electron-nuclear interaction.

The molecular Hamiltonian presented above is the exact electrostatic Hamiltonian in the sense that all of the forces involved are simple Coulomb interactions between particles and no approximations have been introduced except for neglect of spin-orbit (magnetic) coupling terms. The only attractive (i.e. negative) term in the Hamiltonian is the electron-nuclear interaction term, V_{en}. Further, it is important to note that this term is the only coupling term in that it involves both electronic and nuclear coordinates, and is thus the binding potential for the molecule. The presence of this term in the molecular Hamiltonian complicates the solution of the Schrödinger equation since it makes it impossible to express the Hamiltonian as a simple sum of an electronic Hamiltonian and a nuclear Hamiltonian. In this sense, the coupling term is the crux t

term of the Hamiltonian since it makes rigorous separation of electronic and nuclear degrees of freedom an impossibility.

If we rewrite the molecular Hamiltonian by grouping terms involving electronic and nuclear coordinates, we obtain

$$H = [\, T_e(\mathbf{x}) + V_{ee}(\mathbf{x}) + V_{en}(\mathbf{x},\mathbf{q}) \,] + [\, T_n(\mathbf{q}) + V_{nn}(\mathbf{q}) \,].$$

It is worthwhile to consider the above Hamiltonian on physical grounds. First, electrons are much lighter (by at least a factor of 1836) than nuclei, and our intuition suggests that the electronic motion is much faster than the nuclear motion. Thus, to a very good approximation, the electrons can adjust "instantaneously" to the relatively slow motion of the nuclei. Within this level of approximation, we can approach the above Hamiltonian by treating the nuclear framework as being "clamped" in a particular configuration (specified by fixed nuclear coordinates, $\mathbf{q}$) and solving the Schrödinger equation for that molecular geometry. This procedure is repeated over serveral molecular geometries to obtain the total molecular energy as a function of nuclear coordinates.

This separation of electronic and nuclear motions is, in fact, the physical basis for the celebrated Born-Oppenheimer Approximation (42). The original paper by M. Born and R. Oppenheimer was based on time-independent perturbation theory in which a perturbation parameter involving the ratio of electronic to nuclear masses was introduced to treat the nuclear kinetic energy as a perturbation on a zeroth-order Hamiltonian equal to the sum of the electron kinetic energy and the total Coulomb energy. It is possible, however, to pursue the Born-Oppenheimer Approximation on well-motivated physical grounds without having to employ the methods of perturbation theory. In some sense, this approach consists of a Ansatz in which the Born-

Oppenheimer first-order perturbation expansion wavefunction is chosen as the correct wavefunction for the molecular Hamiltonian. In fact, this line of development has now become standard (43,47,84) and has relegated the original derivation by Born and Oppenheimer to the status of culture. The advantage of avoiding the language of perturbation theory, as will be demonstrated below, is that the concept of potential energy surfaces for the nuclear motion arises immediately in the development. Further, the development has a much more intuitive physical appeal which is not exhibited by perturbation-theoretic arguments.

We begin the development by treating the separation of time scales for nuclear and electronic motions. Formally, this procedure corresponds to treating the nuclear coordinate dependence of the Hamiltonian as a parameter. For a given molecular geometry, $\mathbf{q}^*$, the parametic Hamiltonian can be written

$$H(\mathbf{x};\mathbf{q}^*) = [\,T_e(\mathbf{x}) + V_{ee}(\mathbf{x}) + V_{en}(\mathbf{x};\mathbf{q}^*)\,] + [\,T_n(\mathbf{q}^*) + V_{nn}(\mathbf{q}^*)\,]$$

which represents a function of the electronic coordinates with the nuclei clampled at the geometry specified by $\mathbf{q}^*$. In this case, then, the parametric Hamiltonian does exhibit an effective separation in terms of electronic and nuclear degrees of freedom. Corresponding to this Hamiltonian we can construct an appropriate molecular wavefunction (with the same parametric dependence on nuclear coordinates as the Hamiltonian) as a product of separate electronic and nuclear wavefunctions

$$\Psi_{BO} = \psi_\zeta(\mathbf{x},\mathbf{q})\chi_\zeta^\eta(\mathbf{q})$$

where the subscript "BO" is to remind us that we are invoking the Born-Oppenheimer separation. The first term represents an eigenfunction of the terms involving electronic

coordinates at the specified nuclear coordinates. The second term involves only the nuclear coordinates and represents the wavefunction which describes the nuclear motion. Following this Ansatz through we write the time-independent Schrödinger equation in terms of the separated electron-nuclear wavefunction and evaluate the effect of the operators to obtain (after some rearrangement);

$$H\Psi_{B\text{-}O} = \psi_\zeta \left[\frac{-1}{2M} \frac{\partial^2}{\partial q^2} + V_{nn} + \varepsilon_\zeta \right] \chi_\zeta^\eta + \left(\frac{-1}{2M}\right)\left[2\frac{\partial\psi\partial\chi}{\partial q\,\partial q} + \chi_\zeta^\eta \frac{\partial^2\psi}{\partial q^2} \right]$$

$$= E_{\zeta,\eta}\, \psi_\zeta \chi_\zeta^\eta + \left(\frac{-1}{2M}\right)\left[2\frac{\partial\psi_\zeta}{\partial q}\frac{\partial\chi_\zeta^\eta}{\partial q} + \chi_\zeta^\eta \frac{\partial^2\psi_\zeta}{\partial q^2} \right]$$

and in which the term $\varepsilon_{\zeta\eta}$ is identified as the electronic energy for a given nuclear configuration, **q**. The subscripts, ζ and η, denote the electronic state and vibrational level, respectively. The latter terms in this expression involve, respectively, the slopes of the electronic and nuclear wavefunctions with respect to nuclear coordinates, and the curvature of the electronic wavefunction w.r.t. nuclear coordinates. It is the dependence of the electronic wavefunction on nuclear coordinates which is important here. These terms are, of course, a direct consequence of the coupling term -- they represent nuclear kinetic energy coupling.

In view of the expressions above, it is instructive to evaluate the matrix elements corresponding to the Hamiltonian. Proceeding in the usual manner, we obtain

$$\left\langle\, \zeta' n' \,|\, H \,|\, \zeta\, n \,\right\rangle = \int d\mathbf{x} \int d\mathbf{q}\; \psi_{\zeta'}^{*} \chi_{n'}^{*}\, H\, \psi_\zeta \chi_n$$

$$= E_{\zeta n}\, \delta_{\zeta\zeta'}\, \delta_{nn'} + \left(-\frac{1}{2M}\right) \int d\mathbf{x} \int d\mathbf{q}\; \psi_{\zeta'}^{*} \chi_{n'}^{*} H\, \psi_\zeta \chi_n \left\{ 2\frac{\partial\psi}{\partial q}\frac{\partial\chi}{\partial q} + \chi \frac{\partial^2\psi}{\partial q^2} \right\} .$$

Thus, the nuclear kinetic energy coupling terms do not vanish upon integration over electronic and nuclear coordinates, in general, and make some contribution to the

expectation value of the energy. These terms are referred to as "non-adiabatic" terms. Nonetheless, these terms are likely to be small relative to the electronic energy term, $E_{\zeta\eta}$, and can be neglected to a first approximation. In fact, it is precisely the neglect of these terms which define the form of the potential energy surface(s) for nuclear motion in the standard Born-Oppenheimer Approximation. For this reason, the Born-Oppenheimer Approximation is more correctly termed the "Adiabatic Born-Oppenheimer Approximation", and the resulting potential energy surfaces are referred to as "adiabatic potential energy surfaces".

Classical Treatment of Molecular Vibrations

The previous development provides formal expressions for the electronic potential energy surfaces through an effective separation of electronic and nuclear motions. In principle, then, the construction of the potential surfaces proceeds via solution of the separate Schrödinger equations for vibrational (nuclear) and electronic wavefunctions. The former problem can be handled to a very good approximation by the application of a classical model which describes the nuclear motions and leads to quantum mechanical wavefunctions for a familiar, elementary soluble problem: the simple harmonic oscillator. The electronic problem, on the other hand, is somewhat more complicated and requires a fully quantum-mechanical treatment for its solution. We focus here on the solution for the vibrational wavefunctions. The calculation of the electronic wavefunctions is described in detail in a later section.

We begin by envisioning a molecule in terms of a classical model in which the atoms are treated as point masses and the bonds are regarded as springs. We will not be concerned with the details of the electronic structure of the molecule at this point, but instead will focus simply on the classical mechanics of this simplified model.

For N atoms, we require 3N Cartesian coordinates to specify the location of all the

particles. If we then define x_i as the Cartesian displacement from equilibrium for atom "i", we can specify an arbitrary distortion of the molecule by 3N displacement coordinates. For small displacements from equilibrium, we can expand the potential energy in terms of the displacement coordinates as

$$V(\mathbf{x}) = V(\mathbf{x}^{(0)}) + \mathbf{F}\,\mathbf{x} + (1/2)\ \mathbf{x}^{T}\,\mathbf{K}\,\mathbf{x} + (\text{higher-order terms})....$$

where **F** and **K** are the matrices of first and second derivatives, respectively, of the potential. We require that the net force vanish at the equilibrium configuration, so the first derivative terms are zero. Also, we are interested only in the change in energy with respect to the equilibrium configuration, so we may therefore define the term $V(\mathbf{x}^{(0)})$ as zero and gauge the potential energy with respect to this reference. Since we are interested in infinitesimally small displacements from equilibrium, we can neglect the higher order terms in the expansion and obtain for the (approximate) potential energy of vibrational distortion

$$V(\mathbf{x}) = (1/2)\ \mathbf{x}^{T}\,\mathbf{K}\,\mathbf{x}\,.$$

This expression has a very simple physical interpretation: it is just Hooke's Law for a system of masses connected by springs. The coefficients, k_{ij}, are the force constants associated with the springs and represent the restoring force which tends to pull the masses back to their equilibrium positions. Note that this expression exhibits a quadratic dependence of the potential on the displacments, i.e. a harmonic potential. The higher-order terms, which have been neglected, are the so-called anharmonic contributions to the potential. These terms, when included, result in potential wells which are not parabolic.

Now that the form of the potential has been specified, it is possible to write down the equations of motion for the system. If we assume the springs are frictionless the system is conservative and the force is completely specified by the gradient of the potential. Therefore, we can immediately write the equation of motion for the i-th particle from Newton's Second Law as

$$m_i (d^2x_i/dt^2) = F_i = -(\partial V/\partial x_i) = -\sum_j k_{ij} x_j .$$

This represents a system of 3N simultaneous, second-order differential equations which must be solved to obtain the motion for each particle. We can solve this immediately by noting that the solution must be a function of time such that the second derivative of the function is proportional to the function itself. We are free to choose the solution to be of the form

$$x_i(t) = a_i \cos(\omega t + \phi)$$

which can be shown to have the desired property by direct substitution;

$$d^2x_i/dt^2 = -a_i \omega^2 \cos(\omega t + \phi).$$

Inserting this solution into the above set of coupled equations of motion yields

$$-m_i a_i \omega^2 \cos(\omega t + \phi) = -\sum_j k_{ij} a_j \cos(\omega t + \phi)$$

or more simply

$$-m_i a_i \omega^2 = -\sum_j k_{ij} a_j$$

which represents a set of 3N coupled, linear, homogeneous equations in the amplitudes, a_i, which must be solved to obtain the motion for the system. This last expression represents the secular equation which must be solved in order to obtain the vibrational frequencies for the system. In principle as well as in practice this is essentially a trivial problem in that all we are required to do is perform a reasonably simple matrix diagonalization.

On the other hand, we really do not need to carry out the diagonalization to know the

structure of the solution. We have already specified an oscillatory solution for the time dependence of the coordinates. That is, physically, all the masses (atoms) oscillating about their equilibrium positions with the same frequency and phase relationship. Thus, all the atoms move through their equilibrium positions at the same time, reach their classical turning points at the same time, and then reverse the motion. The phase for the motions is of no interest, and so may be arbitrarily set to zero. In fact, the only details of the solution that we do not know are the exact frequency of the motion and the absolute amplitudes of the motion. It turns out, however, that such a system of equations cannot produce a unique set of amplitudes (44,50). Rather, the closest we can obtain to a mathematically complete solution is the relative amplitudes.

Returning to the secular equations obtained previously, we can express this set of 3N simultaneous equations more compactly in matrix-vector notation as

$$\mathbf{Ka} = \omega^2 \mathbf{ma}$$

where **m** represents a diagonal mass matrix. Formally, this expression has the appearance of an eigenvalue equation except for the presence of the mass terms, i.e. each amplitude is multiplied by a different mass. We can convert this expression into an eigenvalue equation by transforming to mass-weighted form in the following manner; (i) replace each a_i by $m_i^{1/2} a_i$ and divide the i-th column of the K-matrix by $m_i^{1/2}$, and (ii) divide the i-th row of the K-matrix by $m_i^{1/2}$. Denoting the transformed **K**-matrix by **U**, and the transformed amplitude vector by **L**, we now have

$$\mathbf{UL_k} = \omega^2_k \mathbf{L_k} \quad (k = 1 \text{ to } 3N)$$

which is in the form of an eigenvalue equation. We denote the mass-scaled amplitude components as $L_{ik} = m_i^{1/2} a_{ik}$. In the language of eigenvalue problems the ω_k are the eigenvalues and the $\mathbf{L_k}$ are the eigenvectors.

The procedure of mass-adjusting described above may seem awkward and ill-motivated at first sight. Nonetheless, it does serve to transform the secular equation into

an eigenvalue equation. It turns out, in fact, that the same eigenvalue problem will result automatically if we define at the beginning a set of mass-scaled displacement coordinates, $m_i^{1/2}\, x_i$, and derive the equations of motion in terms of them. Formally and physically, the results obtained are identical.

The advantage of being able to define an eigenvalue problem via mass-scaled displacement coordinates is that eigenvalue problems are tractable. In matrix language, the solution requires a similarity transformation, which is easy to perform. If we define **L** (without the subscript, k) as the square matrix in which the eigenvectors ($\mathbf{L_k}$) are the columns, and ω the diagonal matrix of eigenvalues ω^2_k, we have

$$\mathbf{UL} = \omega\,\mathbf{L}$$

which can be diagonalized directly by the similarity transform

$$\mathbf{L^{-1}UL} = \mathbf{L^{-1}}\omega\,\mathbf{L} = \omega\,\mathbf{L^{-1}L} = \omega$$

and we can take advantage of the fact that **L** is an orthogonal matrix to obtain

$$\mathbf{L^T UL} = \omega,$$

where the "T" superscript denotes the transpose operation.

Transformation to Normal Coordinates

Recall the original expression for the potential energy change for vibrational distortion in terms of Cartesian displacement coordinates;

$$V(\mathbf{x}) = (1/2)\,\mathbf{x^T K x}.$$

If we now mass-scale the displacement coordinates and the force constants according to the prescription of the previous section, we obtain

$$V(\mathbf{q}) = (1/2)\,\mathbf{q^T U q}$$

where $q_i = m_i^{1/2}\, x_i$ and $U_{ij} = K_{ij}/(m_i^{1/2}\, m_j^{1/2})$.

If we now insert the identity $\mathbf{LL^T = 1}$ before and after **U** in the potential energy expression we can effectively diagonalize the (mass-adjusted) matrix of force constants t

to obtain

$$V(\mathbf{q}) = (1/2)\,\mathbf{q}^T \mathbf{L}\mathbf{L}^T \mathbf{U}\,\mathbf{L}\mathbf{L}^T \mathbf{q} = (1/2)\,\mathbf{Q}^T \omega^2 \mathbf{Q} = (1/2) \sum_k \omega^2_k Q^2_k$$

where we have defined

$$\mathbf{Q} = \mathbf{L}^T \mathbf{q}\,; \quad Q_k = \sum_i L_{ik}\, q_i.$$

The important point regarding the above transformation of the potential energy is that by recasting the change in energy for infinitesimal displacements in terms of the new coordiantes, **Q**, we obtain a simplified energy expression in which there are no cross terms between coordinates. The new coordinates, termed normal coordinates (due to the orthogonality of the eigenvectors, **L**), therefore provide a separable energy expression which can be identified as a sum of individual quadratic terms for each mode of vibration. Therefore, in principle, we have completely solved the classical mechanics of molecular vibration: by diagonalizing the matrix of mass-adjusted force constants in a basis of mass-weighted Cartesian displacment coordinates, we generate the normal modes of vibration.

Quantum Mechanical Consequences

The previous result shows that we can express the potential energy for molecular vibration as a sum of independent harmonic oscillators. This result is based on a model in which the molecule is treated classically, as point masses connected by springs. Nonetheless, an energy expression which is a simple summation implies a separable quantum mechanical wavefunction which is a product of individual wavefunctions. Therefore, by construction, we can write the total vibrational wavefunction for this model as the product of 3N separate harmonic oscillator wavefunctions, one for each normal coordinate. This vibrational wavefunction will be valid to the extent that the approximation of small displacements is valid.

In this sense, we do not require a solution of the vibrational Schrödinger equation. If

we adopt normal coordinates as an approximation to describe the vibrational problem, the vibrational wavefunctions are essentially solved since they are simply harmonic oscillator wavefunctions. An advantage of using a harmonic description of the vibrations, when possible, is that much of the phenomenon involving harmonic oscillators is mathematically tractable (e.g. matrix elements) in closed form. In addition, even for situations where there are anharmonic effects, many of the essential features of the problem will be captured by a zeroth-order description in terms of harmonic oscillators, therefore giving such an approximate description a very satisfying physical appeal. For these reasons, calculations carried out within the harmonic approximation are well justified: in the event that a harmonic calculation does not agree with experiment, we gain the understanding that the phenomenon is anharmonic in character and some quantitative understanding of the degree of anharmonicity.

Semiempirical Molecular Orbital Theory

LCAO-MO-SCF Calculations

Although the Born-Oppenheimer approximation, in conjunction with the adaptation of a normal coordinate description of the vibrational modes, effectively solves the vibrational part of the problem, the electronic Schrödinger equation presents a unique computational problem. Much of the difficulty is due to the presence of electron-electron repulsion terms in the Hamiltonian, which makes impossible the decoupling of the electronic Schrödinger equation into separate one-electron equations. Further, the calculation of quantum mechanical expectation values requires the evaluation of an extremely large number of integrals, thus making the calculation of molecular properties a computationally expensive process. For these reasons, it is necessary to introduce approximations to make the solution of the electronic structure problem a tractable one.

We begin by adopting the linear combination of atomic orbitals (LCAO) approximation, in which the molecular orbitals are expanded in a basis of atomic orbitals centered on the atoms comprising the molecule. If the LCAO-MO wavefunction is then antisymmetrized to insure that the Pauli exclusion principle is not violated, it can be shown that the orbitals which minimize the total energy are those which are solutions to the Hartree-Fock equations (45,47,48) . This series of approximations leads to the familiar secular determinant for the eigenvalues and the secular equations for the eigenvalues;

$$| F_{\mu\nu} - \varepsilon_i S_{\mu\nu} | = 0$$

$$\Sigma_\nu \{ F_{\mu\nu} - \varepsilon_i S_{\mu\nu} \} c_{\nu i} = 0 \quad \text{for } i = 1,2,...,M$$

where $F_{\mu\nu} = [\mu | F | \nu]$ and $S_{\mu\nu} = \int dr_1 \chi_\mu^*(1) \chi_\nu(1)$ are the Fock matrix elements and overlap integrals, respectively.

The Fock operator can be written explicitly as a sum of one- and two-electron operators, in which case

$$F = h + \Sigma_j (2J_j + K_j)$$

so that the Fock matrix elements, in terms of the AO basis functions, can be expressed

$$F_{\mu\nu} = h_{\mu\nu} + \Sigma_\lambda \Sigma_\sigma \rho_{\lambda\sigma} \{ (\mu\nu | \lambda\sigma) - (1/2) (\mu\lambda | \nu\sigma) \}$$

where

$$h_{\mu\nu} = [\mu | h | \nu] \text{ and } (\mu\nu | \lambda\sigma) = \iint dr_1 \, dr_2 \chi_\mu^*(1) \chi_\nu^*(1) (1/r_{12}) \chi_\lambda(2) \chi_\sigma(2).$$

Generally, we are interested in evaluating the electronic energy at a particular molecular geometry. Formally, this corresponds to evaluating the expectation value of the Fock operator, i.e. for a closed shell

$$E_{el} = 2 \Sigma_i \varepsilon_i - (1/2) \Sigma_\mu \Sigma_\nu \Sigma_\lambda \Sigma_\sigma \rho_{\mu\nu} \rho_{\lambda\sigma} \{ (\mu\nu | \lambda\sigma) - (1/2) (\mu\lambda | \nu\sigma) \}$$

which provides an explicit energy expression in terms of the AO basis.

In practice, the Hartree-Fock equations are solved by the self-consistent field (SCF) procedure, in which the coefficients representing the eigenvectors are optimized

iteratively, and the final electronic energy is evaluated after convergence is achieved. In light of the above formalism this procedure, termed Hartree-Fock LCAO-MO-SCF, can be outlined in the form of an algorithm as follows:

(1) Select a set of M basis orbitals, χ_μ (where μ=1,2,...,M), and evaluate the integrals ($h_{\mu\nu}$, $S_{\mu\nu}$, $(\mu\nu \mid \lambda\sigma)$);

(2) Choose a set of coefficients, $\{c_{\mu i}\}$, for the occupied orbitals, perform the LCAO expansion, and evaluate the density matrix, $\rho_{\lambda\sigma} = 2 \Sigma_i c_{\lambda i} c_{\sigma i}$, for all λ,σ, where the summation extends over all doubly-occupied orbitals (i.e. N/2).

(3) Evaluate the Fock matrix elements, $F_{\mu\nu}$;

(4) Find the roots of the secular determinant and solve the secular equations for the eigenvectors, $\{c_{vi}\}$, corresponding to each eigenvalue, ε_i.

(5) Compare the $\{c_{vi}\}$ for i=1,2,...,N/2, with those assumed in step (2). If the two sets of coefficients agree within the desired tolerance, go on to step (6). Otherwise, go to step (2) with the new set of coefficients, $\{c_{vi}\}$, and repeat steps (2)-(5).

(6) Compute the total electronic energy

$$E_{el} = 2 \Sigma_i \varepsilon_i - (1/2) \Sigma_\mu \Sigma_\nu \Sigma_\lambda \Sigma_\sigma \rho_{\mu\nu} \rho_{\lambda\sigma} \{ (\mu\nu \mid \lambda\sigma) - (1/2) (\mu\lambda \mid \nu\sigma) \}$$

and identify the ε_i's as the MO energies and the optimized eigenvectors as the SCF MO's. From the converged SCF orbitals, any further molecular properties of interest may then be evaluated.

The above algorithm is standard to most quantum chemistry codes. Solution of the secular equations requires a matrix diagonalization routine, which is not problem-dependent, and the only differences in the various codes are primarily in terms of the basis set employed. In fact, this algorithm is common to both ab-initio and semiempirical MO theories and the fundamental difference between these two schemes is in terms of the evaluation of the relevant integrals in the SCF procedure.

Inclusion of Configuration Interaction (CI)

The above LCAO-MO-SCF procedure provides a tractable quantum chemical route for the calculation of molecular properties of interest. It is limited, however, to closed shell systems in the present form and thus provides only ground state information. Further, this method cannot provide the exact electronic energy since a single Slater determinantal wavefunction has been used to represent the electron configuration.

The electronic energy can be improved by attempting to incorporate the effect of electron correlation into the calculation of the molecular wavefunction. The natural extension of the procedure thus far outlined is to introduce configuration interaction (CI) into the wavefunction, and expand the total wavefunction as a linear combination of Slater determinants as follows;

$\Psi_{CI} = c_0 D_0 + \sum_i c_i^{(1)} D_i^{(1)} + \sum_i c_i^{(2)} D_i^{(2)} +$ (higher-excitations)...

where D_0 is the Slater determinant representing the (closed-shell) ground state, and the determinants $D_i^{(n)}$ represent excited state electron configurations involving promotion of n=1,2,... electrons. Inclusion of only the n=0,1 determinants in the CI wavefunction is termed "CI singles" (CIS), while including determinants through n=2 corresponds to "CI doubles" (CISD). It is important to note, however, that it can be shown (46,47) through the application of the Slater-Condon rules that the ground state configuration (D_0) does not mix with singly excited configurations (Brillouin's theorem, (45,46,47)), and thus a CI singles calculation does <u>not</u> improve the energy of the ground state but has a dominant effect for excited states. In the course of this work utilizing the QCFF routine, all calculations were carried out to include CI singles, or single excitations.

This extension of the SCF procedure in terms of configuration interaction then proceeds in a manner directly analogous to the LCAO-MO-SCF calculations previously outlined. The relevant energy matrix constructed and diagonalized in the CI calculation, termed the "CI-matrix" or "CI-Hamiltonian matrix", provides the eigenvalues and

eigenvectors corresponding to the ground and excited electronic states of the molecule. In fact, since the diagonalization requirements of both the LCAO-MO-SCF procedure and the CI calculations are identical, the same diagonalization subroutine can be utilized for both types of calculations (as well as for obtaining the normal modes of vibration).

The only remaining point is the evaluation of the integrals required in the SCF calculations. In ab-initio methods, all integrals are evaluated (generally by numerical quadrature routines) explicitly at each step in the SCF. It can be shown that for N-basis functions that the number of integrals required scales as N^4 (46,48). In semiempirical MO methods, the number of integrals required is reduced considerably by introducing various approximations to eliminate altogether certain integrals or, for those which are not neglected, suitable empirical forms are introduced which are flexible enough to accurately represent the integrals over the range of coordinates (45,48). A particularly useful method for reduction of the integrals is the method of zero differential overlap (ZDO), which is discussed next within the context of the Pariser-Parr-Pople method.

The Pariser-Parr-Pople (PPP) Method

One of the most useful semiempirical molecular orbital theories for the treatment of pi-electron systems is the Pariser-Parr-Pople (PPP) method. In spirit and language the PPP method is very similar to Hückel theory, in that many of the concepts and objects of the PPP theory are essentially a reintroduction of parameters which are neglected in Hückel MO theory. More accurately, the PPP method combines the Hückel MO theory with the SCF and CI procedures to produce a method which provides for the calculation of optimized molecular geometries and electronically excited states.

On a formal level, the PPP method is perhaps more well-motivated than the brutal approximations employed in the standard Hückel theory. If we recall the expression for the Fock matrix elements in the AO basis language,

$$F_{\mu\nu} = h_{\mu\nu} + \Sigma_{\lambda} \Sigma_{\sigma} \rho_{\lambda\sigma} \{ (\mu\nu \mid \lambda\sigma) - (1/2) (\mu\lambda \mid \nu\sigma) \},$$

it is important to realize that the electron repulsion integrals, $(\mu\nu \mid \lambda\sigma)$, and the density matrix elements, $\rho_{\lambda\sigma}$, can be either positive or negative in sign. Further, a great number of the repulsion integrals will tend to be small, since their functional form is essentially dominated by an integral over a (screened) Coulomb potential. The upshot of this competition between the absolute signs of the integrals and the density matrix weighting factors in their contributions to each Fock matrix element is that it is both possible and probable for a delicate cancellation to occur, resulting in matrix elements which are nearly zero. In view of the extensive computational labor required to evaluate all the integrals, only to have a large number of them cancel to (near) zero, the general utility of this approach is called into question. In other words, "Why bother (to evalute all the integrals)?"

Pople (48) devised several schemes, generally termed "Neglect of Differential Overlap" (NDO) methods, to reduce the computational effort involved in evaluation of the Fock matrix. In particular, the zero-differential overlap (ZDO) method reduces considerably the number of integrals to be explicitly evaluated by making the approximation

$$(\mu\nu \mid \lambda\sigma) = (\mu\mu \mid \lambda\lambda) \; \delta_{\mu\nu} \, \delta_{\lambda\sigma}$$

where δ_{ij} is the Kronecker delta symbol. In terms of the ZDO approximation, then, the Fock matrix elements are reduced to

$$F_{\mu\mu} = h_{\mu\mu} - (1/2)\rho_{\mu\mu} (\mu\mu \mid \mu\mu) + \Sigma_{\lambda}\rho_{\mu\mu}(\mu\mu \mid \lambda\lambda),$$

and the off-diagonal elements are given by

$$F_{\mu\nu} = h_{\mu\nu} - (1/2)\rho_{\mu\nu} (\mu\mu \mid \nu\nu) \qquad (\mu \neq \nu).$$

Finally, in order to retain invariance of the results to axis rotation, it is necessary to ensure that the two-electron integrals depend only on the type of atoms to which the

basis functions belong. This can be accomplished by making the further approximation that

$(\mu\mu \mid \lambda\lambda) = \gamma_{AB}$, for all μ on atom A, all λ on atom B.

Further, we introduce a simplified notation for the one- and two-electron integrals in the expression for the Fock matrix, making the identifications

$h_{\mu\mu} = \omega_\mu$ $\qquad$ $h_{\mu\nu} = \beta_{\mu\nu}$ (for $\mu \neq \nu$)

and

$(\mu\mu \mid \mu\mu) = \gamma_{\mu\mu}$ $\qquad$ $(\mu\mu \mid \nu\nu) = \gamma_{\mu\nu}$ (for $\mu \neq \nu$).

Within this set of approximations, the Fock matrix in terms of the PPP method may finally be expressed as

$F_{\mu\mu} = \omega_\mu - (1/2)\rho_{\mu\mu}\gamma_{\mu\mu} + \Sigma_{\nu\neq\mu}\gamma_{\mu\nu} Q_\nu$ (diagonal)

$F_{\mu\nu} = \beta_{\mu\nu} - (1/2)\rho_{\mu\nu}\gamma_{\mu\nu}$ $\qquad$ $(\mu \neq \nu)$ $\qquad$ (off-diagonal).

The above expressions for the PPP form of the Fock matrix are still quite general, despite the extensive approximations introduced in arriving at them. What remains is the evaluation of the integrals in these matrix elements by introduction of suitable, flexible, analytic forms or empirical values. The specific forms chosen for the integrals are generally problem (i.e. molecule) dependent. The Quantum Consistent Force Field (QCFF) method, to be described next, is unique in that it provides analytic forms for the integrals and is applicable to a large class of molecules.

The Quantum Consistent Force Field (QCFF)

The Quantum Consistent Force Field (QCFF) semiempirical method was introduced by A. Warshel and M. Karplus (34,35) in an attempt to provide consistent calculation of ground and excited state potential energy surfaces and related spectroscopic properties for conjugated molecules. The fundamental concept behind QCFF was to develop a

unified approach to quantum chemical calculations for a large class of molecules in which a single set of parameters is used in the calculation of all properties.

From a coarse-grained perspective, the QCFF method exploits the physical meaning of each term in the generalized molecular potential energy surface in order to produce equilibrium molecular geometries, normal modes of vibration, and molecular properties (e.g. thermodynamic, transition dipoles, IR intensities, etc.). The general form of the potential energy is expanded around the equilibrium configuration of the molecule, $\mathbf{r}_0$ as follows;

$$V(\mathbf{r}) = V(\mathbf{r}_0) + \Sigma_i (\partial V / \partial r_i) \delta r_i + (1/2) \Sigma_i \Sigma_j (\partial^2 V / \partial r_i \partial r_j) \delta r_i \delta r_j + ...,$$

in which the first term defines the system energy at equilibrium. The second term, which defines the distortion of the molecular framework from equilibrium, produces a set of equations which, when solved, provide the equilibrium molecular geometry;

$$(\partial V / \partial r_i) = 0.$$

This set of equations specifies the condition of balanced forces within the molecule and can be solved by a Newton-Raphson minimization procedure. The third term in the above expansion defines the potential energy for molecular vibration and is solved (as discussed previously) by diagonalization of the matrix of mass-scaled force constants. In principle, all that is required to utilize the above expression to derive molecular properties is an appropriate set of potential functions (and derivatives) for the molecule(s) of interest, and the necessary routines for solution of the energy minimization and matrix diagonalization problems. The QCFF routines combine all these tasks into one convenient package.

Formally, the QCFF invokes a separation of sigma and pi electrons. The sigma electrons are treated in terms of a set of empirical potential functions, and the pi electrons are handled by a semiempirical Pariser-Parr-Pople (PPP) Hamiltonian modified for nearest-neighbor overlap. This modification is incorporated into the

existing ZDO formalism by using an orthogonalized, or Löwdin, basis.

An advantage of the QCFF formalism is that potential energy surfaces are given as an explicit function of the nuclear coordinates, which permits analytic evaluation of the first- and second-derivatives of the surface with respect to the coordinates. These analytic expressions are then used in a hybrid steepest descent/Newton-Raphson energy minimization procedure in order to locate the equilibrium geometry and potential minimum.

Excited state potential surfaces and related properties are obtained by incorporating configuration interaction (CI) in the wavefunction. In the usual manner, the wavefunction is expanded as a linear combination of individual Slater determinantal wavefunctions for various electronic configurations. The CI-matrix is then constructed and diagonalized, and the lowest root obtained is identified with the ground electronic state of the system.

The QCFF potential energy surface for the N-th excited state is expressed as a sum of separate sigma and pi electron surfaces plus the CI excitation energy for the N-th state, i.e. $V(\mathbf{x}) = V_{\sigma}(\mathbf{x}) + V_{\pi}^{(0)}(\mathbf{x}) + \Delta V_{\pi}^{N}(\mathbf{x})$.

The total sigma-electron energy is expressed in terms of model empirical potentials and the pi-electron energy term is obtained as the SCF-MO energy for the closed-shell ground state. The appropriate CI excitation energy for the electronic state of interest is then appended to these two terms to obtain the excited state energy at the molecular geometry specified by the Cartesian coordinates, **x**. It is worthwhile now to consider each of these contributions to the PES in detail.

The Sigma-Electron Potential

The σ-electron potential surface can be written as a sum of contributions from saturated (sat), conjugated (conj), and the connections between saturated and conjugated

(sat-conj) parts of the molecular framework;

$$V_\sigma(\mathbf{x}) = V(\mathbf{x})_{sat} + V(\mathbf{x})_{conj} + V(\mathbf{x})_{sat\text{-}conj}$$

The most appropriate representation of these potentials is in terms of internal coordinates; bond lengths (**b**), bond angles (θ), and torsional angles (φ). Also, when non-bonded interactions are important, these must be included and will be a function of non-bonded distances (**R**) We denote by **S** the set of internal coordinates, i.e. **S** = { **b**, θ, φ, **R** }, and write the general model potential in the form

$$V(\mathbf{S}) = \sum_i V_b(b_i) + \sum_i V_\theta(\theta_i) + \sum_{i,j} V_{b,\theta}(b_i,\theta_i) + \sum_i V_\varphi(\varphi_i) + \sum_{i,j} V_{nb}(R_{ij})$$

The specific forms for the individual empirical functions are contained in the original papers of Warshel, et al. (34-37). Since we have utilized these potentials without modification in our work with the QCFF package, no further discussion of their detailed functional forms is necessary here.

The Pi-Electron Potential

As stated above, the pi-electron energy is computed quantum-mechanically by a SCF-MO calculation. The SCF-MO calculation involves diagonalization of the Fock matrix, which is written in PPP form as

$$F_{\mu\mu} = \omega_\mu + (1/2)\rho_{\mu\mu}\gamma_{\mu\mu} - \Sigma_\nu Q_\nu \gamma_{\mu\nu} \qquad (\nu \neq \mu),$$

$$F_{\mu\nu} = \beta_{\mu\nu} - (1/2)\rho_{\mu\nu}\gamma_{\mu\nu} \qquad (\mu \neq \nu).$$

In terms of the Fock matrix elements we may then express the pi-electron energy for a given molecular geometry as

$$V_\pi^{(0)}(\mathbf{x}) = \Sigma_\mu \rho_{\mu\mu}(\mathbf{x}) \{ W_\mu + (1/4)\rho_{\mu\mu}\gamma_{\mu\mu} \} + 2\Sigma_{\nu>\mu}\rho_{\mu\nu}(\mathbf{x})\beta_{\mu\nu} - \Sigma_{\nu>\mu}\{ (1/2)\rho_{\mu\nu}\rho_{\mu\nu} - Q_\mu Q_\nu \}\gamma_{\mu\nu}.$$

The core, Coulomb, and resonance integrals in this expression are represented by empirical formulas, which is consistent with the PPP method. We present here without

derivation the basic analytical forms of the QCFF integrals, which were used without modification in this work. The Coulomb integrals are, in fact, chosen to be of the Nishimoto-Mataga form, modified by an exponential to provide the flexibility required within the QCFF approach;

$$\gamma_{\mu\nu} = G' \exp\{-\mu_\gamma b_{\mu,\nu}\} + e^2/(D + b_{\mu\nu})$$

in which $G' = (I - A) - G_0$ and $D = e^2 / G_0$, and for the off-diagonal Coulomb integrals;

$$\gamma_{\mu\mu} = (I - A) + G_s [\exp\{-2\mu_\beta (b_{\mu,\mu+1} - b_0^1)\}] \cos^2\tau_{\mu,\mu+1} + \exp\{-2\mu_\beta (b_{\mu,\mu-1} - b_0^1)\} \cos^2\tau_{\mu,\mu-1}]$$

in which $\tau = (\phi_1 + \phi_2 + \phi_3 + \phi_4)/4$, where ϕ_i are the torsional angles associated with the conjugated bond between two carbon atoms. The resonance integrals are given by the form

$$\beta_{\mu,\nu} = \beta_0 \exp\{-\mu_\beta (b_{\mu,\nu} - b_0^1)\} [\, 1 + k_\beta (b_{\mu,\nu} - b_0^1) \,] \times [\cos\tau_{\mu,\nu} (1 - \varepsilon_\tau \rho_{\mu,\nu} \cos\tau_{\mu,\nu})] / [1 - \varepsilon_\tau \rho_{\mu,\nu}]$$

and the core integrals are defined by

$$W_\mu = W_{2p}^0 + \beta \exp\{-2\mu_\beta (b_{\mu,\mu+1} - b_0^1)\} \cos^2\tau_{\mu,\mu+1} + \exp\{-2\mu_\beta (b_{\mu,\mu-1} - b_0^1)\} \cos^2\tau_{\mu,\mu-1}]$$

for which only diagonal terms are required (hence the single subscript, μ). In the off-diagonal integral expressions presented above, the subscript $\nu \neq \mu$ and within the framework of zero differential overlap (ZDO) the condition $\nu = \mu \pm 1$ must hold for a non-zero integral. What remains is to specify the parameters required for explicit evaluation of the π-electron integrals contained in the above forms. The original parameterization

of Warshel and Karplus was adopted without modification; these values are tabulated below (Table 1.).

TABLE 1. QCFF π-electron integral parameters.

integral	parameter	value
ß	$ß_0$	-2.438 eV
	$\mu_ß$	2.035 Å^{-1}
	$k_ß$	0.405 Å^{-1}
	ε_τ	0.03
	b_0^1	1.397 Å
W	W^0_{2p}	-9.97 eV
	ß'	0.235 eV
γ	I-A	9.81 eV
	G_0	5.14 eV
	G_s	0.69 eV
	μ_γ	0.232 Å^{-1}

In the energy minimization procedure, it is necessary to compute the pi-energy at several different geometries. The initial values for the bond orders in the SCF calculation are taken to be the values obtained from a Hückel MO calculation. An SCF iteration then provides improved bond orders at the given geometry, and the pi-energy is computed using the above expression. The geometry is then shifted, and the bond orders for the new geometry are approximated by those from the previous SCF iteration. The SCF calculation is then repeated to provide updated bond orders and pi-energy. This procedure is repeated until convergence in the energy is achieved and the geometry so obtained is identified as the minimum for the surface.

In this procedure, the gradient and second derivatives of the potential are required in order to determine the direction which the geometry must be shifted in order to converge towards the minimum along the multidimensional surface. The evaluation of the derivatives is accomplished in analytic form by regarding the bond orders as constants and differentiating only the integrals. In fact, this procedure yields first derivatives with respect to **r** which are exact at the point $\mathbf{r}_S$. The exactness of the first derivatives is a property of all SCF-LCAO-MO surface and can be demonstrated by the Hellmann-Feynman theorem (49).

To summarize, then, the minimization procedure is as follows;

(i) The core, Coulomb, and resonance integrals are evaluated at **r**.

(ii) The Fock matrix, **F(r)** is constructed and the bond orders are determined.

(iii) First and second derivatives are evaluated and the geometry is shifted to **r'**.

(iv) Steps (i)-(iii) are repeated at the new geometry, **r'**.

This is, of course, the same process as is involved in the SCF algorithm described in section (2.3), with the addition of the geometry optimization procedure.

The Excitation Energy

The CI excitation energy, $\Delta V_\pi^N(x)$, determines the excited state potential energy surface(s) and thus is the central quantity of interest in an excited state calculation. We therefore seek an expression for the vertical excitation energy from the ground state PES to the N-th electronic state as a function of the molecular geometry. The most straightforward way to derive this expression is to begin with the configuration interaction matrix, derive the CI eigenvalue problem, and diagonalize the CI matrix by a similarity transform.

We begin by considering the diagonal elements of the CI matrix. We denote the excited state wavefunction by

$$\psi_N(\mathbf{r}) = \sum_n C_{Nn}(\mathbf{r})\ {}^1\psi_n \quad \text{where} \quad {}^1\psi_n = {}^1\psi_{n1\to n2}$$

represents the wavefuntion for promotion of an electron from MO n1 to MO n2, and express the eigenvalue problem for the CI coefficients (eigenvectors) as

$$\mathbf{A}(\mathbf{r})\mathbf{C}_N(\mathbf{r}) = \Delta V_\pi^N(\mathbf{r})\mathbf{C}_N(\mathbf{r})$$

The diagonal elements of the CI matrix are of the form

$$\mathbf{A}_{nn} = \left\langle {}^1\psi_{n1\to n2} \mid H \mid {}^1\psi_{n1\to n2} \right\rangle - \left\langle {}^1\psi_0 \mid H \mid {}^1\psi_0 \right\rangle$$

$$= \varepsilon_{n2} - \varepsilon_{n1} - \left\langle n_1 n_2 \mid n_1 n_2 \right\rangle + 2\left\langle n_1 n_2 \mid n_2 n_1 \right\rangle$$

and the off-diagonal elements are

$$\mathbf{A}_{nm} = 2\left\langle m_1 n_2 \mid m_2 n_1 \right\rangle - \left\langle m_2 n_2 \mid n_1 m_2 \right\rangle$$

In these matrix elements, the Dirac bra-ket notation is employed. For example, the off-diagonal CI matrix elements in wavefunction language are of the form

$$\int \sum_m C_m \psi_{m_1\to m_2} \{ \sum_i H_i^{core} + \sum_{i,j} \frac{1}{r_{ij}} \} \sum_n C_n \psi_{n_1\to n_2}\, d\tau$$

which, although more transparent, is much more complicated to write. For this reason, we invoke the Dirac notation to simplify these expressions.

We can immediately write down the similarity transform which diagonalizes the CI matrix and obtain the formal expression for the excitation energies;

$$\Delta V_\pi^N(\mathbf{r}) = \mathbf{C}_N\, \mathbf{A}(\mathbf{r})\, \mathbf{C}_N = \sum_m (\mathbf{C}_{Nm})^2 (\mathbf{A}(\mathbf{r}))_{mm} + 2\sum_{k>m} \mathbf{C}_{Nm}\mathbf{C}_{Nk}(\mathbf{A}(\mathbf{r}))_{mk}$$

The explicit forms for the CI matrix elements in terms of the empirical integrals are then used in this expression to compute the excitation energies.

At this point in the development, Warshel (34,35) derives an expression involving separate terms for the core integrals, diagonal and off-diagonal Coulomb integrals, and the resonance integrals. This expression involves defining a set of coefficients for each of the integral contributions which can be regarded as the set of effective bond orders for the particular electronic state. In this way, the excitation energy can be written compactly as

$$\Delta V_{\pi}^{N}(\mathbf{r}) = \sum_{\mu} R_{\mu}^{W} W_{\mu} + \sum_{\nu>\mu} R_{\mu\nu}^{\beta} \beta_{\mu\nu} + \sum_{\mu} R_{\mu\mu}^{\gamma} \gamma_{\mu} + \sum_{\nu>\mu} R_{\mu}^{\gamma} \gamma_{\mu\nu}$$

where the sets of coefficients, $\{R^{g}\}$, can be derived from the previous energy expression by comparing and grouping terms involving the integrals. Warshel, et al. (34,35) provide expressions for these coefficients in terms of the AO basis for CI singles; the coefficients for CI doubles are given by Lasaga et al. (38). The coefficients of the core integrals are prescribed by the expression

$$R_{\nu}^{W} = \sum_{m} (C_{Nm})^{2}(\nu_{m_2\nu}\nu_{m_2\nu} - \nu_{m_1\nu}\nu_{m_1\nu})$$

and the coefficients of the diagonal Coulomb integrals are

$$R_{\nu\nu}^{\gamma} = \sum_{m} (C_{Nm})^{2}[(\nu_{m_2\nu}\nu_{m_2\nu} - \nu_{m_1\nu}\nu_{m_1\nu})\left(\frac{\rho_{\nu\nu}}{2}\right) + (\nu_{m1\nu}\nu_{m2\nu})^{2}] + \sum_{k>m} 2\, C_{Nm}\, C_{Nk}\ \ (\nu_{m_1\nu}\nu_{m_2\nu}\nu_{k1\nu}\nu_{k2\nu})$$

while the resonance integral coefficients are;

$R^{\beta}_{\mu\nu} = \Sigma_{m}\, 2\, (C_{Nm})^{2}\, \{\, \nu_{m2\nu}\, \nu_{m2\mu} - \nu_{m1\nu}\, \nu_{m1\mu}\, \}, \quad (\mu\neq\nu)$

where the term in backets, { ... }, is seen to be the <u>difference</u> <u>density</u> matrix between the orbitals indexed by m_2 and m_1. Finally, the expression for the coefficients of the off-diagonal Coulomb integrals is given by the rather complicted expression;

$$R^{\gamma}_{\mu\nu} = \sum_{m} 2(C_{Nm})^2 \{ - (\nu_{m_2\nu}\nu_{m_2\mu} - \nu_{m_1\nu}\nu_{m_1\mu}) \left(\frac{\rho_{\mu\nu}}{2}\right)$$
$$+ 2 (\nu_{m_1\nu}\nu_{m_1\mu}\nu_{m_2\nu}\nu_{m_2\mu}) - \frac{1}{2} [(\nu_{m_1\nu}\nu_{m_2\mu})^2 + (\nu_{m_1\mu}\nu_{m_2\nu})^2]$$
$$+ (\nu_{m_2\nu}\nu_{m_2\nu} - \nu_{m_1\nu}\nu_{m_1\nu}) Q_{\mu} + (\nu_{m_2\mu}\nu_{m_2\mu} - \nu_{m_1\mu}\nu_{m_1\mu}) Q_{\nu} \}$$
$$+ \sum_{k>m} 2 C_{Nm} C_{Nk} \{ 2 (\nu_{m_1\nu}\nu_{m_2\nu}\nu_{k_1\mu}\nu_{k_2\mu} +$$
$$\nu_{m_1\mu}\nu_{m_2\mu}\nu_{k_1\nu}\nu_{k_2\nu}) - (\nu_{m_1\nu}\nu_{m_2\mu}\nu_{k_1\nu}\nu_{k_2\mu} +$$
$$\nu_{m_1\mu}\nu_{m_2\nu}\nu_{k_1\mu}\nu_{k_2\nu}) \}$$

and the difference density term, $\{ \nu_{m2\nu}\nu_{m2\mu} - \nu_{m1\nu}\nu_{m1\mu} \}$, is revealed in this expression as well. This dependence of the coefficients of the resonance and off-diagonal Coulomb integrals on difference density is particularly important in terms of bond length changes on excitation. These coefficients are also the vehicle which make possible the QCFF parameterization in terms of a single set of empirical integrals for all the electronic states of a molecule: all energy changes are expressed through the set of the coefficients, which represent effective bond order changes for excitation.

The advantage of this approach is that it does serve to isolate the contributions from the various integrals to the total vertical excitation energy. In fact, this form of the energy is motivated by analogy with the familiar energy expressions which result from Hartree-Fock theory in which the total energy is written in terms of the core energy and the total electron repulsion energy. On the other hand, however, the coefficients in the above expression are not simply bond order matrix elements. For this reason, as noted by Warshel (35), first derivatives of the excitation energy computed with this expression are not exact if the coefficients are regarded as constants. In fact, these coefficients are slowly varying functions of the coordinates, and do not possess the exactness of the SCF bond orders, as evidenced by their forms presented above.

Franck-Condon Factors and Vibronic Bandshapes

Within the Born-Oppenheimer approximation the transition dipole between two vibronic states may be expressed

$$\int\int \psi'^{*}(\mathbf{x};\mathbf{q})\chi'^{*}(\mathbf{q})\,\mu\,\psi''(\mathbf{x};\mathbf{q})\chi''(\mathbf{q})\,d\mathbf{x}\,d\mathbf{q}$$

which represents an integral over both electronic and nuclear coordinates. The time required for an electronic transition between vibronic states is fast relative to typical vibrational frequencies, which means that to a very good approximation the nuclei are stationary during the course of the electronic transition. Thus, in terms of the familiar Born-Oppenheimer potential energy surfaces, transitions between surfaces occur with fixed nuclear coordinates. This approximation is known as the Franck-Condon principle. Although this approximation of vertical electronic transtions arises from essentially the same assumption which defines the Born-Oppenheimer adiabatic approximation -- i.e. a separation of time scales for electronic and nuclear motions -- a distinction should be pointed out. The Born-Oppenheimer approximation, on the one hand, is an approximation regarding the form of the total molecular wavefunction. The Franck-Condon principle, on the other, is an approximation involving the nature of an electronic transition.

We now consider how to evaluate the above integral within the Born-Oppenheimer approximation. If we express the dipole operator as a sum of contributions from electrons and nuclei and take advantage of the separation in electronic and nuclear degrees of freedom, we obtain

$$\int\int \psi'^{*}(\mathbf{x};\mathbf{q})\chi'^{*}(\mathbf{q})\,\{\mu_e+\mu_n\}\,\psi''(\mathbf{x};\mathbf{q})\chi''(\mathbf{q})\,d\mathbf{x}\,d\mathbf{q}$$

$$= \int \psi'^{*}\psi''\,d\mathbf{x}\int \chi'^{*}\mu_n\chi''\,d\mathbf{q} + \int \chi'^{*}\chi''\,d\mathbf{q}\int \psi'^{*}\mu_e\psi''\,d\mathbf{x}$$

Owing to the fact that the electronic states are orthonormal the first term vanishes and the integral collapses to

$$\int \chi'^{*}\chi'' \, dq \int \psi'^{*}\mu_e\psi'' \, dx$$

If we define the electronic transition moment as

$$M_e \equiv \int \psi'^{*}\mu_e\psi'' \, dx$$

the integral may now be written

$$M_e \int \chi'^{*}\chi'' \, dq$$

which is a product of the electronic transition moment and a vibrational overlap integral, i.e. the overlap between vibrational wavefunctions in different electronic states. The square of this overlap integral is known as a Franck-Condon factor.

The Franck-Condon factors determine quantitatively the distribution of intensity for individual vibronic transitions. Note that since no assumptions have been made regarding the relative energies of the different states involved in the transitions the Franck-Condon factors so derived are applicable to both excitation (absorption) and emission (fluorescence) processes. In fact, the general validity of the derivation includes multi-photon excitation and emission processes, as well as non-radiative processes. It is also worth noting that since the vibrational wavefunctions involved in the Franck-Condon integral are time-independent (i.e. stationary states) the FC factors are also time-independent. Physically, the FC factors represent time-independent state-to-state transition probabilities and thus determine the vibronic spectrum.

Generally, we are only interested in the relative transition probabilities for a particular experiment. In this case, we need not evaluate the electronic transition

moment prefactors, and concentrate on evaluating only the Franck-Condon integrals. Of course, the FC integrals do not contain any information about the strength of electronic transitions, but from the approximations which lead to the final form of the integral we are free to evaluate these quantities separately.

We are interested in the explicit evaluation of the above Franck-Condon integrals, which requires knowledge of the vibrational wavefunctions for the electronic states involved in the transition. If we adopt a normal coordinate description (harmonic approximation) of the vibrations we simply expand the vibrational wavefunctions as products of (3N-6) harmonic oscillator wavefunctions and evaluate a (3N-6)-fold integral. Of course, the normal coordinate treatment greatly simplifies this multidimensional integral in that the coordinates are separable. If all normal coordinates are the same in the ground and excited state (except for changes in the equilibrium position), all that is required is to evaluate a set of (3N-6) individual integrals, one in each normal coordinate, and then form the product to obtain the total integral. The square of this integral will be the Franck-Condon factor.

In fact, we can reduce the work even further if we realize that each of the (3N-6) integrals involved are simply overlap integrals between two harmonic oscillator wavefunctions which are displaced with respect to each other. Therefore, the general analytic form of all (3N-6) integrals will be identical and we really need to evaluate only one integral in order to formally solve the problem in terms of normal coordinates. The result for this integral is standard (50) and may be written in terms of the Laguerre Polynomials as

$$\left\langle f, n \mid i, n' \right\rangle = \exp\{-s^2/4\}\left(\frac{s}{\sqrt{2}} \right)^{n-n'} \frac{n'!}{n!} \frac{L_n^{n-n'}(s^2/4)}{n!}$$

where $s = \Delta Q/Q^{(0)}$ is defined as the dimensionless displacment in normal coordinate space, $Q^{(0)}$ is the classical turning point for the normal mode. The number of

vibrational quanta in the initial (i) and final (f) states are denoted by n' and n (unprimed), respectively.

If we consider transitions from a vibrationless initial state, the Franck-Condon factors obtained from the square of the above integral for all n'=0 are found to be

$$f_{0n} = \langle f, n \mid i, 0 \rangle^2 = \frac{\lambda^n}{n!} e^{-\lambda} \qquad \lambda = \frac{1}{2} s^2$$

which is seen to be of the form of a Poisson distribution. Despite the seemingly great number of approximations introduced in deriving this rather amazing result, it is worth noting that this expression is valid for transitions originating from vibrationless levels of electronic states and is accurate to the extent that the harmonic, Born-Oppenheimer, and Franck-Condon approximations are accurate. Further, a great number of general features of vibronic spectra are contained in this beautifully simple equation, and it provides an immediately available "back-of-the-envelope" method for calculating Franck-Condon factors. Alternatively, the expression may be combined with FC factors from experiments to extract potential surface displacements.

Several features of this expression are worth noting. First, if we take the derivative with respect to λ and set this equal to zero to find the maximum in the intensity distribution, we find that this occurs for $n = \lambda$. Alternatively, we can obtain this result on physical grounds by arguing that transitions with the highest probability will originate at the expectation value for the coordinate which is, of course, the center of the harmonic well. In the final state, this configuration will define a classical turning point, so that the final state energy is approximately

$n'\omega \sim (1/2)\, k\, (\Delta Q)^2$

If we rearrange this equation to solve for n', we obtain the same result as before.

Thus we know simply by computing the parameter λ the approximate location of the

band maximum. Although we have simply regarded λ as a convenient mathematic parameter, there is much pleasure to be had in noting that since

$$\lambda = (1/2)\, S^2 = (1/2)\, (\Delta Q / Q^{(0)})^2 = (1/2)\, \{ \Delta Q / \omega^{1/2} \}^2$$

this parameter is essentially the "spring energy" in units of ω which is caused by the sudden change in potential due to the electronic transition. From the above expression we also observe that this spring energy is directly related to the square of the relative displacement of the two potential surfaces involved in the transition. The beauty of this model is that it allows us to predict vibronic spectra in a very simple way or, alternatively, to interpret vibrational progressions in experimental spectra and derive information about the potential surfaces involved in the transitions.

Duschinsky Rotation of Normal Coordinates

The previous model for Franck-Condon factors contains a hidden assumption which needs to be addressed. Thus far, we have invoked a series of approximations which are well-motivated on physical grounds and greatly simplify the problem of calculating the Franck-Condon integrals. To recap, these principal approximations are as follow;

(i) The Born-Oppenheimer approximation for the molecular wavefunction.

(ii) The Franck-Condon Principle for the nature of the electronic transition.

(iii) The harmonic approximation for the vibrational motion (i.e. normal coordinates).

Despite having identified, isolated, and characterized all these approximations, it has also been assumed, implicitly, that the (3N-6) normal coordinates for the different potential surfaces are identical except for displacement of the potential minima. However, the forces responsible for the vibrations are a direct result of the electronic structure which determines the potential energy surfaces on which the nuclear motion takes place. Having recognized this, along with the obvious fact that the electronic structure of excited states is different from that of the ground state, it follows

immediately that the normal coordinates for an excited electronic state can be different from the normal coordinates of the ground state.

The first and most obvious way in which two normal coordinates may differ is in terms of the relative displacement of the potential surfaces, which arises from the difference in equilibrium molecular geometries between different electronic states. This has already been incorporated into the previous model for Franck-Condon factors which results in a Poisson-distribution expression for the intensities.

In addition to this, the vibrational frequencies can be different between states. This phenomenon, termed frequency distortion, results in harmonic potential wells which differ in width in electronically excited states. Nonetheless, frequency distortion can be an important contribution to the observed intensity for a given mode. In fact, for non-totally symmetric vibrations, there is no displacement in normal coordinate space, and these modes gain intensity from frequency changes. It can be shown (51,52), for example, that overtone and combination transitions are the only vibronically active transitions for non-totally symmetric modes, i.e. the overlap integrals for fundamental transitions vanish. Therefore, to correctly predict the vibronic spectrum we must incorporate frequency distortion into the formalism.

Nonetheless, even if a particular mode -- whether belonging to totally- or non-totally symmetric irreducible representation -- has the same frequency in two different electronic states, the vibration can still "look" different. That is, the relative displacements of the atoms may be sufficiently different in the two states that the general appearance of the mode is changed. In fact, this difference in appearance of a particular vibration is a consequence of the different electronic structure of the states, as outlined above.

Experimentally, this difference in vibrational modes can manifest itself as a breakdown of the mirror-image symmetry relationship of the excitation and emission

spectra associated with the same transition. By this it is meant that transtions which appear prominently in an absorption spectrum may appear weaker in the emission spectrum (and vice-versa) or in extreme cases have no counterparts whatsoever in emission. In the absence of non-radiative processes, this lack of mirror-image symmetry for the two experiments is attributed to vibrational mode-mixing. In fact, this mode-mixing is a ficticious effect in the sense that there is really a one-to-one correspondence between (albeit different) vibrations on the two electronic surfaces and the final state mode is truely a single mode. In a group theoretic sense, if there is no change in point group for the molecule in undergoing an electronic transition, each vibration still defines an irreducible representation of the point group and the total representation of the vibrations is conserved.

Although the final state mode for a transition is in reality a single mode, it is useful to think of it in terms of a basis of initial state modes. This is the essential difference between the problem of calculating Franck-Condon factors for diatomics (where there is exactly one vibration) and calculating them for polyatomic molecules (for which there are 3N-6 vibrations). We therefore expand the final state modes (Q') in a basis of initial state modes (Q")

$$\mathbf{Q'} = \mathbf{S}\,\mathbf{Q''} + \Delta\mathbf{Q'}$$

where $\mathbf{S} = \mathbf{Q'^{T}Q}$ and $\Delta\mathbf{Q'}$ is the vector of displacements in normal coordinate space. This transformation was first proposed by Duschinsky (41) and the **S** matrix so defined is known as the Duschinsky rotation matrix. There is an exact isomorphism between the Duschinsky transformation and the parameterization of coordinate system rotations, and for this reason the mode-mixing phenomenon is often referred to as normal coordinate rotation or the Duschinsky rotation effect.

From a practical viewpoint we can take stock in the fact that the overall quality of a normal mode calculation for a ground state will always be better than one for an excited

state and so we can adopt a literal interpretation of the Duschinsky transformation and expand the excited state normal coordinates in a basis of ground state coordinates. We thus require a method for the calculation of Franck-Condon factors which takes into account the effects of displacement, frequency distortion, and Duschinsky rotation.

The Doktorov-Malkin-Man'ko (DMM) Method

Several methods have been proposed for the calculation of polyatomic Franck-Condon factors, and each method has certain advantages and limitations depending upon the problem of interest. Indeed, many of the earliest methods (53-57) developed were computationally limited by storage space and computing speed and/or by the fact that some of these methods (54,55) preceeded the advent of modern electronic computers. As a result, the principal differences that exist among these methods in terms of implementation are more a matter of the level of approximation involved than any formal distinction.

Today, however, we have several orders of magnitude more computing power than any of the early methods may have anticipated. As a result, much of the more recently developed formalism for calculation of Franck-Condon factors avoids altogether any approximations beyond the standard assumption of harmonic potentials, permitting calculation of FC factors which are exact within the harmonic approximation.

In particular, Sharp and Rosenstock (53) have generalized the generating functions of Hutchinson (54) to triatomics to derive algebraic expressions for relative transition probabilities for transitions originating from the ground vibrationless level. Cederbaum and Domcke (58) have derived recursion relations for FC factors by defining a homogeneous, linear transformation of boson operators between distorted oscillators and introducing a unitary transformation to account for displacement. In a series of papers, Kupka, et al. (59-62) derived a multidimensional intramolecular distribution

(ID) function which has the form of the square of the vibrational overlap integrals convoluted with a Lorentzian to obtain directly the spectral bandshape. Faulkner and Richardson (63) (FR) define separate coordinate transformations for both ground and excited state modes which effectively eliminates Duschinsky rotation from the FC integral. In a second method (63), FR propose an alternative approach based on canonical transformation of the Hamiltonian and performing a perturbation expansion in terms of ground state (unperturbed) wavefunctions to produce FC integrals as expansions of ground state overlap integrals. Roche (64) has derived recursion relations for polyatomic FC factors using a general linear transformation of boson operators which essentially combines the separate transformations of Cederbaum and Domcke (58) into a single inhomogeneous transformation. In a remarkable and elegant piece of work, Yan and Mukamel (65) circumvented altogether the problem of computing individual FC factors for vibronic lines and derived bandshapes in terms of Fourier transforms of dipole correlation functions within a Green function formalism. Their eigenstate-free Green function calculation incorporates displacements, frequency shifts, and Duschinsky rotation and is exact within the harmonic and Condon approximations. Finally, Doktorov, Malkin, and Man'ko (39,40) (DMM) have derived recursion relation for FC integrals by means of a coherent-state formalism. The overlap integrals are shown to be matrix elements of an operator belonging to the Lie group Sp(2N,R)*H(N), which is a dynamical symmetry group of the vibrational Hamiltonian.

Roche (64) has pointed out that a disadvantage of the method of DMM is that it "...involves Lie groups and coherent states which are not familiar to the average physical chemist". While it is true that Lie groups are quite foreign to physical chemists, coherent states are quite accessible from a conceptual perspective and can be argued to be well within the territory of physical chemistry (66,67). Whatever the case, the great advantage of the DMM recursion relations for polyatmic FC factors is in the fact that

they are exact within the harmonic approximation and incorporate the effects of displacement, frequency distortion, and Duschinsky rotation. Further, the DMM method is applicable to calculation of FC factors for both excitation and emission processes and the recursion relations are not subject to the restriction of transitions from vibrationless initial states. Lastly, the DMM method is reasonably straightforward to implement in terms of the closed-form analytic recursion formulae. Thus, despite the potentially unfamiliar formalism in which these expressions are derived, they are sufficiently general and accurate to warrant their use.

The only proponents of the DMM method, to date, have been Gruner and Brumer (68,70), who developed an efficient algorithm for evaluation of the DMM recursion relations in terms of a binary tree. Their algorithm was implemented in the PL/1 language and used as a test case the emission from the vibrationless level of the first excited singlet state of trans-Stilbene (72 modes). They included 1.3×10^5 states in the calculation, requiring 8-10 Mbyte of virtual storage, 20 Mbyte of scratch disk space, and 10-12 min CPU on an IBM 4361, thus requiring approximately 0.005 sec CPU per Franck-Condon factor. In a later piece of work (69), they coupled the DMM FC algorithm with the QCFF semiempirical method (35) to compute dispersed fluorescence spectra in alkylbenzenes in efforts to interpret features of intramolecular vibrational redistribution (IVR) experiments (71-74).

We have implemented the DMM recursion relations in VAX VMS fortran (77) to compute absorption and fluorescence spectra from vibrationless levels. To accomplish this, we have adopted directly the auxillary matrices and vectors derived by Doktorov, et al. (39,40). We note here that there is a minor discrepancy between the equations derived in the original papers of Doktorov, et al., and those presented Gruner and Brumer (68,70), due to trivial errata which exist in both works. The correct expressions are presented in what follows.

For convenience, we here adopt the convention of unprimed quantities for the final state, and double primes to indicate initial state information. The final state vibrational eigenvectors (normal modes) are expressed in a basis of initial state eigenvectors through the Duschinsky transformation in the usual manner

$$\mathbf{Q} = \mathbf{S}\mathbf{Q}'' + \Delta\mathbf{Q}$$

where the Duschinsky rotation matrix is prescribed by $\mathbf{S} = \mathbf{L}^{\mathbf{T}}\mathbf{L}''$ and the displacements are defined in terms of the final state eigenvector components

$$\Delta\mathbf{Q} = \mathbf{L}^{\mathbf{T}}\,\mathbf{m}^{1/2}\,(\mathbf{r} - \mathbf{r}'')$$

which expresses the projection of the final state modes on the difference geometry vector between the two states. In this expression, **m** represents the diagonal matrix of 3n atomic masses. We define the following auxillary matrices and vectors in terms of the normal mode basis: a diagonal matrix of the root-frequencies for the 3n normal modes (i.e. the six trivial modes with zero frequency are included);

$$\lambda_{\omega} = \begin{pmatrix} \omega_1^{1/2} & & & \\ & \omega_2^{1/2} & 0 & \\ & & \ddots & \\ & 0 & & \omega_{3n}^{1/2} \end{pmatrix}$$

a matrix which accounts for the frequency reordering associated with the Duschinsky mixing;

$$\mathbf{J} = \lambda_{\omega}\mathbf{S}\,(\lambda_{\omega''})^{-1}$$

and the auxillary matrices which describe the interplay between Duschinsky mixing, and frequency distortion;

$$\mathbf{Z} = (\mathbf{1} + \mathbf{J}^{\mathbf{T}}\mathbf{J})^{-1}, \quad \mathbf{R} = \mathbf{Z}\,\mathbf{J}^{\mathbf{T}}, \quad \mathbf{P} = \mathbf{J}\,\mathbf{Z}\,\mathbf{J}^{\mathbf{T}}$$

and a vector which gives the frequency-weighted normal coordinate displacments;

$$\delta = (2\pi/h)^{1/2}\,\lambda_{\omega}\Delta\mathbf{Q}.$$

In terms of these definitions DMM (39,40) find that the overlap integral for the vibrationless transition (i.e. the origin) is given by

$$\left\langle 0' \mid 0'' \right\rangle = 2^{N/2} \prod_{i=1}^{N} \left(\frac{\omega_i}{\omega_i''}\right)^{1/4} [\det \mathbf{Z}]^{1/2} \exp\{ -\frac{1}{2}\, \delta\, (\, 1 - \mathbf{P}\,)\, \delta \}$$

and the square of this integral is, of course, the Franck-Condon factor for the origin.

The overlap integrals for both absorption and emission processes are then given by the DMM recursion relations. We adopt here an occupation number formalism for the vibrational wavefunctions, in which the number of quanta distributed in each vibrational mode is represented by the quantum numbers, v_k. The general relations for absorption are then given by

$$\begin{aligned}\langle v' \mid v_1,\ldots, v_i+1,\ldots, v_N \rangle = 2\sum_{k=1}^{N} \mathbf{R}_{ik} \left(\frac{v'_i}{v_i+1}\right)^{1/2} \langle v'_1,\ldots, v'_k-1,\ldots, v'_N \mid v_1,\ldots, v_i,\ldots, v_N \rangle \\ + \sum_{j=1}^{N} (2\mathbf{Z}-1)_{ij} \left(\frac{v_j}{v_i+1}\right)^{1/2} \langle v' \mid v_1,\cdots, v_j - 1,\cdots, v_N \rangle \\ - (\mathbf{R}\delta)_i \left(\frac{2}{v_i+1}\right)^{1/2} \langle v' \mid v_1,\cdots, v_i,\cdots, v_N \rangle\end{aligned}$$

and for emission

$$\begin{aligned}\langle v'_1,\ldots, v'_k+1,\ldots, v'_N \mid v \rangle = 2\sum_{i=1}^{N} \mathbf{R}_{ki} \left(\frac{v_i}{v'_k+1}\right)^{1/2} \langle v'_1,\ldots, v'_k,\ldots, v'_N \mid v_1,\ldots, v_i-1,\ldots, v_N \rangle \\ + \sum_{m=1}^{N} (2\mathbf{P}-1)_{km} \left(\frac{v'_m}{v'_k+1}\right)^{1/2} \langle v'_1,\cdots, v'_m - 1,\cdots, v'_N \mid v \rangle \\ - [\, (1-\mathbf{P})\, \delta\,]_k \left(\frac{2}{v'_k+1}\right)^{1/2} \langle v'_1,\cdots, v'_k,\cdots, v'_N \mid v \rangle\end{aligned}$$

The squared overlap integrals are the usual Franck-Condon factors.

We note here that a simplification occurs for cold spectra (as is the case for jet

cooled molecules). If all normal modes in the initial state have zero quanta, i.e. the atoms undergo only zero-point motions, the second term in the absorption equation will vanish for all quantum numbers zero. Similarly, in the emission expression, the same simplification occurs, and we have for the "jet-cooled" versions of the recursion relations

$$\langle \nu' \mid \nu_1,\ldots, \nu_i+1,\ldots, \nu_N \rangle = \sum_{j=1}^{N} (2\mathbf{Z}\text{-}1)_{ij} \left(\frac{\nu_j}{\nu_i+1}\right)^{1/2} \langle \nu' \mid \nu_1,\cdots, \nu_j - 1,\cdots, \nu_N \rangle$$

$$- (\mathbf{R}\delta)_i \left(\frac{2}{\nu_i+1}\right)^{1/2} \langle \nu' \mid \nu_1,\cdots, \nu_i,\cdots, \nu_N \rangle$$

for absorption, and

$$\langle \nu'_1,\ldots, \nu'_k+1,\ldots, \nu'_N \mid \nu \rangle = \sum_{m=1}^{N} (2\mathbf{P}\text{-}1)_{km} \left(\frac{\nu'_m}{\nu'_k+1}\right)^{1/2} \langle \nu'_1,\cdots, \nu'_m - 1,\cdots, \nu'_N \mid \nu \rangle$$

$$- [\,(1\text{-}\mathbf{P})\,\delta\,]_k \left(\frac{2}{\nu'_k+1}\right)^{1/2} \langle \nu'_1,\cdots, \nu'_k,\cdots, \nu'_N \mid \nu \rangle$$

for emission. This reduces the computational labor involved in the integral evaluation to some degree and provides expressions which are appropriate to the calculation of zero-Kelvin "stick" spectra to represent experimental jet-cooled spectra.

The recursion relations are not nearly as complicated as they appear. For example, the expression for a fundamental absorption (one quantum of vibration in one mode) obtained from the jet-cooled form is simply

$$\langle 0' \mid 1_i \rangle = - (\mathbf{R}\delta)_i \sqrt{2}\, \langle 0' \mid 0 \rangle$$

which is seen to be of the form of a vector pre-factor times the origin transition integral. Expressions for overtones and multi-mode combinations are only slightly more complicated. Details of the calculation of Franck-Condon factors from the jet-cooled recursion relations are contained in Chapter Three.

CHAPTER 3

COMPUTATIONAL METHODS

The QCFFBOZE Suite

The Quantum Consistent Force Field (QCFF) program and associated routines which were developed in this work comprise a library of codes which shall be referred to throughout as the QCFFBOZE Suite. Briefly, the Suite is a seamless set of programs which can be maintained in an individual file directory and utilized for semiempirical quantum chemical calculations, calculation of spectroscopic information (molecular geometries, potential surface displacements, excitation energies, oscillator strengths), spectral bandshape calculations (absorption, fluorescence) using various models, and potential energy surfaces. The nucleus of the Suite is a modified version of the QCFF program (to be described below), which supplies the input parameters required for bandshape calculations. All routines were written in VAX VMS fortran (77). The codes can be executed in batch or interactive mode. In addition, a collection of DCL command (.COM) files were developed which control input-output streams for calculations on specific molecules.

Operating System Information

We obtained the QCFF program from the Quantum Chemistry Program Exchange (75), Indiana University (QCPE 534: VAX version) on magnetic tape. The tape was logged into the Montana State University Computing System as MSU #U2104 and compiled without errors.

As a preliminary test of the code, the sample input for the ground state of benzene was run and compared with the sample results in the QCPE 534 manual, which were

obtained by D.E. Bugay and W.R. Leenstra of the University of Vermont. The initial results were in agreement with the test case supplied by Bugay and Leenstra, whose results were obtained on a VAX 8600 system, fortran compiler version 4.5-219.

All the computational results obtained in this work were run on the Montana State University Computing and Network Services VAX computers in VMS fortran. Most calculations were run on the TREX node, a VAX 6520. Other calculations were run on the Montana State University Department of Chemistry microVAX Earth nodes, which were later converted to a VAX 4000 system (May, 1993). The only notable differences between machines were in overall execution (CPU) times, with the VAX 6520 being a factor of 10-12 times faster than the microVAX, and the VAX 4000 being approximately 3-4 times faster than the microVAX. (Detailed execution times for various calculations are contained in Appendix 1.)

On a practical note, it is worth pointing out that these calculations were not expensive in terms of CPU time. Typical approximate VAX 6520 CPU times for indole (N=42 modes) were ca. 60 sec. per electronic state, ca. 30 sec. for peripheral routines in the QCFFBOZE Suite, and ca. 60 sec. for computation of Franck-Condon factors. Thus, a typical 0K stick spectrum, which requires running the two electronic states involved, requires approximately 240 sec. (4 min.) CPU. The "rate-limiting-step" in any bandshape calculation is in the final application of Gaussian broadening to the FC factors; broadening factors on the order of 100 cm^{-1} required ca. 200 sec. CPU to compute. In addition, potential energy surface calculations are reasonably efficient, requiring ca. 1 sec. per point on the surface. All times reported here are approximate; actual CPU times are, of course, molecule dependent, scaling as the number of vibrational modes, number of FC factors specified in a calculation, maximum energy specified, etc. (cf. Appendix 1).

Modifications to QCFF: QCFFBOZE

We have suitably modified the canonical QCFF routine of Warshel and Levitt for the specific problem of performing calculations of spectral bandshapes and potential energy surfaces. The final form of the modified code is referred to as QCFFBOZE.

The first set of modifications involved specifying output channels to write QCFF results to disk which are computed but not written in the standard QCPE program. These modifications, although somewhat tedious, were straightforward to perform and thus do not require extensive discussion. These modifications are well documented within the QCFFBOZE code and can be located by using the "FIND" function of the TPU editor and typing "boze" at the prompt.

Another minor but important modification was the replacement of the standard QCFF matrix diagonalization subroutine (EIGEN) with the EISPACK (76) diagonalization codes. The EISPACK fortran subroutines RSP, EPSETA, TRED3, TQLRAT, TQL2, and TREAK3 were adopted with two modifications to perform all required diagonalization procedures within QCFF. The first modification, which is not of necessity, was to remove the implicit double precision statement from these six subroutines. Since QCFF is written in single precision (real*4), this modification was performed to avoid any possible problems of compatibility. The second modification was to remove the statement "include 'sizes' " from routine RSP.

In order to complete the union of QCFF diagonalization tasks to EISPACK, it was necessary to write a short subroutine (MATPACK) to pack a row-wise vector from the lower triangle of real, symmetric matrices, which is the required format as specified in the routine RSP. The QCFF routine EIGEN was designed to perform diagonalization on vectors packed from the upper diagonal. In addition, it was necessary to create a short subroutine (WRITETEN) to write eigenvalue-eigenvector information files to Channel 10, as this task was previously handled within the EIGEN routine.

In addition to these modifications, a considerable amount of documentation was added within the program (i.e. QCFFBOZE.FOR), based on the original QCFF papers of Warshel, et al. (35-37), to make the code more readable. An intact version, free from any modifications, of the canonical QCPE #534 version was maintained as QCFF0.FOR. It is worth noting that none of the QCFF force field and molecular parameters (which are stored as block data in the code) were modified.

All of the modifications described above are, in essence, trivial in that they either (a) required no writing of additional fortran code, or (b) required minimal modifications of existing code or incorporation of canned routines (EISPACK). The distinction being that these modifications did not in any way require either new method-development or modifications to the existing formalism contained in the QCFF program.

The two significant modifications which do not meet the above criteria were the development of a difference density matrix scaling procedure and a routine to compute potential energy surfaces. These modifications are sufficiently involved and original to warrant discussion under separate headings.

Difference-Density Scaling Procedure

In our preliminary work with the QCFF routine, benzene was adopted as the test-case molecule for most calculations. The reasons for choosing benzene are multi-fold. First, benzene is relatively simple (compared to indole) in many respects. Second, the spectroscopy of the first excited singlet state of benzene is very well characterized in terms of a comprehensive vibrational assignment, and the geometric distortion involved in the excitation is reasonably simple. In addition, benzene defines a paradigm for theoretical studies of pi-electron systems, particularly the polyacenes, and is one of the more well-studied molecules from a theoretical perspective. Further, and particularly relevant to this work, the QCFF package is based on a semiempirical parameterization

which incorporates molecular properties for benzene to a great extent. In particular, the empirical form for the resonance integral in QCFF is parameterized specifically in terms of benzene properties. All of these factors combine to make benzene a very good candidate for testing semiempirical predictions.

On the other hand, benzene is not simple in many respects. It possesses thirty (30) normal modes of vibration, with 20 unique frequencies (due to degenerate irreducible representations). Unfortunately, not all the frequencies are established experimentally due to the complexity of selection rules in a molecule of such high symmetry, and certain ambiguities persist in the force field for these modes as a result. In addition, there exist several subtle vibronic-coupling mechanisms in benzene which cannot be predicted without incorporating Herzberg-Teller (HT) expansion of the transition dipole into the calculation of the oscillator strength of a transition. The main issue in the vibronic coupling mechanisms is the ability of certain vibrations to induce false origins which permit violation of rigorous selection rules and lead to complex features in electronic spectra. Further challenges to theory lie in the "Channel Three" problem, which is the term given to the rapid onset of radiationless transitions ca. 3200 cm^{-1} above the origin of the first excited singlet.

Most, if not all, of these problems can be avoided altogether, simply by acknowledging the experimental results. In particular, in the absorption spectrum for the first excited singlet state, the oscillator strength computed within the Born-Oppenheimer approximation (i.e. without HT terms, with a hexagonal geometry) will be exactly zero. Nonetheless, Franck-Condon factors computed at the same level of approximation will show a progression in the a(1g) vibrational mode, with an intensity of zero when weighted by oscillator strength. Of course, to predict the correct absolute intensities requires taking into account the nuclear-coordinate dependence of the transition dipole. It is only when we ask questions regarding the absolute intensities that we need to invoke

vibronic-coupling to obtain the full answer. The point is that we do not need to perform a complete vibronic-coupling calculations via HT expansion in order to predict the correct trend in relative intensities from FC factors.

For benzene, the first excited electronic state L_b ($^1B_{2u}$) is a singlet which is essentially HOMO-->LUMO in character (as are the L_a ($^1B_{1u}$) and $B_{a,b}$ ($^1E_{1u}$) excited states). In the Platt notation (1) for aromatic hydrocarbons, this state is labeled L_b. The transition density topology (77), or transition bond orders, for this state reveal that the changes in electron density with respect to the ground state consist predominantly of a symmetric decrease in electron density between carbon atoms. This decrease in electron density results in weaker bonds, and this is reflected in an increase in carbon-carbon bond lengths in the excited state. Thus, the major geometry change upon excitation is a uniform increase of the six-carbon ring.

In fact, this correlation between difference density matrices and bond lengths is a general phenomenon and the fundamental link between the quantum mechanical wavefunction and molecular geometries. The bond lengths are "tuned" according to the electron density defining the bonds in a particular electronic state, and the changes in bond lengths are directly related to the difference density.

In the course of this work, we developed a difference density scaling procedure to allow variation of excited state bond lengths in an effort to fit computed spectra and potential energy surfaces to experimental data. The method is motivated in part by existing semiempirical correlations between bond lengths and bond orders for ground states. In particular, Salem (47) provides a set of linear bond order - bond length curves based on fitting carbon-carbon bond lengths in ethylene, benzene, and graphite. Coulson (78) developed a non-linear expression for conjugated systems which provides bond orders in terms of experimental bond lengths.

One problem is that these correlations, which are obtained by fitting experimental bond length data, are applicable only to ground states. As pointed out by Berry, et al. (78), "The difficulty in the present context is in the level of subtlety required to isolate a connection between bond length or bond order and aromatic character." On the other hand, however, the relationship between bond order and bond length for ground states can be obtained by doing SCF-LCAO-MO calculations, relegating semiemprical correlations to the status of a convenient tool for approximations which play a secondary role in light of the actual calculations.

The central issue raised by Berry, et al. (78), is that the semiempirical correlations are vulnerable to the problem of transferability between molecules. A reasonable approach, then, would be to develop correlations on molecule-to-molecule basis, in which a correlation is constructed for each molecule. Any generality or transferability that might exist could be revealed by such an approach, in which there is a solid emphasis on doing MO calculations for individual molecules. In this approach, however, the results of the calculations themselves are of more value than an extrapolation to different molecules.

The situation for excited states is more difficult. To date, our knowledge of excited state electronic structure from both experimental and theoretical perspectives has lagged behind that of ground states. In some sense, a satisfactory and consistent theory of electronic excited states has yet to be developed. To that end, reliable semiempirical correlations for excited states are not yet available.

If we consider the underlying assumption of bond lengths which vary smoothly with electron density (i.e. bond orders), a reasonable approach is to construct a relationship between changes in bond length and the associated changes in electron density (i.e. difference bond orders). In fact, this approach was adopted by Miller and Murrell (79) in their calculations of FC factors for the polyacenes. In their approach, the bond order

change on excitation for the benzene (260 nm band) was related to the bond length change measured by Dunn, et al. (106), and this correlation was extended to naphthalene, anthracene, tetracene, and pentacene, to provide displacement vectors for evaluation of FC factors.

Miller and Murrell (79) point out that this extension of the idea of semiempirical correlations to excited states may not be accurate due to the fact that an electron in an anti-bonding orbital may have a greater effect on bond length than an electron in an bonding orbital. This is true, to some extent, in that comparison of bond order changes calculated in the framework of Hückel theory with calculations including configuration interaction suggest that the Hückel bond orders will slightly underestimate bond length changes. This is only a problem, of course, if the correlation is developed on the basis of Hückel MO bond orders (as Miller and Murrell go on to do). Inclusion of configuration interaction (as is the case with QCFF) will improve the situation.

We have developed a semiempirical scaling procedure based on bond orders calculated from QCFF which includes CI singles excitations. This correlation, which is essentially an extension of the method proposed by Miller and Murrell, is based on fitting the correct change in C-C bond length in benzene upon excitation. The ground state geometry of benzene has been accurately determined through various high-resolution studies (80,81). The ground state carbon-carbon bond length is predicted to be 1.397 Å (±0.0004 Å), which represents an upper bound on the error for all the experimental methods.

The geometry in the first excited electronic state is not nearly as well characterized. In high-resolution spectroscopic studies, the common approach is to fit the change in geometry for excitation (fluorescence) in accordance with the observed $6_0{}^1 1_0{}^n$ ($6_1{}^0 1_n{}^0$) progression. Parmenter, et al. (80,81) performed single vibronic level fluorescence (SVLF) experiments on benzene vapor and fit the relative intensity of the $6_1{}^0 1_n{}^0$

progression for n=(0-3) to obtain a C-C bond length change of 0.034 Å (±0.001 Å), corresponding to an excited state C-C bond length of 1.431 Å (ground state 1.397 Å). Alternatively, Callomon, et al. (107) performed high-resolution spectroscopy which allowed analysis of rotational band contours and fitting of the excited state rotational constant (B) to determine a C-C bond length change of 0.038 Å, corresponding to an excited state C-C bond length of 1.435 Å. Subsequent refinement (108) of the rotational band analysis resulted in a C-C bond length change of 0.034 Å, bringing the values from SVLF and band contours into agreement.

More recently, Hiraya and Shobatake (HS) (82) performed direct absorption studies of jet-cooled benzene which included the 130-260 nm region. They determined the absolute absorption intensities of the $6_0^1 1_0^n$ (n=0-5) progression for the 260 nm band but did not fit the geometry change. However, HS point out that their results are in good agreement with the relative intensities calculated by Fischer, et al. (86), which correspond to a change in C-C bond length of 0.034 Å, which is in agreement with the value obtained from SVLF by Parmenter et al..

One difficulty in the present context is that all of the various fitting procedures involve fitting the ring-breathing mode Franck-Condon progression in terms of a single parameter. The jet-cooled absorption spectra of Hiraya and Shobatake are perhaps the best data available for isolated benzene, and so the FC progression intensities they obtained are the appropriate experimental values for comparison with FC factors computed at zero Kelvin. Still, the problem remains that the fitting procedure involves only a single parameter (the change in C-C bond length), and so there will certainly be some compromise in the fit of all but one FC factor.

Most fitting procedures are based implicitly on fitting the fundamental (for totally symmetric modes, as is the case here) or, in the present case, the ratio of the fundamental to the origin. It is possible, then, to adjust the bond length change or, alternatively, the

normal coordinate displacement, to fit the exact ratio which is measured. The fact admits itself, then, that fitting computed spectral bandshapes (and, to a greater extent, assigning the experimental spectrum) is an iterative process (70,87).

In terms of the calculation of spectral bandshapes, the principal objective is to fit the vibronic progressions with sufficient accuracy to capture the features of the experimental spectrum. The standard approach is to compute the frequencies and displacements of the normal modes, evaluate the Franck-Condon factors, and compare the calculated spectrum with the experimental spectrum. The problem then becomes an empirical analysis in which the computed displacements are adjusted to fit a limited set of experimental intensities.

An example of this empirical approach is that of Hemley, et al. (87) in the vibrational analysis of the uv spectrum of the singlet states of styrene. In this work, an extended PPP-CI method (38) which is essentially the QCFF method extended to include CI doubles was used to compute molecular geometries, normal modes, and displacements for calculation of the multidimensional FC factors. The normal coordinate displacements (i.e. for in-plane vibrations) were then adjusted by comparison with the experimental vibrational assignment. The empirically adjusted displacements were then used to recompute the FC factors and thus provide a fitted spectrum.

In a very similar approach, Gruner and Brumer (70) developed an iterative algorithm in which an empirical analysis provides adjusted surface displacements which are then used to correct the equilibrium molecular geometry. Since the FC factors depend on the geometry difference, GB opt to adjust only the excited state geometry. The corrected difference geometry vector is then used to recompute FC factors, and the refined spectrum is again compared with experiment. In practice, however, this procedure is not simply iterative: it involves a trial-and-error component which has its roots in the recursive nature of the Franck-Condon factors and the fact that the FC factors depend on

the square of the displacements. This method takes advantage of the fact that the recursion relation for fundamentals

$$\langle 0' \mid 1_i \rangle = -(\mathbf{R}\delta)_i \sqrt{2} \langle 0' \mid 0 \rangle$$

provides the overlap integral in terms of a vector, $(\mathbf{R}\delta)$. Thus, we can express the intensity of a fundamental line as

$$I_i = \mathbf{A}_i I_{00}$$

where $\mathbf{A}$ is defined for convenience as $\{2(\mathbf{R}\delta)_i^2\}$. The relative intensity is seen to be directly proportional to $\mathbf{A}_i$, and this vector component can be adjusted to reproduce the correct intensity simply by inserting the experimental relative intensity of the fundamental; $\mathbf{A}_i = \{ I_i / I_{00} \}_{exptl.}$

The difficulty arises in fitting lines which depend, through recursion, on the fundamental. Although the above algorithm will provide adjusted fundamentals which are in exact agreement with the experimental values used in the fitting procedure, there is still a sign indeterminacy in the vector $(\mathbf{R}\delta)$ which can compromise the fit of the overtones and combinations which depend on the (adjusted) fundamentals through the recursion relations. This uncertainty in sign for each normal coordinate presents considerable problems for large molecules; for example, for ten displaced modes, there are 1024 possible sign combinations (obtained by summation of binomial coefficients (50)). This presents considerable difficulties in terms of determination of the optimum set of adjusted vectors.

The common thread in the above empirical methods of displacement analysis and bandshape fitting procedures is that the information required for evaluation of FC factors is obtained from a semiempirical calculation, and then this information (frequencies, displacements, geometries) is adjusted by appeal to experiment. This is perfectly acceptable at the level of a fitting procedure, but it must be borne in mind that this fitting

procedure is undertaken due to a flaw in some level of the semiempirical treatment which provides the normal coordinates. A very reasonable line of approach, then, is underscored in the question: Is it possible to correct the normal coordinate displacements at the level of the semiempirical treatment itself?

The answer requires a formulation of the SCF-LCAO-MO+CI calculation such that the dependence on the difference density is explicit. Since the geometry changes on excitation depend sensitively on the difference density, we propose scaling this difference density, i.e. the bond-order matrix elements, to adjust the bond lengths such that the results of the QCFF semiempirical calculation are consistent. We accomplish this by observing that the excitation energy expression for QCFF CI-singles calculation is given by

$$\Delta V_{\pi}^{N}(\mathbf{r}) = \mathbf{C}_N \mathbf{A}(\mathbf{r}) \mathbf{C}_N = \sum_{m} (\mathbf{C}_{Nm})^2 (\mathbf{A}(\mathbf{r}))_{mm} + 2 \sum_{k>m} \mathbf{C}_{Nm}\mathbf{C}_{Nk} (\mathbf{A}(\mathbf{r}))_{mk}$$

in which the diagonal elements may be written

$$\mathbf{A}_{nn} = \left\langle {}^1\psi_{n1\rightarrow n2} \mid H \mid {}^1\psi_{n1\rightarrow n2} \right\rangle - \left\langle {}^1\psi_0 \mid H \mid {}^1\psi_0 \right\rangle$$

$$= \varepsilon_{n2} - \varepsilon_{n1} - \left\langle n_1 n_2 \mid n_1 n_2 \right\rangle + 2 \left\langle n_1 n_2 \mid n_2 n_1 \right\rangle$$

for excitation from MO n_1 to MO n_2. We now recast the SCF orbital energy difference in terms of the Fock matrix elements

$$\varepsilon_{n2} - \varepsilon_{n1} = \sum_{\mu} (\nu_{n_2\mu}^2 - \nu_{n_1\mu}^2) F_{\mu\mu} + 2 \sum_{\nu>\mu} (\nu_{n_2\mu}\nu_{n_2\nu} - \nu_{n_1\mu}\nu_{n_1\nu}) F_{\mu\nu}$$

Finally, we recall the QCFF excitation energy expression which is given in terms of the semiempirical integrals, i.e.,

$$\Delta V_{\pi}^{N}(\mathbf{r}) = \sum_{\mu} R_{\mu}^{W} W_{\mu} + \sum_{\nu>\mu} R_{\mu\nu}^{\beta} \beta_{\mu\nu} + \sum_{\mu} R_{\mu\mu}^{\gamma} \gamma_{\mu} + \sum_{\nu>\mu} R_{\mu}^{\gamma} \gamma_{\mu\nu}$$

and note the dependence of the resonance integral and off-diagonal Coulomb integral coefficients on the difference density;

$$R^{\beta}_{\mu\nu} = \Sigma_m 2 (C_{Nm})^2 \{ \nu_{m2\nu} \nu_{m2\mu} - \nu_{m1\nu} \nu_{m1\mu} \}$$

$$\begin{aligned} R_{\mu\nu}^{\gamma} = \sum_{m} 2(C_{Nm})^2 \{ & - (\nu_{m_2\nu}\nu_{m_2\mu} - \nu_{m_1\nu}\nu_{m_1\mu}) \left(\frac{\rho_{\mu\nu}}{2}\right) \\ & + 2 (\nu_{m_1\nu}\nu_{m_1\mu}\nu_{m_2\nu}\nu_{m_2\mu}) - \frac{1}{2} [(\nu_{m_1\nu}\nu_{m_2\mu})^2 + (\nu_{m_1\mu}\nu_{m_2\nu})^2] \\ & + (\nu_{m_2\nu}\nu_{m_2\nu} - \nu_{m_1\nu}\nu_{m_1\nu}) Q_{\mu} + (\nu_{m_2\mu}\nu_{m_2\mu} - \nu_{m_1\mu}\nu_{m_1\mu}) Q_{\nu} \} \\ & + \sum_{k>m} 2 C_{Nm} C_{Nk} \{ 2 (\nu_{m_1\nu}\nu_{m_2\nu}\nu_{k_1\mu}\nu_{k_2\mu} + \\ & \quad \nu_{m_1\mu}\nu_{m_2\mu}\nu_{k_1\nu}\nu_{k_2\nu}) - (\nu_{m_1\nu}\nu_{m_2\mu}\nu_{k_1\nu}\nu_{k_2\mu} + \\ & \quad \nu_{m_1\mu}\nu_{m_2\nu}\nu_{k_1\mu}\nu_{k_2\nu}) \} \end{aligned}$$

in which the term $\{ \nu_{m2\nu}\nu_{m2\mu} - \nu_{m1\nu}\nu_{m1\mu} \}$ is the difference density for the excitation.

We now introduce a scaling parameter for the difference density, χ, which we multiply the difference density by in order to amplify the bond-order changes for an excitation. Thus, we define a scaled resonance integral coefficient, $\chi R^{\beta}_{\mu\nu}$, which is simply

$$\chi R^{\beta}_{\mu\nu} = \chi \Sigma_m 2 (C_{Nm})^2 \{ \nu_{m2\nu} \nu_{m2\mu} - \nu_{m1\nu} \nu_{m1\mu} \},$$

or, equivalently, a scaled difference density, $\mathbf{D}\mu\nu$,

$$\mathbf{D}_{\mu\nu} = \chi \{ \nu_{m2\nu} \nu_{m2\mu} - \nu_{m1\nu} \nu_{m1\mu} \}.$$

This same scaling of the difference density terms is applied within the expression for the coefficients of the off-diagonal Coulomb integrals; note that it is not possible to simply multiply these coefficients as is the case with the beta integrals, due to the additonal terms which are not formally difference densities.

In order to be consistent we must append the correct energy change in the diagonal

elements of the CI matrix. Thus, for a bond-order change of magnitude χ, we must add this amount into the SCF orbital energy difference terms in the CI matrix elements;

$2(\chi - 1) \sum_{\nu>\mu}\{ \nu_{m2\nu} \nu_{m2\mu} - \nu_{m1\nu} \nu_{m1\mu} \} F_{\mu\nu}$.

This additional term in the CI Hamiltonian will raise the excitation energies (by roughly χ-percent), but makes very little overall contribution to the geometry shifts since these are governed primarily by the resonance integrals.

To summarize, the difference-density scaling procedure involves scaling all difference density terms in the coefficients of the integrals and the CI energy expression. This provides a much more direct and consistent approach to adjusting the geometry shift upon excitation (and, by extension, the normal coordinate displacements) and represents an improvement over the standard approach of empirically adjusting the displacements at the level of a fitting procedure for the Franck-Condon factors which determine the spectrum.

Calculation of Franck-Condon Factors and Vibronic Bandshapes

The Franck-Condon factors required for calculation of spectral bandshapes were computed using an algorithm based on the recursion relations of Doktorov, et al. (39,40), as outlined in Chapter Two. For calculation of fluorescence excitation (absorption) spectra of jet-cooled molecules, we have developed the program FCEXFL. For calculation of dispersed fluorescence from the vibrationless level of an excited electronic state, the program DISPFLU was developed. The two codes differ only in terms of which states are defined as the initial and final states involved in the transition, and the recursion relations relevant to the set of states.

As follows from the definitions of the auxillary matrices and vectors and the expression for the origin, the calculations required routines for matrix inversion, transpose operation, and evaluation of determinants. The matrix inversion task was

accomplished by performing lower-upper (LU) decomposition coupled with Gaussian elimination backsubstitution. The fortran routines LUDCMP and LUBKSB from Numerical Recipes (88) were adopted without modification within the Franck-Condon codes for this purpose. The evaluation of matrix determinants was accomplished by taking the product of the diagonal elements of the LU decomposed matrix, as suggested in Numerical Recipes (88).

Although the calculations required dealing with matrices typically of dimension 42x42 or 48x48, as is the case for the indole normal modes, no problems were encountered with overflow or underflow of the floating point dynamic range on any of the VAX computers used in this work. This is a potential problem when evaluating the determinant of any matrix of substantial size which we were fortunate not to encounter. Subsequent users are referred to the discussion by Press, et al. (88), in the event that the codes are adopted to different operating systems.

Although the recursive structure of the DMM overlap integrals has potential for highly efficient evaluation of Franck-Condon factors, there are several problems which arise in the fortran implementation of these equations which prohibit a fully recursive algorithm. In the first place, fortran does not contain pointer manipulation operations, as is the case with Pascal, PL/1, and C (68). Also, it is not possible to pass function subprogram names through common blocks (89) in fortran. Further, as will be seen in what follows, for even a moderate number of normal modes the number of FC factors which must be stored in arrays for a fully recursive algorithm is prohibitively large.

For these reasons, the codes FCEXFL and DISPFLU were written to compute the FC factors by a brute force approach, with minimal regard for overall efficiency. This circumvents the problem of storing integrals in dimensioned arrays, with the trade off being an increase in CPU expense. In practice, however, the algorithm we employ turns out to be fast enough for our purposes.

In this algorithm we store the fundamentals and overtones in a two-dimensional array, and since these transitions involve n-quanta excitation of single modes, they are completely specified by indices for the mode and number of quanta;

F(mode,nquanta), mode=1-42 (for indole), nquanta=1,2,...,n.

A convenient notation for a particular transition is to utilize the occupation-number formalism for coherent states and specify the number of quanta (n) and the mode excited by a subscript (k). We can thus specify a general excitation of N modes as

$\{ n_1, n_2, ..., n_k, ..., n_N \}$.

The advantage of this representation is that the set of fundamentals may be represented

$\{ 1_k \}$, where k=1,2,...,N (for N modes),

and the overtones, for n=2,3,... quanta of excitation are compactly expressed by $\{ n_k \}$. For combinations, we can denote the sets in this formalism very compactly from the general expression. For example, single quanta excitation of two individual modes (labeled i,j) is written $\{ 1_i, 1_j \}$, i.e. a combination transition for modes "i" and "j".

In the routines FCEXFL and DISPFLU, all integrals (FC factors) through five-quanta of excitation are calculated. The set of integrals is presented in Table 2. These sets of modes define a hierarchy in terms of total quanta of excitation. The fundamentals define, trivially, the one-quanta excitation set. First overtones and { 1,1 } combinations define the two-quanta excitations. Thus, we compute all Franck-Condon factors for transitions up to five-quanta excitations.

TABLE 2. Franck-Condon integrals computed for 0_0 fluorescence excitation and 0^0 dispersed fluorescence.

occupation (quanta)	total quanta	spectroscopic designation
$\{ 1_k \}, \{ n_k \}$	1-n	fundamentals and overtones
{ 1,1 }	2	combinations
{ 2,1 }, { 1,1,1 }	3	combinations
{ 2,2 }, { 2,1,1 }, { 1,1,1,1 }	4	combinations
{ n,1 } for n ≥3	4+	combinations
{ 3,1,1 }, { 2,2,1 }, { 2,1,1,1 }		
{ n,2 } for n≥3,, { 1,1,1,1,1 }	5+	combinations

The storage requirements for the entire set rapidly becomes excessive. For example, in order to store the five-quanta combination integrals for indole would require 42^5 (130,691,232) separate storage locations, which is of the order $O(10^8)$. This is clearly not practical. To get around this problem, we store only those Franck-Condon factors within a set tolerance in a vector. The algorithm -- common to both FCEXFL and DISPFLU -- is then a straightforward procedure which can be outlined as follows;

(**1**) Input the normal mode frequencies, displacements, and eigenvector components.

(**2**) Compute the Duschinsky transformation.

(**3**) Dimension and compute the auxillary matrices and vectors for the DMM relations.

(**4**) Compute the origin (0-0) Franck-Condon factor from the closed-form expression.

(**5**) Set the lower limit for storage of FC factors as a fraction of the origin and the maximum energy range for the calculation.

(**6**) Compute the set of Franck-Condon factors from the recursion relations and store those which fit the intensity and energy criteria in the vector, FVEC.

This vector is then sorted by increasing frequency into a new array. This array, then, defines the zero Kelvin "stick" spectrum for the molecule. The frequency of the origin transition defines the zero of the energy scale, and all FC factors are expressed in terms of energy in excess of the 0-0 (as is common to experimental jet-spectra). In practice, the sort procedure is performed by a subroutine, "SORT", which is a direct adaptation of the Heapsort algorithm provided in Numerical Recipes (88). The sorted vector is then written to a file for graphics.

Gaussian Broadening

In addition to the Franck-Condon factor evaluation codes, we developed a separate routine for the application of Gaussian broadening to the zero K stick spectra. The convolution of the computed spectrum with Gaussian functions allows us to incorporate phenomenological broadening in the bandshape. The Gaussian function, which is appropriate to inhomogeneous broadening mechanisms (e.g. sequence bands), builds resolution into the spectrum. We represent the stick spectrum by $I(\omega_0)$, then numerically evaluate the convolution integral (90)

$$I_\Gamma(\omega') = \int_{-\infty}^{+\infty} d\omega_0 \, G_\Gamma(\omega' - \omega_0) \, I(\omega_0)$$

in which $G_\Gamma (\omega' - \omega_0) = \exp\{ - (\omega' - \omega_0)^2 / \Gamma^2 \}$

is the Gaussian function. The integral is standard and it follows from the Gaussian property that since $\int \exp\{- x^2 / a \} \, dx = a \, \pi^{1/2}$, that Γ is related to the full-width at half-maximum (FWHM) of a band, W, by $\Gamma^2 = W^2 / 4 \ln(2)$. We may thus discretize the integral and numerically evaluate it via

$$I_\Gamma(\omega') \cong \sum_{\forall \omega_0} \exp\{ - (\omega' - \omega_0)^2 / \Gamma^2 \} \, I(\omega_0) \, \Delta\omega_0$$

$$= \sum^{N} \exp\{ - (\omega' - k\Delta\omega_0)^2 / \Gamma^2 \} \, I(k\Delta\omega_0)$$

in which we have chosen to use an equally spaced interval.

This then allows us to compute spectral bandshapes with arbitrarily specified broadening factors to simulate the effects of inhomogeneous broadening.

Excitation Energies and Potential Energy Surfaces

As outlined in Chapter Two, QCFF provides for the calculation of excitation energies at a given molecular geometry by diagonalization of the configuration interaction matrix. The eigenvalues so obtained are the excitation energies for the various electronic states of the molecule; the energy at the ground state equilibrium geometry is defined as the zero of energy.

In canned form, QCFF thus provides those points on a potential energy surface corresponding to a minimum energy. We have modified QCFF to extend the potential energy surface calculation procedure to obtain the PES along an arbitrary coordinate for ground and excited states. The subroutine, PSURF, is contained in Appendix 2. The potential energy surface algorithm can be summarized as follows:

(i) QCFFBOZE is run to obtain the equilibrium molecular geometries for the electronic states of interest;

(ii) The coordinate along which the PES is to be computed is specified and input as a vector.

(iii) The number of points at which to compute the surface is specified and the step-size is computed.

(iv) The starting geometry (generally away from an equilibrium molecular geometry) is specified and input as a vector.

(v) The ground state PES is computed along the vector;

(vi) The PES for the specified electronic state is computed.

In practice, steps (ii)-(iii) are accomplished by defining the coordinate along which

the PES is to be computed as a vector, **r**, in Cartesian space and the step size ($\Delta\mathbf{r}$) is defined by $\Delta\mathbf{r} = \mathbf{r}/N$, where N is the number of points specified. In component form we have $\Delta x_i = dx_i /N$, for i=1,2,...,3n. This defines the metric for the potential surface calculation such that the vector is normalized in the 3n-dimensional Cartesian space of the molecule.

If the coordinate of interest is the difference in equilibrium molecular geometries for two electronic states, the metric as defined above allows a uniform change in molecular geometry from one state to the next. Calculation of the PES along various normal coordinates is also possible by defining the vector in terms of the eigenvectors representing the normal modes of vibration. This is particularly useful for those vibrations for which there is displacement of the potential surfaces (in normal coordinate space) and a given vibration "projects" one equilibrium molecular geometry onto another.

The QCFF potential energy surface is given as an explicit function of the 3n Cartesian coordinates as

$$V(\mathbf{x}) = V_\sigma(\mathbf{x}) + V_\pi{}^0(\mathbf{x}) + \Delta V_\pi{}^N(\mathbf{x})$$

which can be recast in the form

$$V(\mathbf{x}) = V^{(0)}(\mathbf{x}) + \Delta V_\pi{}^N(\mathbf{x})$$

which is essentially a sum of a ground state surface plus the configuration interaction excitation energy appropriate to the N-th electronic state. Thus, in practice, we need only append the CI excitation energy to the ground state surface at a given molecular geometry to obtain the excited state surface.

The step-size for the PES calculations or, alternatively, the number of points along a coordinate, is arbitrary. Since the PES calculations are not performed to locate minima on the surfaces, there is no convergence problem or error associated with the choice of step-size. Also, since the potential energy surfaces reported for indole required ca. 1 sec.

CPU per point (cf. Appendix 1), computing typically 10^2 PES points posed no problems in terms of execution time.

In addition to computing potential surfaces, it is also possible to compute "excitation surfaces", since the CI excitation energy is computed at each geometry by QCFF. These surfaces, although not Born-Oppenheimer PE surfaces, are important in that they reflect the qualitative features of the true potential surfaces. In particular, excitation surfaces exhibit exactly the same crossing and avoided crossing behavior of the true potential surfaces which they comprise. In the event that two excited electronic states cross, there will be a degeneracy at the crossing region which is manifest as identical excitation for both surfaces at the point(s) in question. Alternatively, an avoided crossing of two surfaces can be elucidated as a non-crossing of the excitation energies since no degeneracy of the surfaces (excitations) can exist at any point.

A major component of this investigation was the question of avoided crossings of the L_b and L_a potential surfaces in indole. Since these surfaces possess the same symmetry, the von Neumann-Wigner Crossing Theorem (91) states that these surfaces cannot cross, except for the case of "accidental degeneracies". We therefore have two equivalent means at our disposal for elucidation of avoided crossings; examination of the "excitation surfaces", and the true Born-Oppenheimer adiabatic potential surfaces. By taking the difference in excitation energies at a given configuration or, alternatively, the PES difference (these will be identical), we are then able to determine the magnitude of the avoided crossing.

CHAPTER 4

RESULTS and DISCUSSION

Preliminary QCFF Results

Benzene Geometry and Surface Displacement

The canonical QCFF results for the benzene geometry in the A_{1g} (S_0, ground) and B_{2u} (S_1) electronic states are presented in Table 3, along with the experimental values for the carbon-carbon bond length. The calculated change in the C-C bond length is 0.0252 Å, which is 0.0088 Å lower than the experimental value (0.034 Å).

TABLE 3. QCFF calculation of benzene geometry in the A_{1g} and B_{2u} electronic states.

state	C-C bond length / Å	C-H bond length / Å
A_{1g}	1.4062 (1.3974)[a]	1.0829
B_{2u}	1.4314 (1.4314)	1.0799
	Δr(C-C)/Å = 0.0252 (0.0340)	

(a)Experimental values in parenthesis. (ref. 80)

The QCFF value for the excitation energy for the B_{2u}<--A_{1g} transition from the ground state equilibrium geometry is 39,081 cm^{-1}, with an oscillator strength of zero. This is in agreement with the experimental value for the origin of the 260 nm band (ca. 38,462 cm^{-1}), which exhibits an oscillator strength of zero in the absence of solvent.

In experiments on the benzene 260 nm band, the one-photon absorption (fluorescence excitation) spectrum which is measured is a result of Herzberg-Teller (HT)

vibronic coupling mechanism involving e_{2g} vibrations which make allowed the dipole-forbidden B_{2u}<--A_{1g} transitions by distorting the benzene geometry away from a perfectly hexagonal structure. Since the QCFF package calculates molecular properties at the equilibrium molecular geometry (hexagonal), the zero oscillator strength result computed means that the absolute intensity of the B_{2u} band will also be zero, as per the expression for the electronic transition intensities, $M_e \int \chi'^* \chi \, d\mathbf{q}$, the square of which is a product of an electronic transition moment, squared, times the Franck-Condon factor.

Nonetheless, the relative intensities are determined solely by the Franck-Condon factors. To that end, we compute the surface displacements and determine the FC spectrum for the benzene molecular geometries in Table 3. There is only one vibrational mode in benzene which is appreciably displaced in normal coordinate space; the a_{1g} "ring-breathing" mode. The geometric distortion caused by motion of the atoms along this coordinate, Q_1, is primarily a lengthening of the carbon-carbon bonds. The QCFF computed frequencies in the A_{1g} and B_{2u} states, and coordinate displacement information for this mode are displayed in Table 4.

TABLE 4. QCFF calculation of the benzene a_{1g} normal coordinate, Q_1.

state	ω / cm^{-1}	ω (exptl.)[a]	ΔQ[b]	$Q^{(0)}$ [b,c]	$S=\Delta Q/Q^{(0)}$	λ
A_{1g}	1037.	993.	.2205	.1835	1.2017	0.7220
B_{2u}	1001.	923.				

(a)(ref. 80)
(b)Values in mass-weighted normal coordinate, $(amu)^{1/2}$Å.
(c)Classical turning point.

The frequency calculated for the a_{1g} normal mode in the first excited singlet state is seen to be lower than in the ground state. This is reasonable, and can be easily

rationalized in terms of the one-dimensional harmonic oscillator model for the vibrational motion. Since the force constant for the motion along a coordinate within the harmonic approximation is $k=\mu\omega^2$, a weakening of the bonds in the excited state corresponds to a lower restoring force, and thus a lower frequency, i.e. $\omega = (k/\mu)^{1/2}$. In terms of bond order changes, this is completely consistent with (and, indeed, follows from) a decrease in bond order upon excitation. We note also that the ground state value of the Q_1 vibrational frequency is in basic agreement with the value reported by Warshel, et al. (34,35), 1046 cm^{-1}. In both electronic states the QCFF computed frequencies are found to be higher than the experimental values, by ~5% in the ground state and ~8% in the B_{2u} state. This frequency overestimation is, in fact, a common feature to vibrational frequencies computed by QCFF as well as most quantum chemistry packages, and has been noted previously (35,71,87).

Further, we note that no Duschinsky rotation exists between the two a_{1g} vibrational modes in benzene. The other a_{1g} mode, which is characterized as predominantly a C-H stretch mode at ca. 3000 cm^{-1}, could mix with the ring-breathing mode since it belongs to the same irreducible representation. However, since the geometry change for excitation conserves the point group (D_{6h}) and is primarily a lengthening of the C-C bond framework, little if any mixing of these coordinates is expected. In addition, since these vibrations differ by nearly 2000 cm^{-1}, they are effectively "adiabatically" separated (44,92), which is consistent with intuitive ideas involving two-state mixing in terms of a variational picture. The a_{1g} block of the Duschinsky rotation matrix supports this; our calculations produce a unit diagonal 2x2 matrix for this symmetry.

QCFF Benzene 260 nm Franck-Condon Progression

On the basis of the QCFF normal modes and their displacements, we have computed the absorption spectrum for benzene at zero Kelvin. The spectrum includes the effects of

surface displacement, frequency shifts, and Duschinsky rotation for all normal modes. However, for the benzene B_{2u}<--A_{1g} spectrum, the dominant feature is the progression in the one significantly displaced coordinate, Q_1, and so we focus our attention on these transitions. For the normal coordinate displacement of Table 4., the corresponding value of λ is computed to be ~0.7. According to the Poisson model for uncoupled, parallel modes without frequency distortion, this corresponds roughly to a maximum in the progression occurring at zero quanta of excitation for the vibration, Q_1, and an intensity ratio for the fundamental to the origin of ~0.7. The Franck-Condon factors which determine the progression (1_0^n) are presented in Table 5(a) and Figure 1., and the experimental values obtained by Hiraya and Shobatake (82) by direct absorption jet-spectroscopy are presented in Table 5(b) for comparison.

TABLE 5a. QCFF Franck-Condon factors for the (1_0^n) progression in benzene.

quanta;	n= 0	1	2	3	4
I_n(abs.)	0.46	0.34	0.12	0.028	0.004
I_n(rel.)	1.00	0.74	0.26	0.06	0.01

TABLE 5b. Experimental Franck-Condon factors for the (1_0^n) progression in benzene. From; A. Hiraya and K. Shobatake, "Direct absorption spectra of jet-cooled benzene in 130-260 nm", J. Chem. Phys. **94** (12), 1991. (pps. 7700-7706).

quanta;	n= 0	1	2	3	4	
f (rel.)	1.00	1.36	0.98	0.62	0.42	{integrated oscillator strengths}
I(rel)[a]	1.00	1.33	0.93	0.58	0.38	

(a) corrected for excitation frequency; $I_n(rel)=f_n(rel)/\omega_n$

The most striking difference between the (1_0^n) progression computed from the QCFF normal modes and that measured by HS is that in the experimental spectrum, the progression maximum appears at the fundamental, with one quantum in the ring-

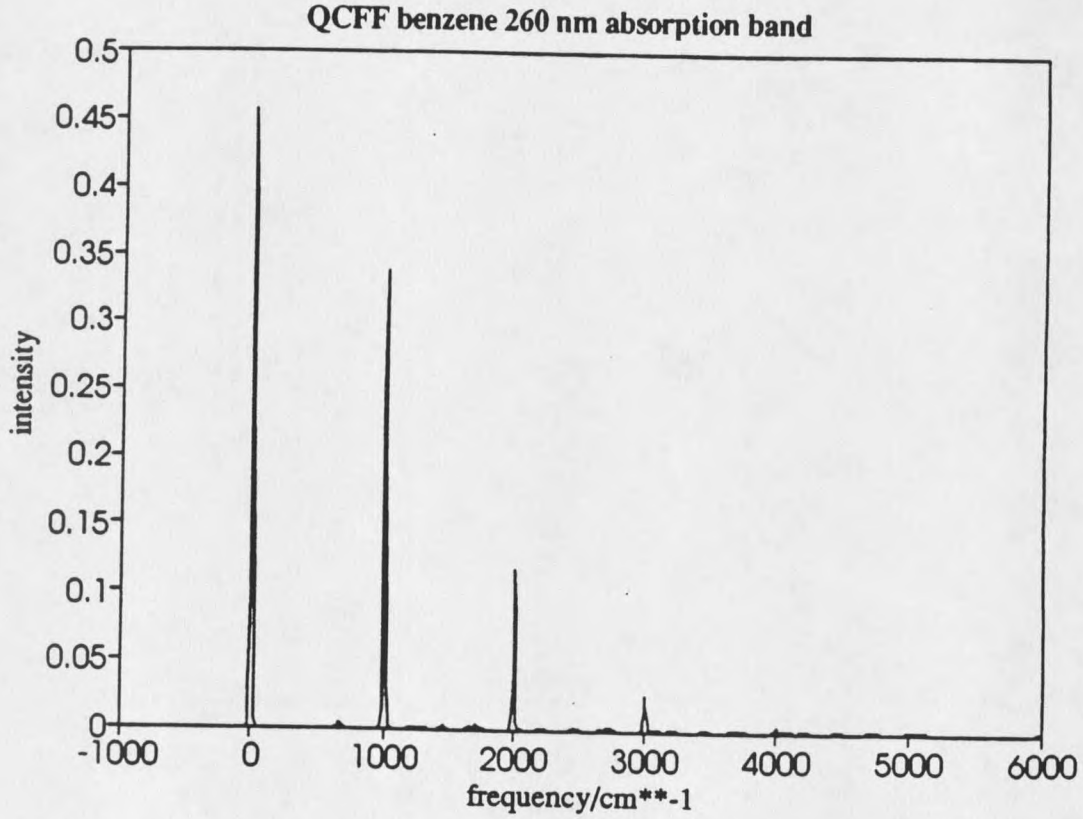

Figure 1. Benzene 260 nm absorption band computed by QCFF. Frequencies (cm^{-1}) are relative to the B_{2u}<--A_{1g} origin, intensities are the Franck-Condon factor values. The a_{1g} "ring-breathing" mode progression is clearly evidenced.

breathing vibration. Of course, this progression is built on the false origin induced by HT vibronic coupling (primarily with one quantum of Q_6), and this plays a role in the comparison of the calculated and experimental intensities at this level of analysis in that the experimental intensities are not strictly Franck-Condon factors. Two points are at issue here; (i) the dependence of the experimental intensities on excitation energy, and (ii) the effects of non-adiabaticity, as noted by Naaman, et al. (86).

In order to work within these issues, we deal with the former case simply by dividing the experimental intensities by the observed frequencies to remove the excitation energy dependence of the observed intensity. The results for this are presented as the last entry in Table 5(b).. The latter problem is considerably more subtle; coupling to the E_{1u} electronic state (at ~55,000 cm^{-1}) provides most (if not all) the intensity of the bands. Whether the mixing is independent of vibrational energy depends on the relative displacements of the B_{2u} and E_{1u} surfaces. Neglecting this effect may lead ultimately to computed intensities which are lower than experimental values. This provides a possible reason why the computed FC factors might be "anomolously" lower than their experimental counterparts. The point is that even if we were able to match the experimentally observed bond length changes for benzene, the intensity distribution computed for this geometry change would still be somewhat lower than what is observed. With this in mind, we proceed to analyze the computed progression members from Table 5(a).

The computed relative intensities of Table 5(a) are what we anticipate on the basis of the value of the parameter, λ, and the intuitive Poisson model for the Franck-Condon factors. However, it is clear by comparison with Table 5(b) that the general trend of the experimental progression is <u>not</u> reproduced by the QCFF calculation. The ratio of the fundamental to the origin, which is determined by the parameter, λ~.70, is not in agreement with experiment. Higher members of the calculated progression are also

anomolously lower than the experimental values.

The cause of this lack of agreement between theory and the experiment lies primarily in the value of the displacement. The computed change in the C-C bond length, 0.0252 Å, is considerably lower than the experimental value of ~0.034 Å, as noted above. This has dramatic consequences in terms of the Franck-Condon factors; it represents an error of ~26% in the bond length change, but the error in the relative intensity of the fundamental is on the order of 50%. In addition, the most disturbing feature of the QCFF computed progression is that it does not even capture the general trend in the relative intensities (~1.0 origin, ~1.3 fundamental, ~1.0 first overtone). The root of the problem, which can be stated succinctly in the form of a conclusion, is thus: QCFF underestimates the bond length changes upon electronic excitation for benzene.

This poses considerable problems, since we are interested in accomplishing two complementary goals in this work. First, we wish to explain, on the basis of semiempirical MO calculations, some of the general trends in the spectroscopy of the two lowest singlet states in the electronic manifold of indole. By this is meant a reasonably comprehensive vibrational assignment in which the calculated Franck-Condon factors might corroborate existing experimental assignments. Secondly, we are interested in obtaining information about the potential energy surfaces of these electronic states since these surfaces provide, in principle, a key to understanding both the nature of the vibrational wavefunctions away from the PES minima and the associated dynamics of these molecular excited states which have presented experimental issues which are still unresolved.

Neither of these goals can be accomplished within a theoretical framework which cannot account for the correct general trends in the spectroscopy of a reasonably simple system such as benzene. To that end, as outlined in the formalism of Chapter Two, we developed the difference-density scaling procedure to attempt to correct the QCFF C-C

bond length change for the benzene B_{2u} state.

The formalism of the scaling procedure requires only the introduction of a multiplicative parameter, χ, which is applied to all difference-density terms in the excitation energy expression and CI-matrix elements. In this way, we are able to "tune" the excited state bond lengths by varying the bond-order matrix elements. By running a series of benzene B_{2u} electronic state calculations with QCFF, varying the scaling factor, we were able to fit the correct change in the C-C bond length in efforts to reproduce with reasonable accuracy the experimental 1_0^n progression.

QCFFBOZE Difference Density Scaled Benzene 260 nm Band

The results for the scaling procedure are summarized in Table 6 and Figure 2. The "default" value of the scale factor, $\chi = 1$, produces the standard QCFF results. Note that no scaling is applied to the ground state; the scaling procedure serves only to amplify the difference density, resulting in bond length changes upon excitation. Thus, we fit the change in bond length upon electronic excitation at the level of the QCFF semiempirical calculation.

TABLE 6. Effect of difference density scaling on the B_{2u} C-C bond length in benzene.

χ	1.0	1.27	1.28	1.30	1.31	1.32	1.33	1.34
r_{CC}/Å	1.4313	1.4394	1.4397	1.4403	1.4406	1.4409	1.4412	1.4415
Δr/Å	.0252	.0332	.0335	.0341	.0344	.0347	.0350	.0353

As outlined in detail in Chapter Three, the advantage of this difference density scaling procedure over the more common empirical displacement analysis is that it provides us with information which is consistent throughout the calculation. The

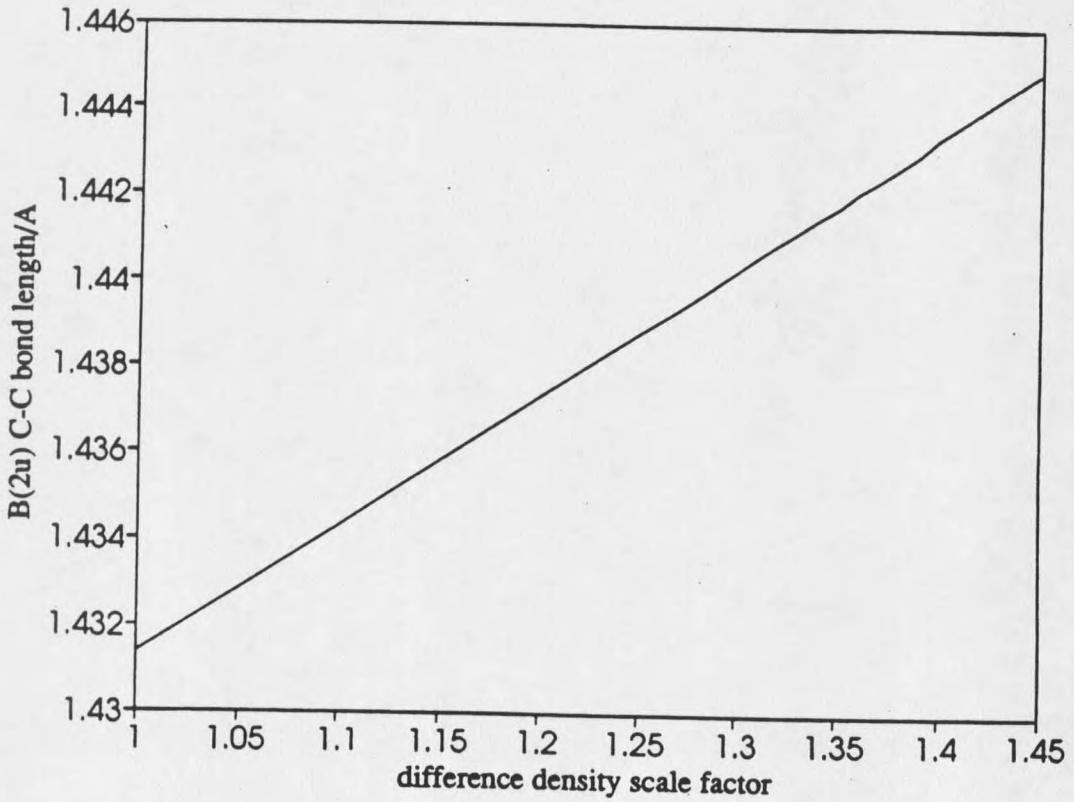

Figure 2. Benzene C-C bond length (Å) in the B_{2u} electronic state computed from QCFFBOZE for various difference-density scaling factors.

calculated Franck-Condon factors and associated spectral bandshapes are consistent with the wavefunctions, potential energy surfaces, and normal modes of vibration which determine them. In this sense, the scaling procedure elevates the bandshape calculations from a simple exercise in fitting normal coordinate displacements to a more rigorous correction of the underlying semiempirical method.

From the scaled bond length results in Table 6, we note that the scale factor value χ = 1.30 produces a change in the C-C bond which is in good quantitative agreement with the experimental value of 0.034 Å. On the basis of this value for the scale factor, we have calculated the normal coordinate information required for the Franck-Condon factors. The results of this calculation are contained in Table 7.

TABLE 7. QCFFBOZE calculation of the benzene a_{1g} normal coordinate Q_1, for a difference density scale factor, χ=1.30.

state	ω / cm^{-1}	ω (exptl.)[a]
A_{1g}	1037.	993.
B_{2u}	988.	923.

ΔQ[b]	$Q^{(0)}$ [b,c]	$S=\Delta Q/Q^{(0)}$	λ
.299	.1848	1.6184	1.3097

(a)(ref. 80)
(b)Values in mass-weighted normal coordinate, $(amu)^{1/2}$Å.
(c)Classical turning point.

The important point with regard to the scaled calculation is that now the value of the parameter λ (~1.3) is in much better agreement with the experimental ratio of the fundamental to the origin. The Franck-Condon factors for the 1_0^n progression were then calculated for this (scaled) surface displacement (Table 8.).

TABLE 8. QCFFBOZE Franck-Condon factors for the (1_0^n) progression in benzene. {difference density scale factor, χ=1.30}

quanta;	n= 0	1	2	3	4
I_n(abs.)	0.24	0.33	0.22	0.09	0.028
I_n(rel.)	1.00	1.38	0.91	0.38	0.12
I_n(exptl.)	1.00	1.33	0.93	0.58	0.38

note; Experimental values from ref. 82.

The result for the scaled benzene Franck-Condon factor (Table 8.) for the origin transition exhibits a significant decrease in intensity from the unscaled case (I_0=0.46). This is precisely what should occur, since the 0-0 transition now occurs with a greater relative displacement of the two electronic surfaces. Interestingly, the absolute intensity of the fundamental does not undergo a significant reduction. Of course, the intensity relative to the origin is in agreement with the larger value of λ, as must be the case, and it is observed to change by a factor of ~2. Higher members of the progression exhibit higher absolute and relative intensities, which is consistent with predictions based on the simple one-dimensional Poisson model.

Figure 3. presents the QCFFBOZE benzene spectrum corresponding to the computed Franck-Condon factors of Table 8.. In addition, the Franck-Condon factors are compared with the experimental relative intensities of Hiraya and Shobatake (82) in Figure 4., in which the relative intensities attributed to the a_{1g} "ring-breathing" mode are given as a function of number of quanta. The important point to note is that the origin-fundamental ratio computed by QCFFBOZE is observed to be in good agreement with experiment, while the calculated overtone relative intensities are seen to decay much faster than is observed. This compromise in the fit of higher members of the progression is a direct

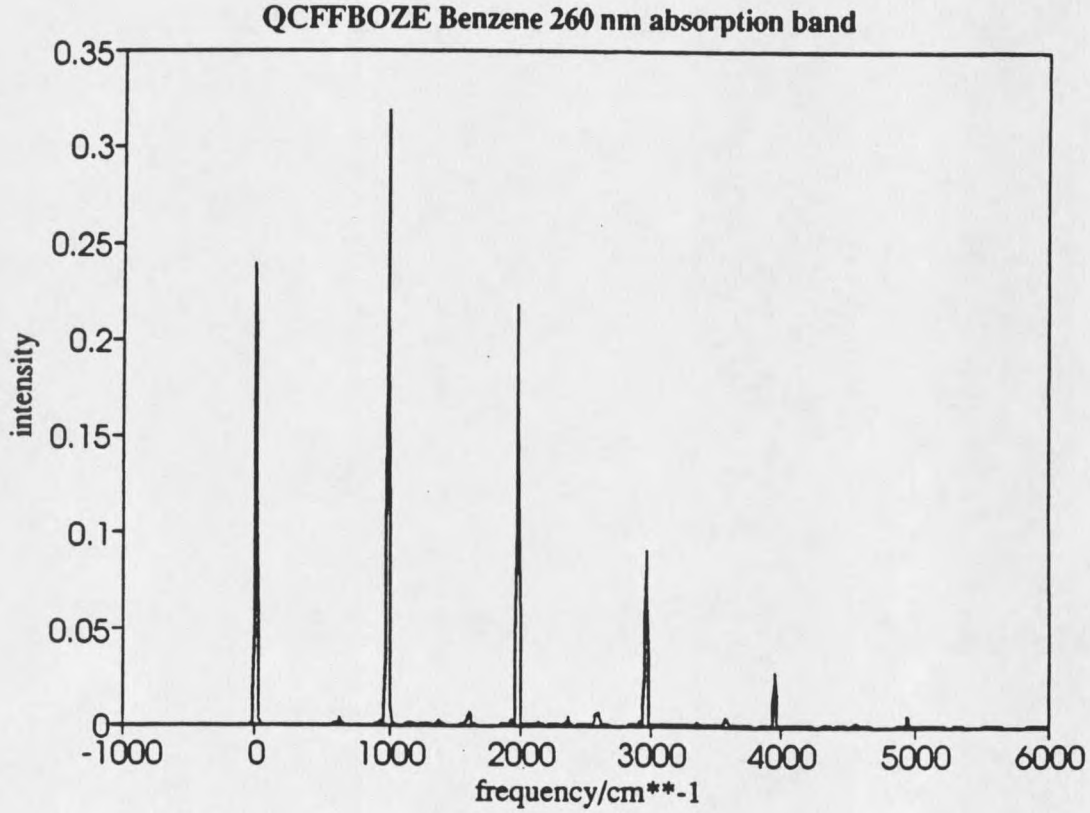

Figure 3. Benzene 260 nm absorption band computed by QCFFBOZE with a difference density scaling factor of χ=1.30. The a_{1g} "ring-breathing" mode progression exhibits a fundamental-origin ratio of ~1.38, in much better agreement with experiment than the QCFF (unscaled) spectrum.

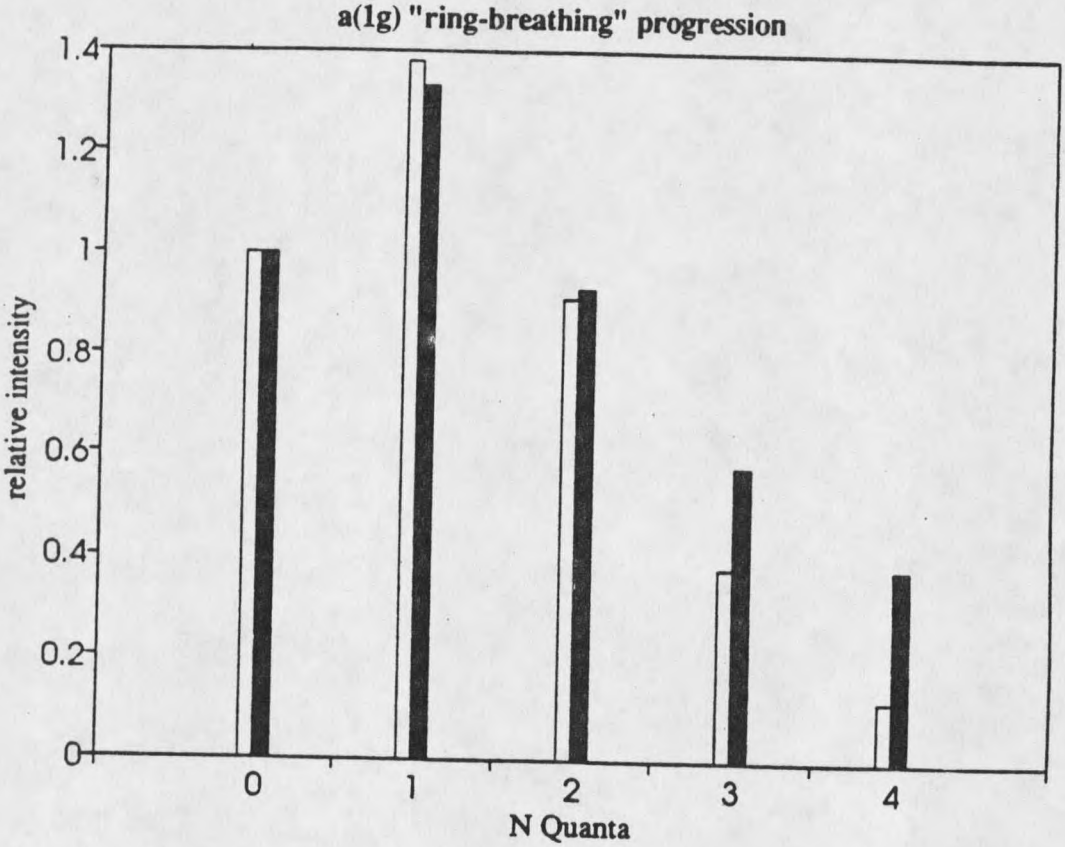

Figure 4. Comparison of benzene a_{1g} "ring-breathing" mode progression relative intensities computed from QCFFBOZE with experimental intensities. Shaded bars correspond to the jet-cooled direct absorption intensities observed by Hiraya and Shobatake (ref. 82).

result of the relatively large displacement of the a_{1g} mode in benzene -- the large value of lambda (i.e. $\lambda>1$) allows a relatively long progression. In this sense, fitting the a_{1g} mode progression is a considerable challenge and shows benzene to be a worst-case scenario: for molecules with small displacements (i.e. all $\lambda<1$) this difficulty may be ignored because the higher members are not observed with accuracy. The discrepancy between the experimental and computed FC progression may be attributed to the coupling to the E_{1u} state, as outlined previously, and although it is (as stated above) a result of the displacement it is not simply an issue of an ill-predicted geometry change. This is seen simply by noting that the agreement between the computed geometry shift and the experimental value is quite good -- the scaling procedure works to fit the geometry changes. Fitting the relative intensities (via the geometry changes) is a closely related and more complicated issue.

Thus, the difference density scaling procedure provides a reasonably accurate method for fitting the 1_0^n progression in benzene and bringing the QCFF computed displacement and FC factors into agreement with experiment in a very direct way: by doing the fitting at the level of the geometry changes. The extension to other molecules -- in particular, to indole -- is straightforward in principle. We apply the scale factor, χ, without modification directly to indole under the assumption of transferrability between molecules.

Indole: QCFF Preliminary Results

From the canonical QCFF results, certain general trends in indole are reasonably well predicted. We consider first the geometries for the ground and first two electronic excited states (L_b and L_a). The emphasis here is on the geometry changes upon excitation, which determine the Franck-Condon progressions, and on the relative energies of the electronic states. From this information, a qualitative picture of the L_b-L_a

electronic manifold emerges which is in reasonable agreement with experiment.

Indole QCFF Geometry

The geometry of the indole molecule is considerably more complicated than benzene simply in terms of the lower symmetry as well as the relative number of bonds, bond angles, and torsional angles which define the internal coordinates. For indole, there are 17 bond lengths, 27 bond angles, and 49 torsional angles in the set of internal coordinates. A simplification occurs, however, if we realize that (as in benzene) the C-H bond lengths are relatively less important than the C-C (and C-N) bond lengths in defining the molecular framework. Further, since the molecule is planar in the ground state (and in the L_b and L_a states as well), it suffices to specify only the bond lengths with the understanding that we mean the bond lengths consistent with the bond angles and torsional coordinates which define the equilibrium molecular geometry.

In this way, we can specify only 10 bond lengths. The numbering of the atoms according to the conventional scheme is as follows;

Indole

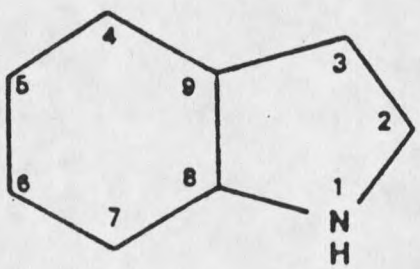

In addition, the N-H bond length is of considerable interest as well, so we include this value in specifying the geometry. The QCFF energy-minimized geometries for the ground, L_b, and L_a electronic states are contained in Table 9. The bonds defining the six-member carbon ring are denoted with an asterisk (*).

TABLE 9. Indole geometry predicted by QCFF (bond lengths in angstroms, Å).

bond	ground	L_b	L_a	
N-C_2	1.4278	1.4212	1.4120	
C_2-C_3	1.3787	1.4152	1.4507	
C_3-C_9	1.4557	1.4323	1.4067	
C_4-C_9	1.4134	1.4145	1.4507	*
C_4-C_5	1.4006	1.4327	1.4164	*
C_5-C_6	1.4261	1.4394	1.4111	*
C_6-C_7	1.4021	1.4151	1.4609	*
C_7-C_8	1.4161	1.4288	1.3937	*
N-C_8	1.4175	1.4056	1.4295	
C_8-C_9	1.4230	1.4606	1.4492	*
N-H	1.0016	1.0014	1.0016	

(*) denotes bonds comprising the six-member ring.

These geometries require some comment. First, with regard to the six-member ring, we note that the C-C bond lengths in the ground state are slightly longer than those calculated for benzene (~1.406 Å), and are not uniform or exactly symmetric about the six-member ring, and this situation persists in the excited states as well. Second, we note that the N-H bond length does not change appreciably upon excitation to either the L_b or L_a electronic states. From this we may tentatively conclude that the L_a state is <u>not</u> predicted to be dissociative at the CI singles level of theory for planar indole (23). Of course, this conclusion must be corroborated by examining the qualitative nature of the potential energy surface along the N-H bond coordinate; if the potential is highly anharmonic for reasonably small displacements, a dissociative mechanism for L_a might be plausible. We present this potential surface calculation in a later section; for now, it suffices that the equilibrium geometry is predicted to be non-dissociative.

The relative changes in bond lengths upon excitation are of great importance in determination of spectral bandshapes, and it is important to recognize the changes associated with the geometries in Table 9. In the L_b state, the only bonds exhibiting a

decrease in length with respect to their ground state values are the C3-C9 and N-C8 bonds, which are calculated to decrease by 0.0234 Å and 0.0119 Å, respectively. All other bonds (except for N-H) are seen to increase significantly (ca. ~0.01 - 0.04 Å). In the L_a state, there are significant decreases in the N-C2, C3-C9, C4-C5, C5-C6, C7-C8, and C8-C9 bonds with respect to the ground state values. Further, we note that the C2-C3 bond length exhibits a dramatic increase upon excitation to both L_b (+0.0365 Å) and L_a (+0.0720 Å). The qualitative nature of these bond length changes are consistent with the difference density computed by INDO/S (33), in that the absolute signs of the changes are in agreement and their magnitudes are consistent. Another important feature of the geometry shifts is that the C2-C3 bond length change for excitation to L_a is very dramatic; the value of 0.0720 Å is the largest change for the molecular framework.

In a systematic sense, the primary feature of the L_b geometry shift is an increase in the size of six-member ring. The L_b INDO/S difference bond orders for this part of the molecule are considerably larger than those for the five-member ring. On the other hand, the L_a geometry shift is a significant increase in the size of the five-member ring and a large increase in the adjacent C4-C9 and C7-C8 bond lengths on the six-member ring, in basic agreement with the INDO/S difference bond orders for L_a. Neither excitation exhibits truly "ring localized" geometry changes, but the basic pattern of bond length changes (as dictated by the difference density) is captured by the noting in both L_b and L_a there is an increase in the size of the six-member ring. In the L_a state, the lengthening of the C4-C9 and C7-C8 bonds roughly corresponds to a ring expansion towards a distorted "prefulvene" geometry (93).

QCFF Excitation Energies and Oscillator Strengths

As stated previously, the QCFF code provides for calculation of excitation energies via CI singles expansion of the wavefunction. The roots obtained from the

diagonalization of the CI matrix provide the excitation energies for the various electronic states, and the oscillator strength is computed by summation of the x- and y-components of the transition moment (the z-component is zero for planar indole) and applying the standard expression for oscillator strength in the context of CI singles (47)

$f = (8\pi^2 m_e \nu / 3he^2) | \mu_{fi} |^2 = (8\pi^2 m_e \nu / 3he^2) 2 | \Sigma_{jk} \Sigma_r C_{jk} \nu_{jr}^* \nu_{kr} e \mathbf{r}_r |^2,$

in which ν_{jr}, ν_{kr} are the AO coefficients of the singly excited configurations $\psi_{j->k}$ for MO's j and k, C_{jk} is the CI coefficient for the configuration, and the coordinate summation runs over all pi atoms (indexed by 'r'). For practical calculations, the transition moment is expressed in terms of the dipole strength (units of Å), and with the transition energy in electron volts (eV) the above expression becomes

$f = 0.0875 \times 2 | \Sigma_{jk} \Sigma_r C_{jk} \nu_{jr}^* \nu_{kr} \mathbf{r}_r |^2,$

which is the form employed in the QCFF routine OSCILL. The standard QCFF values for the L_b and L_a excitations from the ground state equilibrium geometry are presented in Table 10.

TABLE 10. QCFF vertical excitation energies (ν) and oscillator strengths (f) from the ground state equilibrium geometry.

	ν (cm^{-1})	f
L_b	36450.	0.0186
L_a	40424.	0.3511

ex. energy difference $\{ \nu (L_a) - \nu (L_b) \} = 3974.\ cm^{-1}$
oscill. strength ratio $\{ f_a / f_b \} = 18.89$

There are two important features of the L_b-L_a electronic manifold which are revealed by this calculation. First, vertical excitation from the ground state equilibrium geometry to the L_b surfaces occurs at 36,450. cm^{-1}, while the excitation to L_a occurs nearly 4000 cm^{-1} higher in energy. Thus, the gap between the L_b and L_a surfaces at this

molecular geometry is about 4000 cm^{-1}, with L_a being higher in energy. Further, the computed oscillator strength ratio (18.89) shows that L_a excitation is much stronger than L_b excitation. This oscillator strength ratio is however only in qualitative agreement with experiment, and greatly overestimates the observed ratio.

A more comprehensive picture of the L_b-L_a electronic manifold is obtained by performing the excitation energy calculation at the L_b and L_a equilibrium geometries. These results are presented in Table 11.

TABLE 11. QCFF vertical excitation energies (ν) and oscillator strengths (f) from the L_b and L_a equilibrium geometries.

	L(b) geometry		L(a) geometry	
	ν (cm^{-1})	f	ν (cm^{-1})	f
L_b	34979.	0.0205	34962.	0.0299
L_a	38807.	0.3243	36641.	0.5094

The energy gap between the L_b and L_a surfaces is now seen to be 3,828. cm^{-1} for excitation at the L_b geometry, and 1,679. cm^{-1} at the L_a geometry, with oscillator strength ratios of 15.82 and 17.04, respectively. The excitation energy differences at the ground, L_b, and L_a geometries thus provide a qualitative picture of the excited state potential energy surfaces. From these differences and the total molecular energies computed at the three equilibrium geometries, it is possible to construct a schematic profile of the potential energy surface along the coordinate describing the geometry change from the ground state to the excited states. In fact, it is worth noting that such a schematic picture is the only semi-quantitative characterization of the potential surfaces which the QCFF package is designed to provide. It is for this reason that we modified QCFF for construction of potential surfaces away from minimum energy configurations -- to allow us to explore the global surface and gain information on the quantitative

nature of the surfaces.

Nonetheless, the schematic profile based on the three equilibrium geometries provides a simple "rough-cut" at the surfaces, represented by only nine data points. It serves to demonstrate the relative location of the potential minima as well as the separation of the L_b and L_a surfaces. This picture of the surface, which is only one step up in status from the standard "cartoon surfaces" which abound in the literature (94-96), provides our first picture of the L_b-L_a electronic manifold. What remains, of course, is to explicitly compute the profile connecting the three regions in configuration space and generate the full surfaces.

In addition, we can gain further spectroscopic information from the total molecular energies at the equilibrium geometries. The minimized total energies for indole in the ground, L_b, and L_a computed by QCFF are as follows (in kcal mol^{-1}); -1494.78, -1392.52, -1384.43. From these, we compute the difference (in wavenumbers, cm^{-1}) between the ground and excited state minima, which correspond to the "0-0" spectroscopic origin transitions. The L_b origin is computed to be 35754. cm^{-1}, while the L_a origin occurs at 38583. cm^{-1}, the difference in these origins being 2829. cm^{-1}. It needs to be emphasized that this "zeroth-order" picture of the surfaces and band origins must be viewed with caution. The L_a origin, in particular, is <u>not</u> observed at ca. 2800 cm^{-1} above the L_b origin in fluorescence excitation experiments on jet-cooled indole and perhaps more importantly it probably <u>cannot</u> be observed in such experiments (if it does, in fact, exist in this region) due to the rapid loss of quantum yield ca. 1500 cm^{-1} above the observed L_b origin.

Indole: QCFFBOZE Difference Density Scaled Results

Indole QCFFBOZE Geometry

The difference density scale factor obtained from the benzene C-C bond length change, χ=1.30, was applied directly to indole in order to compute new equilibrium geometries, normal coordinates, and displacements. The scaled L_b and L_a state equilibrium geometries are given in Table 12. Since the effect of the scaling is to amplify changes in bond lengths, the same qualitative changes in bond lengths with respect to their ground state values are observed as in the unscaled geometry shifts. Thus, the scaled excited state geometry changes for indole are in qualitative agreement with the INDO/S bond order changes, as was the case for the unscaled geometries. As in the unscaled case, the N-H bond length changes upon excitation are seen to be quite small, corroborating a non-dissociative L_a equilibrium geometry. The C2-C3 bond length changes are now seen to be 0.0487 Å for the L_b state, and 0.0812 Å for L_a.

TABLE 12. Indole geometry predicted by QCFFBOZE (bond lengths in angstroms, Å), difference density scale factor χ=1.30.

bond	ground	L_b	L_a	
N-C_2	1.4278	1.4515	1.4193	
C_2-C_3	1.3787	1.4274	1.4599	
C_3-C_9	1.4557	1.4250	1.4028	
C_4-C_9	1.4134	1.4163	1.4463	*
C_4-C_5	1.4006	1.4419	1.4307	*
C_5-C_6	1.4261	1.4443	1.4174	*
C_6-C_7	1.4021	1.4183	1.4569	*
C_7-C_8	1.4161	1.4337	1.4045	*
N-C_8	1.4175	1.3988	1.4264	
C_8-C_9	1.4230	1.4751	1.4603	*
N-H	1.0016	1.0012	1.0015	

(*) denotes bonds comprising the six-member ring.

QCFFBOZE Excitation Energies and Oscillator Strengths

The scaled indole excitation energies and oscillator strengths are contained in Table 13. The scaling of the diagonal elements of the CI matrix corresponds, roughly, to an increase in the excitation energies by a factor of χ from the unscaled values. However, in comparison with the unscaled vertical excitation energies, the separation of the L_b and L_a surfaces is reduced considerably upon application of difference density scaling. The L_a-L_b separation at the L_b geometry is reduced from 3828. cm^{-1} to 2765 cm^{-1}, while at the L_a geometry it is reduced from 1679 cm^{-1} to 349^{-1}. Again, as with the unscaled case, these excitation energy differences provide a qualitative picture of the excited state potential energy surfaces, the central feature being the reduction of the L_a-L_b surface separation as the indole geometry shifts from L_b to L_a. Detailed examination of the potential energy surfaces is presented in a later section.

The ratio of oscillator strengths for the scaled geometries are observed to decrease from the unscaled values. At the L_b geometry the ratio is now ~12, in contrast to the unscaled ratio of ~16. At the L_a geometry, the scaled ratio is now ~1, which is a dramatic reduction from the unscaled value of ~17. This large change in the oscillator strength ratio at the L_a geometry is consistent with the decreased gap between the two surfaces; there is significantly more mixing of L_b and L_a character. At this molecular configuration, the oscillator strengths for L_b and L_a are very nearly equal, reflecting the similar character of the wavefunctions. It is also important to note that since $(f_a + f_b) \sim 0.72$, the mixing is not strictly between L_b and L_a but includes contributions from a higher state as well. If this were not the case, the oscillator strength sum would stay near 0.35, as it is for canonical QCFF at the L_b geometry.

TABLE 13. Scaled (χ=1.30) QCFFBOZE vertical excitation energies (ν) and oscillator strengths (f) from the L_b and L_a equilibrium geometries.

	L(b) geometry		L(a) geometry	
	ν (cm^{-1})	f	ν (cm^{-1})	f
L_b	43889.	0.0411	43934.	0.3557
L_a	46654.	0.4913	44283.	0.3595

In addition, the effect of the scaling on the total molecular energy is of interest. Of course, as reflected by the increase in excitation energies, the net effect of the scaling will be to shift the energy upward. The scaled total energies for L_b and L_a were calculated to be -1326.165 kcal mol^{-1} and -1323.417 kcal mol^{-1}, respectively. From these values and the total energy of the ground state, we compute the energy of the origin transitions. For L_b, this corresponds to an origin at 58,954.55 cm^{-1}, and for L_a the origin is now at 59,915.35 cm^{-1}. The L_a origin is now seen to be ~961 cm^{-1} above the L_b origin; a net decrease from the unscaled origin difference of ~2829 cm^{-1}. This shift of the calculated L_a origin due to the difference density scaling places this transition into the experimentally accessible region in terms of quantum yield, and is in reasonable agreement with the proposed L_a origin; at this stage, we need only predict a value within the range 455-1450 cm^{-1} in order to have "agreement" with experiment.

Configuration Interaction Eigenvectors

The oscillator strength values corresponding to excitation from the L_a equilibrium presented in Table 13. are seen to be very nearly equal for the L_b and L_a electronic surfaces, which indicates strong mixing of these two states. The eigenvectors of the CI (singles) calculation define which states (L_b, L_a) correspond to the first and second singlet (S_1, S_2) excitations, respectively, through the relative sizes of the CI coefficients.

We present here the approximate form of the CI eigenvectors at the ground, L_b, and L_a equilibrium geometries in order to properly assign the transitions as S_1 and S_2.

We adopt the convention here that ψ represents the CI eigenvector, and ϕ_{ij} represents the wavefunction for excitation of a single electron from MO "i" to MO "j". We present only those CI eigenvector coefficients which are found to be ~0.20, since only these excitations contribute significantly to the CI eigenvector (in fact, only those coefficients ≥ 0.3 contribute $\geq 10\%$, so this is sufficient for our purposes). For excitation from the ground state geometry, the QCFF CI singles eigenvectors for the first and second roots of the CI matrix diagonalization are found to be

$\psi_1 = -0.59\,\phi_{57} - 0.74\,\phi_{46}$ and $\psi_2 = 0.91\,\phi_{56} + 0.18\,\phi_{47}$,

which shows the first excited singlet to be comprised of ~35% 5-->7 excitation, and ~55% 4-->6 excitation, whereas the second excited singlet is ~83% 5-->6 and ~3% 4-->7. To put this in perspective (in more transparent language), the first excited singlet is thus predicted to be a mixture of (HOMO-->LUMO+1) and (HOMO-1-->LUMO), while the second excited singlet is dominated by the (HOMO-->LUMO) transition, plus a minor contribution from (HOMO-1-->LUMO+1). This characterization of the S_1 and S_2 states is in agreement with INDO/S-SCI and INDO/S-SDCI results obtained by Callis (33) and serves to define the electronic structure of the L_b and L_a states.

In terms of this language, then, we conclude that for excitation from the ground state geometry, the S_1 transition is identified unambiguously as L_b and the S_2 transition is seen to be L_a. This situation of S_1=L_b and S_2=L_a correlation persists for the CI wavefunctions computed within the framework of QCFF, i.e. without the application of a difference-density scale factor, for both the L_b and L_a equilibrium geometries, as evidenced by the values of the oscillator strengths at the respective geometries (cf. Table 13.). For completeness, we present here the results for the S_1 and S_2 corresponding to these geometries computed by QCFF;

$\{L_b \text{ geometry}\}$ $\psi_1 = -0.59\,\phi_{57} - 0.75\,\phi_{46}$ and $\psi_2 = -0.91\,\phi_{56} + 0.37\,\phi_{47}$,

$\{L_a \text{ geometry}\}$ $\psi_1 = -0.61\,\phi_{57} - 0.74\,\phi_{46}$ and $\psi_2 = 0.96\,\phi_{56} - 0.24\,\phi_{47}$,

which are apart from (irrelevant) phase factors seen to be very close to the corresponding excited singlets computed at the ground state geometry.

The form of the QCFFBOZE difference-density scaled CI eigenvectors are of considerably more interest, since it is these eigenvectors on which we base our normal mode calculations, potential energy surfaces, and vibrational assignment. Since the scaling procedure does not apply (by definition) to the ground state, the MO's involved are the same and provide the basis for comparison. The results for the CI eigenvectors with difference-density scaling (1.30) are presented below for both the L_b and L_a QCFFBOZE equilibrium geometries of Table 12.

$\{L_b \text{ geometry}\}$ $\psi_1 = -0.57\,\phi_{57} - 0.78\,\phi_{46}$ and $\psi_2 = -0.93\,\phi_{56} + 0.31\,\phi_{47}$,

$\{L_a \text{ geometry}\}$ $\psi_1 = -0.61\,\phi_{56} + 0.47\,\phi_{57} + 0.61\,\phi_{46}$

and $\psi_2 = 0.76\,\phi_{56} + 0.40\,\phi_{57} + 0.44\,\phi_{46}$.

The extent of L_b-L_a mixing is clearly evidenced by the composition of these eigenvectors: at the L_b equilibrium geometry, the S_1 and S_2 vectors retain their respective L_b and L_a character, and are in basic agreement with the QCFF (unscaled) eigenvectors. At the L_a geometry, however, there is extensive mixing; the basic forms of the S_1 and S_2 eigenvectors are observed to be very similar.

At the L_a geometry, as prescribed through the CI eigenvectors, it is not possible to assign strict L_b and L_a character to the first two excited singlets. The nearly identical character of these eigenvectors is a strong indication of a near-crossing of the potential

energy surfaces of the two electronic states (i.e. a near-degeneracy). The true character of this region on the L_b-L_a surfaces will be elucidated in a later section, but there is one important fact which arises from this examination of the CI eigenvectors: The L_b and L_a wavefunctions exhibit strong mixing in the region of the L_a equilibrium geometry, indicating an avoided crossing of these surfaces near the L_a PES minimum because the QCFFBOZE difference-density scaling procedure effectively pushes the L_b and L_a surfaces closer together than their QCFF (unscaled) counterparts.

The implications of this coupling of the sufaces are pervasive in terms of the overall bandshape which QCFFBOZE predicts; the mixed character imparted to both S_1 and S_2 transitions corrupts the "pure" L_b and L_a nature of these states. The S_1 transition is now seen to contain a large component of the (HOMO-->LUMO) configuration attibuted to L_a, while the S_2 transition now contains a significant contribution from the (HOMO-1-->LUMO) configuration. The (HOMO-1-->LUMO+1) configuration generally attributed to L_a makes an insignificant contribution to S_2; the eigenvector coefficient for 4-->7 is observed to be -0.20, corresponding to a contribution of only ~4%. There is thus a sufficient amount of L_b character transferred to S_2 that vibronic bandshapes computed for this transition will appear "L_b-like", since the CI eigenvector for S_2 is no longer dominated by the (HOMO-->LUMO) configuration. The S_1 transition retains a significant amount of L_b character, but this is problematic; we now have S_1 and S_2 transitions which are primarily L_b and the calculated bandshapes will reflect this. Evidently, the Condon approximation breaks down in the region of the S_2 equilibrium geometry, and the electronic wavefunctions in this region are very strongly dependent on the nuclear coordinates, **Q**. In this situation, the more appropriate picture is not one of adiabatic (i.e. Born-Oppenheimer) potential energy surfaces but rather <u>diabatic</u> surfaces in which the nuclear kinetic energy is incorporated into the Hamiltonian. For the diabatic picture, the potential surfaces are allowed to cross. This is due to the nuclear kinetic

energy coupling, which gives rise to non-adiabatic terms which transfer probability amplitude between surfaces (84,102-105). In order to approach the diabatic limit, we require either (a) outright modification of the molecular Hamiltonian or (b) an approximate approach which essentially "turns off" the repulsion of the adiabatic surfaces.

"Frozen" Configuration Interaction (CI) for the S_2 State

In order to correct for the effective repulsion (i.e. avoided crossing) of the L_b and L_a surfaces which is predicted by the difference-density scaling procedure, we propose the following modification of the CI singles calculation for the S_2 (nominally L_a) electronic state;

(i) The L_b geometry is input as the starting geometry for the SCF procedure involving the second excited state (nex=2) in QCFFBOZE.

(ii) The CI Hamiltonian matrix is constructed at the L_b geometry and diagonalized in the usual way to obtain eigenvalues (excitation energies) and eigenvectors (CI coefficients).

(iii) The eigenvalues and eigenvectors obtained in step ii. are saved. In subsequent calls to the CI subroutine, the CI Hamiltonian is constructed but is not diagonalized.

(iv) The excited state coefficients in the potential energy expression are constructed in the usual way, employing the eigenvectors from step ii.

Formally, this procedure corresponds to neglecting the off-diagonal elements of the CI matrix and shall be termed (albeit erroneously) "frozen CI", since the eigenvalues utilized in the calculation are those obtained at the reference geometry. In this way, the potential energy surfaces so constructed are not rigorously adiabatic PE surfaces; rather, they are closer to an effective "diabatic" picture, in which the coupling between the S_1 and S_2 is turned off in the region of the avoided-crossing. The result of invoking a diabatic treatment of the surfaces is that the mixing of the two states is removed,

producing "pure" L_b and L_a surfaces and an L_a equilibrium geometry which is decoupled from the crossing zone. The resulting CI eigenvectors for the "frozen CI" calculation using the L_b reference geometry are as follows;

$$\{L_a \text{ geometry}\} \quad \psi_1 = -0.57\,\phi_{57} - 0.78\,\phi_{46} \quad \text{and} \quad \psi_2 = -0.93\,\phi_{56},$$

which are seen to be very close to those obtained in the standard scaling procedure at the L_b geometry. This is not a surprising result -- these eigenvectors are, in fact, exactly prescribed at the L_b geometry, displaced only very slightly by one SCF iteration.

This "frozen CI" calculation does manage to maintain the L_a character of the S_2 state in the region of the avoided crossing, albeit in an artificial way. This result is more clearly evidenced by the oscillator strength values which are obtained from the above CI eigenvectors. For S_1, an oscillator strength of 0.0470 is obtained, while for S_2 the oscillator strength is 0.551; these values are more representative of L_b and L_a character. In fact, these values are closer to the (unscaled) QCFF values presented in Table 10., which is consistent with the similarity between the QCFF CI eigenvectors and those obtained from the QCFFBOZE frozen CI calculation at the S_2 potential minimum.

The geometry obtained from the frozen CI calculation is of particular interest. This is presented in Table 14., along with the standard QCFFBOZE geometries.

The L_a geometry obtained from the frozen CI calculation mimics the bond length changes of the ground-L_a distortion calculated by the QCFFBOZE scaling procedure in that the sign of the bond length changes are in agreement in all cases. In four of the bonds, however, the bond length changes are observed to be smaller in magnitude than those obtained from the standard scaled calculation. In particular, the N-C_2, C_3-C_9, C_4-C_5, and C_8-C_9 bond length changes for the frozen CI calculation are not as large as the corresponding bond length changes in the QCFFBOZE L_a calculation. The first two of

these bonds, located on the five-member ring, are seen to decrease less in the frozen CI calculation; the last two bonds are seen to increase less. The point is not so much how different the QCFFBOZE L_a geometry is from the frozen CI L_a geometry; rather, it needs to be emphasized how similar they are. In the present context, a "large" bond length change is on the order of ~0.01 Å, while a "small" change is typically ~0.001 Å. In other words, bond length changes of ~1% could well be characterized as "large" -- and bond length changes on the order of a few percent (as is the case for the geometry shift between the ground state and the $L_{a,b}$ states) could well be termed "significantly large".

TABLE 14. Indole geometry predicted by QCFFBOZE (bond lengths in angstroms, Å), difference density scale factor χ=1.30.

bond	ground	L_b	L_a		L_a frozen CI	
N-C_2	1.4278	1.4515	1.4193		1.4148	(< -)
C_2-C_3	1.3787	1.4274	1.4599		1.4703	
C_3-C_9	1.4557	1.4250	1.4028		1.3944	(< -)
C_4-C_9	1.4134	1.4163	1.4463	*	1.4591	
C_4-C_5	1.4006	1.4419	1.4307	*	1.4229	(< +)
C_5-C_6	1.4261	1.4443	1.4174	*	1.4112	
C_6-C_7	1.4021	1.4183	1.4569	*	1.4722	
C_7-C_8	1.4161	1.4337	1.4045	*	1.3928	
N-C_8	1.4175	1.3988	1.4264		1.4325	
C_8-C_9	1.4230	1.4751	1.4603	*	1.4585	(< +)
N-H	1.0016	1.0012	1.0015		1.0013	

note; (<) denotes frozen CI calculated bond length changes which are less than their counterparts calculated from standard QCFFBOZE with difference density scaling.

This is not a trivial point. In fact, it runs counter to the viewpoint of Barstis, et al., who conclude that indole does not significantly change size upon excitation. To put the best face on the whole issue, the relative changes in bond lengths are most accurately charcterized not so much in terms of percent change but rather in terms of the projection

of each normal coordinate onto the geometry shift and, by extrapolation, the spectral bandwidth which results from these bond length changes.

Indole Normal Coordinate Analysis

The normal coordinate analysis for indole is relatively simple from the perspective of group theory. Indole belongs to the Cs point group, for which the only symmetry elements are the identity (the molecule itself) and the horizontal plane of the molecule. The irreducible representation of the (3n-6 = 42) vibrations is comprised of 29 A' (in-plane) and 13 A" (out-of-plane) modes, i.e. Γ_{vib} = 29 A' + 13 A". In the conventional notation for these modes, the in-plane modes are numbered 1-29 in order of decreasing frequency, and out-of-plane modes are issued 30-42, also in order of decreasing frequency. Thus, for example, mode 29 (ν_{29}) is the lowest frequency in-plane vibration. Modes 43-48 are the six trivial vibrations exhibiting zero frequency -- 3 translations and 3 rotations -- and are of no spectroscopic consequence and are omitted from any further discussion.

The signature of the in-plane (A') modes is that they can possess displacement. Since these vibrational motions occur within the plane of the molecule, they can "project" one equilibrium geometry (e.g. the ground state) onto a different equilibrium geometry (e.g. L_b or L_a excited states). The extent of this projection shows how much a particular vibration "looks" like the geometry difference between two states. In fact, this projection or displacement is precisely the normal coordinate displacement defined in Chapter Two in the general discussion of Franck-Condon factors, i.e.

$$\Delta \mathbf{Q}' = (\mathbf{L}')^T \mathbf{m}^{1/2} \Delta \mathbf{r}.$$

Recall that this expression says that the displacement of a normal coordinate, Q, in a particular electronic state is given by the projection of the vibrational coordinates onto the geometry difference between the initial and final states. The root-mass diagonal

matrix is introduced since we have adopted mass-weighted normal coordinates.

The out-of-plane (A") vibrational modes cannot have displacement (i.e. in a planar molecule), and these modes are characterized by $\Delta Q_k = 0$. In this way, we can catagorize the computed normal modes and perform a symmetry assignment simply by grouping modes with non-zero displacement and then sorting these two groups by frequency.

One problem remains. Even after having performed the normal mode calculation and the symmetry assignment, it is difficult (and, in some cases, impossible) to identify vibrational structure in an experimental spectrum with the associated normal modes. This process -- the vibrational assignment of the spectrum -- is complicated by the fact that the measured transitions do not exhibit information which is indicative of particular displacements of atoms during the course of a vibration. The situation is complicated further still by the fact that the harmonic approximation is just that -- an approximation -- and there are terms in the Hamiltonian which have been neglected in performing a normal mode calculation. In a very real sense, molecules "diagonalize their own Hamiltonian" (97), and this (exact) Hamiltonian contains interaction terms which are neglected at the harmonic level of approximation. Thus, a simple frequency-based assignment will in almost all cases lead to significant errors in the assignment of transitions. The situation is improved somewhat through the calculation of Franck-Condon factors, which provides information regarding the transition intensities which are then compared with the spectrum. Even at this level, however, there will remain ambiguity regarding the identification of a particular transition with the relative motion of the atoms for the vibrational mode. For this reason, the vibrational assignment is an altogether complicated, iterative, semiempirical process which must be approached with caution. The first and perhaps most important step in such an assignment is, of course, a thorough normal coordinate analysis.

The normal coordinate analysis can be outlined as follows. First, the normal modes

of vibration for the various electronic surfaces must be computed. Following this, the six trivial vibrations are identified as the zero-frequency modes and removed from the set of vibrations, resulting in 3n-6 true vibrational modes. These modes are then transformed, if necessary, into the coordinate system of choice. QCFF, in particular, provides automatically for normal modes in terms of internal coordinates; we have suitably modified QCFF to extract the modes in Cartesian coordinates, which standard QCFF provides but does not write as output.

The next stage of the analysis requires calculation of the normal coordinate displacements and, in our work, calculation of the Duschinsky rotation matrix since we choose to incorporate this effect. Franck-Condon factors are then computed for the origin, fundamental, overtone, and combination transitions involving the initial and final states of interest. From this information, the vibrational assignment can then be approached. Finally, the computed FC factors can be utilized to prepare a computed spectrum, or spectral bandshape, for comparison with experiment.

Indole Vibrational Frequencies and Displacements

The normal coordinate information for the QCFFBOZE difference density scaled indole L_b and L_a states are displayed in Tables 15a and 15b. The QCFF unscaled ground state frequencies are also presented in the leftmost column of both tables. The modes have been assigned according to the conventional notation; ν_1-ν_{29} are the in-plane A' modes, and ν_{30}-ν_{42} are the out-of-plane A" modes. The units and dimensions are annotated in the key at the bottom of the table.

Modes 1-7 are primarily high-frequency (ca. 3000+ cm^{-1}) N-H and C-H stretch modes which exhibit very small displacements in both the L_b and L_a states. The distinction can be made here between these modes and the spectroscopically important "skeletal modes", 8-29, which experience sufficient displacement to cause significant

TABLE 15a. QCFFBOZE indole L_b normal coordinates.

ω/cm^{-1}	ΔQ	S	λ
3105	-0.0001	-0.0010	0.0000
3099	-0.0036	-0.0345	0.0006
3092	0.0006	0.0058	0.0000
3091	-0.0031	-0.0297	0.0004
3086	0.0002	0.0019	0.0000
3086	0.0034	0.0325	0.0005
3081	-0.0010	-0.0096	0.0000
1630	0.0030	0.0209	0.0002
1544	-0.0102	-0.0691	0.0024
1488	-0.0439	-0.2917	0.0425
1484	0.0210	0.1393	0.0097
1426	-0.0887	-0.5770	0.1665
1406	-0.0263	-0.1699	0.0144
1379	0.0400	0.2558	0.0327
1354	0.0805	0.5103	0.1302
1290	0.0115	0.0711	0.0025
1259	-0.0696	-0.4254	0.0905
1236	-0.0493	-0.2986	0.0446
1153	0.0074	0.0433	0.0009
1107	-0.0332	-0.1902	0.0181
1096	0.0197	0.1124	0.0063
1032	-0.0794	-0.4395	0.0966
1005	0.0980	0.5353	0.1433
896	-0.0186	-0.0959	0.0046
823	0.1910	0.9440	0.4455
757	-0.0082	-0.0389	0.0008
587	0.0018	0.0075	0.0000
545	0.0033	0.0133	0.0001
456	-0.0242	-0.0891	0.0040

NOTE: ΔQ = normal coordinate projection = $m^{1/2}(L'')^T\Delta r$

S = dimensionless displacement

$\lambda = (1/2)\ S^2$

TABLE 15b. QCFFBOZE indole L_a normal coordinates.

ω/cm^{-1}	ΔQ	S	λ
3105	0.0000	0.0000	0.0000
3099	-0.0032	-0.0307	0.0005
3092	0.0000	0.0000	0.0000
3091	-0.0035	-0.0297	0.0004
3087	0.0006	0.0057	0.0000
3086	0.0024	0.0230	0.0003
3081	-0.0008	-0.0077	0.0000
1637	-0.0934	-0.6508	0.2118
1567	-0.0621	-0.4234	0.0896
1497	0.0095	0.0633	0.0020
1473	0.0362	0.2393	0.0286
1447	0.0163	0.1068	0.0057
1385	0.0666	0.4270	0.0912
1373	-0.0991	-0.6326	0.2001
1357	-0.0762	-0.4835	0.1169
1291	-0.0233	-0.1442	0.0104
1254	0.1023	0.6240	0.1947
1224	-0.0206	-0.1242	0.0077
1155	-0.0075	-0.0439	0.0010
1107	0.0414	0.2373	0.0282
1087	-0.0685	-0.3890	0.0757
1045	-0.0897	-0.4996	0.1248
1015	-0.0805	-0.4419	0.0976
896	-0.0022	-0.0114	0.0001
832	0.1558	0.7743	0.2997
758	-0.0095	-0.0450	0.0010
589	-0.1619	-0.6770	0.2292
544	0.0762	0.3063	0.0469
453	0.0099	0.0363	0.0007

NOTE: $\Delta \mathbf{Q}$ = normal coordinate projection = $m^{1/2}(L'')^T \Delta \mathbf{r}$

S = dimensionless displacement

$\lambda = (1/2)\ S^2$

decreases in the origin intensity and to exhibit progressions. Although the N-H and C-H stretch modes are in-plane vibrations, the relatively small mass coupled with the small amplitude of the motions leads to very small values of lambda for these modes. We include these modes in all the calculations of Franck-Condon factors, but they are of very little consequence in uv-vis spectroscopy. In addition, modes 1-7 do not mix with the skeletal modes (although they do mix with each other in a trivial sense) due to vibrational adiabaticity (44,92) and the fact that their eigenvectors do not map onto the geometry difference vector for distortion of the molecular frame.

It is immediately obvious by examining the projections of modes 8-29 that the vibrational modes for indole are dramatically different in character than those of benzene. Whereas in benzene there is only one significantly displaced mode, the a_{1g} ring-breathing mode, in indole there are essentially 22 modes exhibiting displacement and all of the displacements are relatively small. This is seen more clearly through the parameter, λ, which is (at the Poisson model level) the ratio of the fundamental to the origin transition for a particular mode. This situation of several modes with small displacements has two immediate consequences in terms of the qualitative appearance of spectral bandshapes computed with these parameters. First, the relatively small values of lambda produce overtone progressions which rapidly decay in intensity with increasing number of quanta in the mode(s). Second, the computed spectrum will be reasonably sparse in terms of the overall density of transitions (this depends, however, on how many modes exhibit displacement). Of course, the out-of-plane modes achieve Franck-Condon intensity through frequency changes, resulting in overtone progressions (and to a lesser extent, combinations) which provide some intensity to the overall bandshape. Nonetheless, the computed progressions can be anticipated to be short in terms of number of vibrational quanta.

It is worthwhile to examine in some detail the quality of the QCFFBOZE vibrational

frequencies and the features of the ground-excited state frequency distortion. Table 16 contains the symmetry-ordered A' and A" mode frequencies for the ground, L_b, and L_a excited states and the associated frequency differences. All calculated frequencies (both A' and A" vibrations) are observed to decrease upon excitation for both excited states, which is consistent with the intuitive idea of weaker force constants in the excited states. The high-frequency (ca. 3000+ cm^{-1}) stretching vibrations are seen to incur very small decreases upon excitation, typically 1-2 cm^{-1}. The remaining A' modes (8-29) exhibit frequency decreases ranging from -1 cm^{-1} to -68 cm^{-1}(for the L_b v_9, representing a decrease of ~4.2%).

In the out-of-plane modes, the frequency shifts are typically larger than for the in-plane modes. For example, v_{30} is seen to decrease by 205 cm^{-1} for the L_a state, representing a change of ~18%. The frequency distortion for the A" modes is of considerable importance, since these modes gain Franck-Condon intensity through frequency changes (rather than displacement). In a later section, we present a model calculation of first overtones (2 quanta) based on the frequency shift to quantitatively demonstrate this phenomenon.

We consider now the error associated with the calculated QCFFBOZE frequencies. For the ground state of indole, reasonably comprehensive vibrational assignments have been possible, due primarily to the one-photon allowed character of all fundamental transitions. In particular, Bickel, et al. (12) obtained 29 ground state frequencies via analysis of SVLF data. Lautie, et al. (98) provide a complete set of (42) ground state frequencies from IR- and resonance Raman spectroscopies. Takeuchi and Harada (T-H) (32) performed a normal coordinate analysis for indole by constructing a force field based on the experimental data of T-H which provides frequencies which are in close agreement with the IR and RR values and allowed corroboration of the assignments by Lautie, et al.. Suwaiyan and Zwarich (99) performed polarized IR experiments on

TABLE 16. QCFFBOZE indole vibrational frequencies for the ground (S_0), L_b, and L_a electronic states.

A' in-plane vibrational frequencies

$\omega(S_0)/cm^{-1}$	$\omega(L_b)/cm^{-1}$	$\omega(L_a)/cm^{-1}$
3105	3105	3105
3101	3099	3099
3093	3092	3092
3093	3091	3091
3088	3086	3087
3087	3086	3086
3082	3081	3081
1647	1630	1637
1612	1544	1567
1532	1488	1497
1501	1484	1473
1476	1426	1447
1434	1406	1385
1407	1379	1373
1371	1354	1357
1293	1290	1291
1260	1259	1254
1248	1236	1224
1157	1153	1155
1116	1107	1107
1113	1096	1087
1050	1032	1045
1027	1005	1015
902	896	896
854	823	832
767	757	758
599	587	589
551	545	544
457	456	453

A" out-of-plane vibrational frequencies

$\omega(S_0)/cm^{-1}$	$\omega(L_b)/cm^{-1}$	$\omega(L_a)/cm^{-1}$
1144	970	939
1057	904	922
1020	875	889
935	845	842
883	767	769
792	713	691
747	664	660
692	602	617
526	473	470
519	448	465
411	359	355
254	225	234
211	190	188

partially oriented ndole crystals to obtain values for the out-of-plane modes. Collier (100) performed IR and Raman experiments coupled with a semiempirical (AM1) force field calculation in an attempt to verify assignments of both A' and A" modes. Majoube and Vergoten (26) performed ab-initio calculations at the 3-21G basis set level to support their FT-IR experiments on indole and deuterated indoles, and provide a complete set of frequencies which involve the introduction of scale factors for in- and out-of-plane frequencies. More recently, Barstis, et al. (25) have performed jet-cooled one-color resonant two-photon ionization (1C R2PI) of indole and deuterated indoles in effort to assign the L_a origin. In conjunction with the 1C-R2PI experiments, they provide an ab-initio calculation of the ground state indole frequencies from Gaussian 90.

In addition to this rather extensive indole "data-base" of vibrational frequencies, Callis, et al. (4-7,19) have focused efforts on indole, deuterated indoles, and methyl-indoles with a solid emphasis on elucidation of L_b and L_a character of one- and two-photon transitions. Calculations utilizing the AMPAC package (101) within the Callis Group have been used as a semi-quantitative guide to the vibrational frequencies in indole and 3-methylindole.

In order to access the accuracy of the QCFFBOZE calculated frequencies, we compare them with the ground state frequencies obtained by Bickel, et al. (SVLF), Takeuchi and Harada (semiempirical force field), and Lautie, et al. (IR and Raman). In addition, Bickel, et al. have provided assignments for nine L_b modes (4 A', 5 A"), and we compare the QCFFBOZE L_b modes with these. The results of this analysis are provided in Tables 17-19.

The agreement between QCFFBOZE in-plane modes and the assignment of Bickel, et al. is rather encouraging. In most cases, the QCFFBOZE calculated ground state modes are higher than the experimental assignment, with a relative error of only a few percent. The lowest frequency in-plane mode, ν_{29}, is seen to be in error by ~15%, which

TABLE 17. Comparison of QCFFBOZE indole ground state vibrational frequencies with experiment (Bickel, et al., ref. 12).

mode	ω(calc.)/cm-1	ω(exp.)/cm-1	Δω/cm-1	rel. error
		A' in-plane modes		
11	1501	1479	- 22.	1.49
12	1476	1459	-17.	1.17
13	1434	1410	-24.	1.70
14	1407	1350	-57.	4.22
15	1371	1278	-93.	7.28
16	1293	1248	-45.	3.61
17	1260	1208	-52.	4.30
18	1248	1185	-63.	5.32
19	1157	1143	-14.	1.22
20	1116	1123	7.	0.62
21	1113	1085	-28.	2.58
22	1050	1068	18.	1.18
23	1027	1015	-12.	2.19
24	902	902	0.	0.00
25	854	876	22.	2.51
26	767	759	-8.	1.05
27	599	609	10.	1.64
28	551	542	-9.	1.66
29	457	396	-61.	15.40
		A" out of plane modes		
30	1144	971	-173.	17.82
31	1057	925	-132.	14.27
32	1020	849	-171.	20.14
33	935	765	-170.	22.22
34	883	738	-145.	19.65
35	792	715	-77.	10.77
36	747	602	-145.	24.09
37	692	570	-122.	21.40
38	526	480	-46.	9.58
39	519	420	-99.	23.57
40	411	403	-8.	1.99
41	254	241	-13.	5.39
42	211	208	- 3.	1.44

TABLE 18. Comparison of QCFFBOZE indole ground state vibrational frequencies with experiment (Takeuchi and Harada, ref. 32).

mode	ω(calc.)/cm^{-1}	ω(exp.)/cm^{-1}	Δω/cm^{-1}	rel. error
		A' in plane modes		
8	1647	1616	-31.	1.92
9	1612	1573	-39.	2.48
10	1532	1508	-24.	1.59
11	1501	1486	-15.	1.01
12	1476	1467	-9.	0.61
13	1434	1413	-21.	1.49
14	1407	1347	-60.	4.45
15	1371	1290	-81.	6.28
16	1293	1246	-47.	3.77
17	1260	1207	-53.	4.39
18	1248	1185	-63.	5.32
19	1157	1146	-11.	0.96
20	1116	1117	1.	0.09
21	1113	1096	-17.	1.55
22	1050	1063	13.	1.22
23	1027	1005	-22.	2.19
24	902	905	3.	0.33
25	854	867	13.	1.50
26	767	763	-4.	0.52
27	599	608	9.	1.48
28	551	543	-8.	1.47
29	457	398	-59.	14.82
		A" out of plane modes		
30	1144	971	-173.	17.82
31	1057	934	-123.	13.17
32	1020	853	-167.	19.58
33	935	780	-155.	19.87
34	883	748	-135.	18.05
35	792	722	-70.	9.70
36	747	607	-140.	23.06
37	692	586	-106.	18.09
38	526	488	-38.	7.79
39	519	426	-93.	21.83
40	411	403	-8.	1.99
41	254	256	2.	0.78
42	211	225	14.	6.22

TABLE 19. Comparison of QCFFBOZE indole ground state vibrational frequencies with experiment (Lautie, et al., ref. 32).

mode	ω(calc.)/cm^{-1}	ω(exp.)/cm^{-1}	$\Delta\omega$/cm^{-1}	rel. error
		A' in plane modes		
8	1647	1616	-31.	1.92
9	1612	1576	-36.	2.28
10	1532	1509	-23.	1.52
11	1501	1487	-14.	0.94
12	1476	1455	-21.	1.44
13	1434	1412	-22.	1.56
14	1407	1352	-55.	4.07
15	1371	1276	-95.	7.45
16	1293	1245	-48.	3.86
17	1260	1203	-57.	4.74
18	1248	1191	-57.	4.79
19	1157	1147	-10.	0.87
20	1116	1119	3.	0.27
21	1113	1092	-21.	1.92
22	1050	1064	14.	1.32
23	1027	1010	-17.	1.68
24	902	895	-7.	0.78
25	854	873	19.	2.18
26	767	758	-9.	1.19
27	599	607	8.	1.32
28	551	542	-9.	1.66
29	457	397	-60.	15.11
		A" out of plane modes		
30	1144	970	-174.	17.94
31	1057	930	-127.	13.66
32	1020	848	-172.	20.28
33	935	767	-168.	21.90
34	883	743	-140.	18.84
35	792	725	-67.	9.24
36	747	608	-139.	22.86
37	692	575	-117.	20.35
38	526	487	-39.	8.01
39	519	423	-96.	22.70
40	411	403	-8.	1.99
41	254	240	-14.	5.83
42	211	207	-4.	1.93

TABLE 20. Comparison of QCFFBOZE indole L_b vibrational frequencies with experiment (Bickel, et al., ref. 32).

mode	ω(calc.)/cm^{-1}	ω(exp.)/cm^{-1}	Δω/cm^{-1}	rel. error
		A' in plane modes		
26	757	718	-39.	5.43
27	587	540	-47.	8.70
28	545	480	-65.	13.54
29	456	380	-76.	20.00
		A" out of plane modes		
36	664	498	-166.	33.33
37	602	369	-233.	63.14
39	448	278	-170.	61.15
41	225	183	-42.	22.95
42	190	158	-32.	20.25

is the largest error within the A' set. The out-of-plane modes are not in nearly as good agreement with the values assigned by Bickel, et al.; the relative error in these modes is seen to range from ~2% to as high as ~24%. The situation is very similar for the comparison with the experimental values of Lautie, et al., which leads to the general conclusion that QCFFBOZE predicts in-plane vibrational frequencies much better than out-of-plane frequencies.

Interestingly, the same trend in the relative error is seen in the comparision with the frequencies obtained by Takeuchi and Harada. The force field constructed by T-H is designed specifically for indole, while the QCFF parameterization is much more general. If anything, the close agreement with experiment of the frequencies obtained by T-H demonstrates the greater accuracy of a molecule-specific force field.

Lastly, in Table 20 we present the comparison of QCFFBOZE L_b vibrational frequencies with the available assignment of Bickel, et al.. The four in-plane modes (26,27,28,29) are in reasonable agreement with experiment (≤20%), but only in a qualitative sense. The five out-of-plane modes are considerably worse, with a minimum relative error of ~20%. This poses some difficulty in terms of the quality of calculated Franck-Condon factors for overtone transitions in these modes, but this can be dealt with by performing a simple model calculation to relate the error in the frequency shift to the associated error in the overtone FC factors.

Duschinsky Rotation Analysis; Excited State Mode-Mixing

It is not rigorously correct to make a one-to-one identification of the L_b and L_a modes with their ground state counterparts, even though all modes have been symmetry assigned in exactly the same manner. This is a manifestation of the Duschinsky effect, the net result of which is the excited state modes being described as linear combinations of the ground state modes. In some modes, however, the Duschinsky effect is very

minor and this permits a reasonable "parallel modes" identification of vibrations in different electronic states. We have computed the Duschinsky rotation matrix for the L_b and L_a modes in terms of an expansion in ground state modes, i.e.,

$$\mathbf{Q'} = \mathbf{S}\,\mathbf{Q} + \Delta\mathbf{Q'}$$

in which **S** represents the Duschinsky rotation matrix. In component form, this matrix-vector relation takes on the very transparent appearance;

$$Q'_k = \Sigma_i S_{ki} Q_i + \Delta Q'$$

in which the k-th excited state normal coordinate is seen to be a linear combination of ground state coordinates, plus a displacement term. Formally, this is of the form of a rotation (S) coupled to a translation (Δ) of the coordinate. The ground state modes thus provide the basis set for the expansion.

The results of this Duschinsky rotation analysis for the difference density scaled L_b and L_a modes are presented in Tables 21a and 21b, respectively. In these calculations, we present only those Duschinsky rotation matrix elements S_{ki} (i.e. expansion coefficients) which are $\geq$0.20. In most cases, as evidenced by the coordinate expansions in 14a-b, there is one primary mode with $S_{ki} \geq 0.9$ which makes the major contribution to an excited state mode. Note also that the coefficients are normalized such that the sum of their squares for a given coordinate is equal to unity (or very close).

These expansions provide a quantitative picture of how the excited state modes differ from their parent forms in the ground state. There are two cases of trivial Duschinsky rotation in which an excited state mode is the exact counterpart of a ground state mode. First, there is the case of simple frequency reordering; the only difference between an excited state mode and the corresponding ground state mode is a change in frequency. The other possibility is a trivial change in phase for a given mode; the amplitudes are identical in magnitude for ground and excited state but the sign is reversed. In both cases, these modes are clearly evidenced by a unit matrix element, S_{ki}.

TABLE 21a. Expansion of S_1 normal coordinates in the ground state coordinate basis.

$$Q_{11} = 0.2180\,Q''_{9} - 0.8653\,Q''_{10} + 0.4256\,Q''_{12}$$

$$Q_{12} = 0.2339\,Q''_{10} + 0.2643\,Q''_{11} + 0.5447\,Q''_{12} + 0.6371\,Q''_{13} + 0.3810\,Q''_{14}$$

$$Q_{13} = 0.3162\,Q''_{10} + 0.6699\,Q''_{12} - 0.4655\,Q''_{13} - 0.4525\,Q''_{14}$$

$$Q_{14} = 0.3927\,Q''_{13} - 0.5501\,Q''_{14} + 0.7128\,Q''_{15}$$

$$Q_{15} = 0.4067\,Q''_{13} - 0.5758\,Q''_{14} - 0.6934\,Q''_{15}$$

$$Q_{17} = -0.8948\,Q''_{17} + 0.4051\,Q''_{18}$$

$$Q_{18} = 0.3847\,Q''_{17} + 0.9012\,Q''_{18}$$

$$Q_{31} = -0.7760\,Q''_{31} + 0.6091\,Q''_{32}$$

$$Q_{33} = 0.6043\,Q''_{31} + 0.7841\,Q''_{32}$$

$$Q_{34} = 0.2005\,Q''_{33} + 0.9767\,Q''_{34}$$

$$Q_{35} = 0.2309\,Q''_{30} + 0.8736\,Q''_{35} - 0.3946\,Q''_{36}$$

$$Q_{36} = -0.4247\,Q''_{35} - 0.8943\,Q''_{36}$$

$$Q_{38} = -0.8142\,Q''_{38} + 0.5731\,Q''_{39}$$

$$Q_{39} = 0.5669\,Q''_{38} + 0.8015\,Q''_{39}$$

TABLE 21b. Expansion of S_2 normal coordinates in the ground state coordinate basis.

$$Q_8 = 0.9234\,Q''_8 + 0.2897\,Q''_9$$
$$Q_9 = 0.2678\,Q''_8 - 0.8863\,Q''_9 - 0.2460\,Q''_{10} - 0.2562\,Q''_{11}$$
$$Q_{10} = -0.3221\,Q''_9 + 0.4426\,Q''_{10} + 0.5925\,Q''_{11} - 0.2057\,Q''_{14}$$
$$Q_{11} = 0.2146\,Q''_8 - 0.6344\,Q''_{10} + 0.6517\,Q''_{11} + 0.2940\,Q''_{12}$$
$$Q_{12} = -0.2630\,Q''_{11} - 0.8679\,Q''_{13} - 0.3226\,Q''_{14}$$
$$Q_{13} = -0.4286\,Q''_{10} - 0.6883\,Q''_{12} + 0.4571\,Q''_{14} - 0.2563\,Q''_{15}$$
$$Q_{14} = 0.2691\,Q''_{10} + 0.2950\,Q''_{12} - 0.3325\,Q''_{13} + 0.4750\,Q''_{14} - 0.6570\,Q''_{15}$$
$$Q_{15} = -0.2864\,Q''_{13} + 0.6016\,Q''_{14} + 0.6932\,Q''_{15}$$
$$Q_{16} = 0.8682\,Q''_{16} + 0.4165\,Q''_{18}$$
$$Q_{17} = 0.4455\,Q''_{16} + 0.4486\,Q''_{17} - 0.7357\,Q''_{18}$$
$$Q_{18} = 0.8364\,Q''_{17} + 0.4609\,Q''_{18}$$
$$Q_{20} = 0.9606\,Q''_{20} - 0.2211\,Q''_{22}$$
$$Q_{30} = 0.9111\,Q''_{30} - 0.2307\,Q''_{33} - 0.2214\,Q''_{35} - 0.2214\,Q''_{36}$$
$$Q_{31} = -0.9411\,Q''_{31} - 0.2683\,Q''_{34}$$
$$Q_{32} = -0.2121\,Q''_{30} - 0.9439\,Q''_{33} + 0.2050\,Q''_{34}$$
$$Q_{33} = -0.2109\,Q''_{31} + 0.9465\,Q''_{32} + 0.2082\,Q''_{34}$$
$$Q_{34} = 0.2064\,Q''_{31} - 0.2427\,Q''_{32} - 0.2062\,Q''_{33} - 0.8819\,Q''_{34} - 0.2525\,Q''_{35}$$
$$Q_{35} = 0.2613\,Q''_{30} - 0.2172\,Q''_{34} + 0.9228\,Q''_{35}$$
$$Q_{38} = 0.4970\,Q''_{38} - 0.8625\,Q''_{39}$$
$$Q_{39} = -0.8598\,Q''_{38} - 0.4892\,Q''_{39}$$

One feature common to both the L_b and L_a normal coordinate expansions is that the in-plane (A') modes cannot mix with the out-of-plane (A") modes, as these sets of modes belong to different irreducible representations. We therefore do not observe any mixing between the sets of modes {1-29} and {30-42}, as must be the case.

By comparison of Table 21a. and 21b., it is immediately clear that more L_a modes are mixed than are L_b modes. It is important to realize that this mode mixing cannot be attributed to the greater displacement of the L_a surface, since the interplay between displacement and Duschinsky rotation is not manifested at the level of the Duschinsky transformation ($Q'_k = \Sigma_i S_{ki} Q_i + \Delta Q'$), which shows these effects are separable. The different extent of mixing for L_b and L_a is a consequence of the different electronic structure in these states, and so a general explanation is that the L_b electronic structure is more similar to that of the ground state than is L_a.

In the L_b normal coordinates, the form of these vibrations is seen to be quite similar to the ground state vibrations. For examples, modes 17 and 18 in the L_b state are seen to be comprised mostly of their corresponding ground state vibrations. The L_b modes 11-15 are seen to be considerably more mixed, as evidenced by contributions from 3-4 ground state modes in these cases. In mode 11, in particular, the corresponding ground state vibration does not contribute significantly, and this mode is truely well-mixed.

Surprisingly, the L_b out-of-plane modes correlate reasonably well with their ground state counterparts. Those modes which are mixed are seen to be comprised of contributions from 2-3 ground state modes and in most cases there is one mode which makes a dominant contribution to the expansion. Modes 31 and 33 are exceptions to this, but in all other modes there is a matrix element >0.80 which indicates that the excited state mode correlates strongly with a ground state counterpart.

The general conclusion which can be drawn regarding the Duschinsky rotation of the L_b modes is that the form of these vibrations correlate strongly with their ground state

counterparts for both A' and A" representations. It is crucial to note, in addition, that the most displaced L_b mode (25, cf. Table 15.) does not undergo any significant Duschinsky rotation.

For the L_a normal coordinates, there is more mixing than there is in the L_b case both in terms of the number of A' and A" modes which are mixed and the extent of this mixing. Nonetheless, examination of Table 21b. demonstrates that the form of the L_a normal coordinates correlate strongly with their ground state counterparts in most cases and that the two most displaced modes (25 and 27) do not exhibit Duschinsky rotation. The L_a modes 8, 14, and 17, which are considerably displaced (cf. Table 15.), do exhibit extensive mixing.

The best illustration of these mixing effects is provided by comparison of the computed $L_{b,a}$<--S_0 Franck-Condon factors for absorption with the corresponding FC factors for emission (fluorescence). These spectra are seen in Figures 5a. and 5b.. Both absorption and emission calculations are performed from vibrationless initial states and all energies are expressed as vibrational energy in excess of the origin). In these four computed spectra, a nominal Gaussian broadening factor (fwhm) of 5 cm^{-1} was applied. In addition, calculated FC spectra with Gaussian broadening of 50 cm^{-1} are overlayed on the "stick" spectra in Figures 5a. and 5b. for comparison and to illustrate the effects of broadening. Note that the separate L_b and L_a spectra have not been weighted by their respective oscillator strengths; we incorporate this effect later in order to construct the full spectrum.

Both the L_b and L_a excitation-emission spectra exhibit a high degree of mirror-image symmetry, which is a direct measure of the extent of Duschinsky rotation. In the calculated L_b absorption spectrum, the origin is observed to be the most intense transition. The first L_b transition with appreciable intensity with respect to the origin is identified as the fundamental of v_{25} (at 823 cm^{-1}). The first overtone for this vibration,

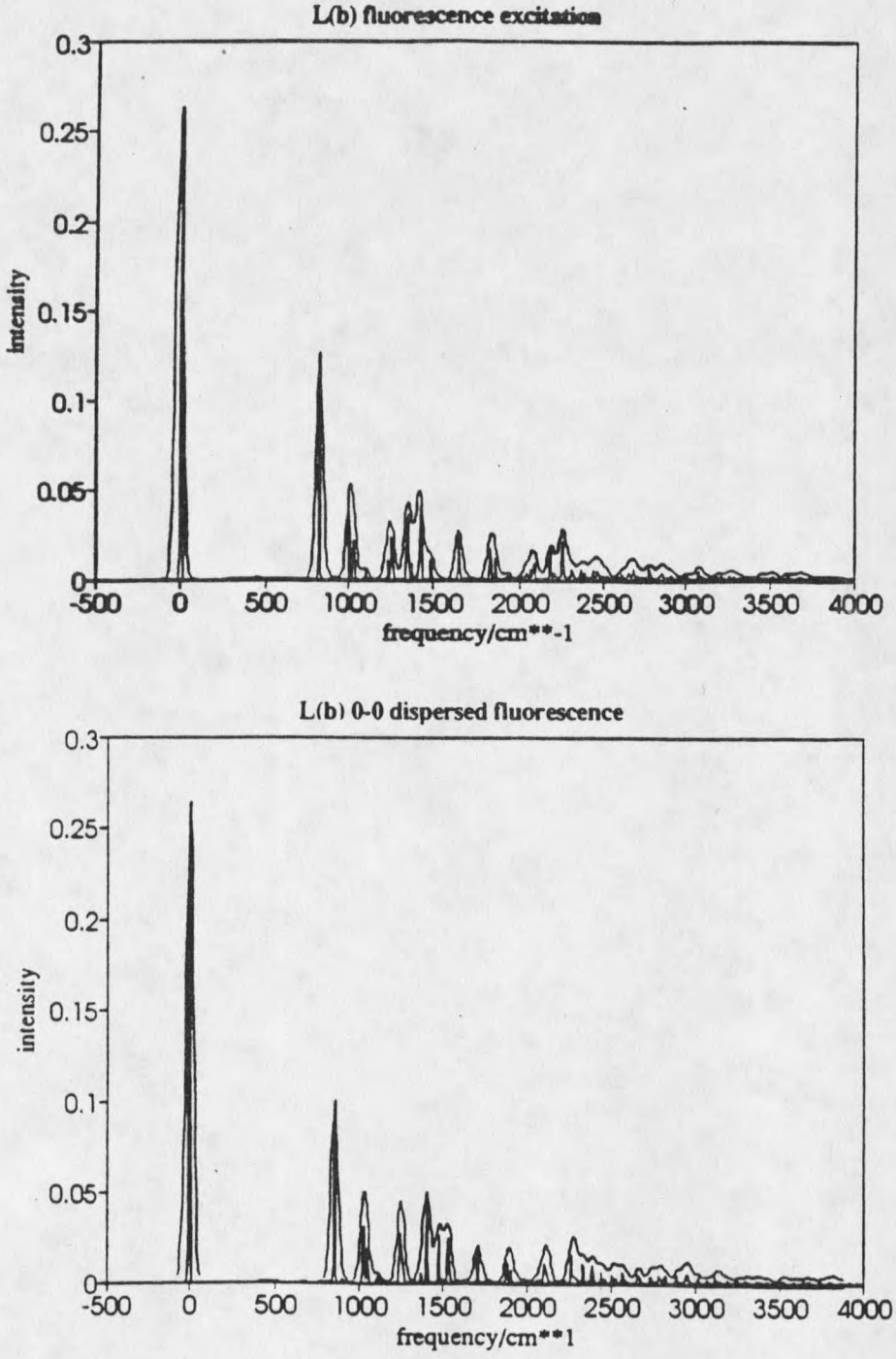

Figure 5. L_b fluorescence excitation and 0-0 dispersed fluorescence spectra computed from QCFFBOZE normal coordinate displacements and frequencies. The effect of Duschinsky rotation is incorporated into the calculation of the spectrum. Overlaid on the zero Kelvin "stick" Franck-Condon factors is the bandshape corresponding to a Gaussian broadening of FWHM 50 cm^{-1}. Note the high degree of mirror image symmetry between excitation and fluorescence.

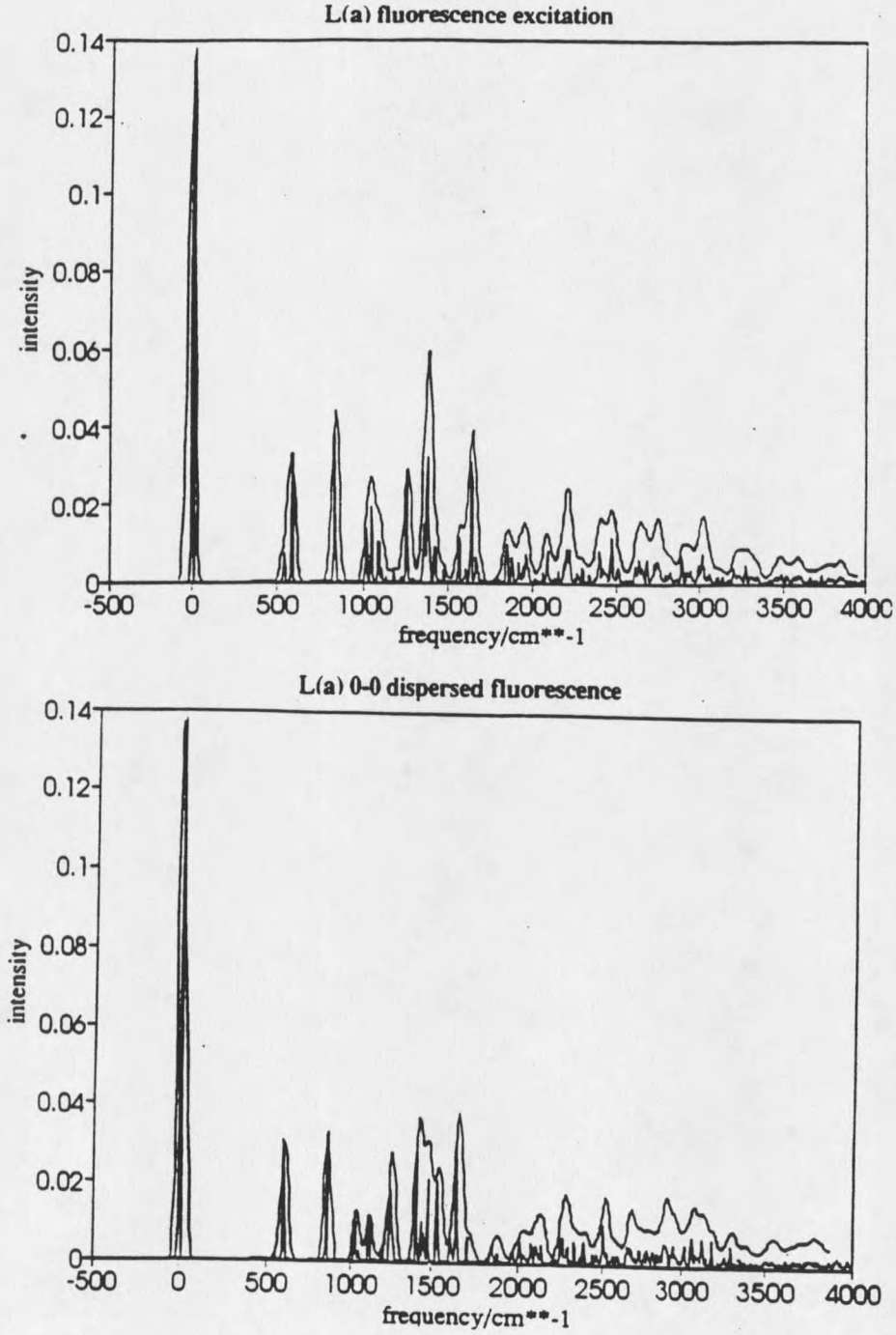

Figure 6. L_a fluorescence excitation and 0-0 dispersed fluorescence spectra computed from QCFFBOZE normal coordinate displacements and frequencies. The effect of Duschinsky rotation is incorporated into the calculation of the spectrum. Overlaid on the zero Kelvin "stick" Franck-Condon factors is the bandshape corresponding to a Gaussian broadening of FWHM 50 cm^{-1}. Note the high degree of mirror image symmetry between excitation and fluorescence.

25_0^2, is observed at 1646 cm^{-1}; the second overtone, 25_0^3 at 2469 cm^{-1}, has negligible intensity. This pattern for the v_{25} progression is observed in the L_b emission spectrum as well, and apart from very minor frequency shifts the absorption and emission spectra for L_b are qualitatively very similar, i.e. they exhibit a high degree of mirror-image symmetry.

A similar situation exists for the L_a state (Figure 6.), although it is worth noting that in the L_a spectra there is sufficient Duschinsky rotation for some breakdown of mirror image symmetry and that in a qualitative sense the L_a fluorescence excitation band exhibits more intensity than does the 0-0 dispersed emission in the first ~2000 cm^{-1}. Nonetheless, L_a fluorescence is relatively less important from an experimental perspective: to date, no L_a fluorescence has been observed from uncomplexed indole, and this is attributed to rapid internal conversion (9) of L_a states to L_b following excitation.

Indole Franck-Condon Factors and Vibrational Assignment

Experimental Survey

The status of the indole vibrational assignment is perhaps best summarized as problematic. On the one hand, recent polarized two-photon fluorescence excitation (PTPFE) experiments on jet-cooled indole (5-7,9,19,20) have provided accurate polarization ratios for a majority of the observed transitions up to ca. 1,500 cm^{-1} above the L_b origin, allowing the identification of L_b and L_a transitions on the basis of these polarization ratios. These experiments, in conjunction with the SVLF studies of Bickel, et al., provide a fairly comprehensive and accurate catalog of transition frequencies for the L_b electronic state, and represent a significant advance in our overall knowledge of the spectroscopy of isolated indole since the pioneering LIF study by Bersohn, Even, and

Jortner (10). The general (and arguably tentative) conclusion that can be drawn in terms of the work of Callis and co-workers (2-7) and the study by Bickel, et al., is that the vibrational assignment of L_b transitions is reasonably well established.

On the other hand, extensive ambiguity remains in regard to the vibrational assignment for L_a not just in terms of which vibrations are active in the transitions but as regards the assigned L_a character of the transitions. In particular, the assignment of the L_a origin has been the subject of considerable effort among various groups (3,5,11,15-18), with a speculative component arising recently (25). The crux of the situation is that it is not possible to do the vibrational assignment unless the band origin has been identified. For this reason, to date, no vibrational assignment of the L_a state has been performed.

As regards the L_a origin, there are essentially two differing schools of thought which can be very clearly delinated in terms of which transition(s) are assigned as the 0-0 for the L_a state. Based primarily on an early assignment by Stickland, et al. (18), considerable attention has been given to a strong transition at ca. 1450 cm^{-1} above the L_b origin (in indole vapor) as a possible candidate for the L_a origin (9,). On the other hand, Callis and co-workers (6,7,19) have established through PTPFE experiments that transitions lower in energy than the ~1450. cm^{-1} band can be unambiguously assigned as L_a in character.

Callis, et al., in particular, have been the only proponents of an L_a origin assignment to the bands at 455 and 480 cm^{-1} above the L_b origin. This assignment of an L_a origin which is "split" by ~25 cm^{-1} has attracted some criticism (25) and evoked a one-sided controversy. Whereas prior to 1990, the status of the L_a origin could be summarized in the question, "Does the L_a origin exist?", the current trend appears to be in the direction of proving what the L_a origin is <u>not</u> and attempting to refute the proposed assignment of Callis, et al..

Certainly, the L_a "origin" exists in the trivial sense that there is an S_2 electronic state with L_a character which is displaced relative to the ground and S_1 (L_b) potential surfaces. The more pointed question is how large the Franck-Condon factor might be for the L_a 0-0 transition or, alternatively, how large the geometry difference vector is between the minima of the ground and L_a surfaces. An answer to these questions is provided, in approximate form, by LCAO-MO-SCF calculations coupled with normal coordinate analysis in the ground, S_1, and S_2 electronic states of indole.

Unfortunately, such calculations almost of necessity must be carried out within the framework of the Born-Oppenheimer and harmonic approximations, and Franck-Condon factors are only tractable within the Condon approximation. Nonetheless, vibrational assignments based on the comparison of computed FC factors with experimental intensities are a considerable improvement over vibrational assignments based solely on comparison of computed vibrational frequencies with experimental data, as has been attempted on at least one occasion for indole (25).

Much of the apparent (and artificial) controversy regarding the proposal of a "split" L_a origin stems from an artifact of the earlier assignment of Bickel, et al. (12), in which the transitions at 455 and 480 cm^{-1} were assigned as the combination $39_0^1 41_0^1$ and fundamental 28_0^1, respectively, involving L_b vibrations. Thus, this assignment provides the fundamental of ν_{28} at 480 cm^{-1}. The fundamentals of modes 39 and 41 were assigned by Bickel, et al., at 278 and 183 cm^{-1}, the sum of these frequencies being 461 cm^{-1}; a discrepancy of +6 cm^{-1} from the assigned combination. On the other hand, Bickel, et al., do <u>not</u> assign a separate transition (weak shoulder) observed at exactly 461 cm^{-1}, and do not report SVLF out of this state. In fact, it seems almost an anomaly that this transition was not assigned as the combination $39_0^1 41_0^1$ simply on the basis of frequency agreement and receives no mention in the paper, nor in the AIP Physics Auxiliary Publication Service (PAPS) reprint of SVLF spectra and tables associated with

the article (13).

Table 22 presents the PTPFE results obtained by Sammeth (9) for jet-cooled indole, with the associated assignments of Bickel, et al. provided for comparison. On the basis of the two-photon polarization ratio, the transitions in the first ca. 400 cm^{-1} of the excitation spectrum are unambiguously assigned as L_b in character. The two-photon polarization ratio for the 455 and 480 cm^{-1} transitions measured by Sammeth are strongly indicative of L_a character; these are the first peaks in the excitation spectrum which exhibit such a relatively low polarization ratio. This assignment was subsequently confirmed by Muiño (20), solidly establishing the L_a character of the 455 and 480 cm^{-1} transitions.

TABLE 22. One-photon fluorescence excitation frequencies, relative one-photon intensities, and two-photon polarization ratios for indole measured by Sammeth.[a] All frequencies relative to the L_b origin at 35,232 cm^{-1}, intensities as % of L_b origin.

ω / cm^{-1}	Intensity	Ω	State Assignment	Bickel, et al. assignment[b]
0.0	100	1.4	L_b	0-0 L_b
315.7	0.8	1.4	L_b	42_0^2 L_b
364.9	1.3	1.4	L_b	41_0^2 L_b
379.5	2.2	1.4	L_b	29_0^1 L_b
454.4	3.2	0.7	L_a	$39_0^1 41_0^1$ L_b
479.9	7.0	0.7	L_a	28_0^1 L_b
540.1	6.0	1.4	L_b	27_0^1 L_b
588.4	1.1	....	....	
718.5	35.0	1.3	L_b	26_0^1 L_b

[a]Excerpt from D.M. Sammeth, Ph.D. thesis, Montana State University (1992), p.48
[b] ref. 12

The one-photon SVLF experiments of the Bickel group were directed at chacterization of the S_1<--S_0 transitions of indole and did not provide polarization information which is inherent in the PTPFE method of Callis, et al.. In view of the polarization ratios, the L_a character of the 455 and 480 cm^{-1} introduces several complex issues regarding the indole vibrational assignment.

In their original paper proposing the "split" L_a origin, Sammeth, et al. (5) raise the following question which serves to summarize and put in perspective the persisting ambiguity regarding the 455 and 480 cm^{-1} transitions: "Is the lowest energy transition observed with the L_a character the L_a origin, or might such a weak band actually be due to a L_b state whose oscillator strength and two-photon intensity come mainly from Herzberg-Teller vibronic coupling to the L_a manifold?"

On the basis of the two-photon polarizaton ratios measured by Sammeth, the assignment of the 455 and 480 cm^{-1} to L_a is particularly compelling. Both transitions exhibit "L_a signature" polarization ratios, with $\Omega = 0.7$. On the other hand, however, the 455 cm^{-1} transition red-shifts by ~129 cm^{-1} upon complexation with water, and the 480 cm^{-1} transition red-shifts by ~140 cm^{-1}in indole-H_2O complex, while all other L_b peaks exhibit red-shifts of ~131 cm^{-1} in indole-H_2O complex and L_a transitions are established as undergoing red-shifts typically on the order of a few hundred wavenumbers (19).

The intensity ratio for the 455 and 480 cm^{-1} peaks (Table 22.) is ~2, with the 480 transition being the larger. Regardless of whether either of these peaks or both are L_b or L_a in character, it is clear that the 480 transition occurs with a greater probability than the 455, i.e. with a greater vibrational overlap. A similar situation persists in 3-methylindole (3MI), in which there exist low energy transitions at 409 cm^{-1} and 420 cm^{-1} above the L_b origin (at 34,876 cm^{-1} in 3MI) with an intensity ratio of ~1.2 (7).

Interestingly, in 5-methylindole (5MI) it is expected that the L_b-L_a origin separation widen by ~950 cm^{-1} relative to indole (7) and in fact there is observed at ~1424 cm^{-1}

above the 5MI L_b origin a transition which appears to be a strong candidate for the L_a origin (7). This is in reasonable agreement with the idea of an indole L_a origin at ~474 cm^{-1}, a value closer to the 480 cm^{-1} transition than the 455 (or the intermediate value, ~468 cm^{-1}), but in reasonable agreement with an L_a origin within this energy range.

Surprisingly, the results for jet-cooled 3MI L_a transitions (7) are not in agreement with the observation of Stickland, et al. (18), in which the L_a band maximum of the 3MI vapor absorption spectrum is shifted to ~270 nm in comparison to a band maximum at ~260 nm for indole. Note that in the vapor absorption experiments of Stickland, et al., the 3MI L_b origin (287 nm) is shifted by only ~4 nm relative to the L_b origin for indole vapor (283 nm). On the basis of the observed shift in the L_a band maximum (10 nm = ~1425 cm^{-1}) for 3MI, one would anticipate that the L_a origin would lie <u>below</u> the L_b origin in 3MI. This is not observed, however; investigation of the region 700 cm^{-1} to the red of the 3MI L_b origin revealed no one-photon excitation intensity greater than 0.10% of the L_b 0-0, leading to the conclusion that the L_a origin is not shifted as significantly as might be expected on the basis of the band maximum shift.

To summarize, it appears that the origin shift for 5MI supports the assignment of an indole L_a origin in the region 455-480 cm^{-1}, while experiments on 3MI raise further questions about the validity of a "split" L_a origin. In addition, differential solvent shifts for indole-H_2O complexes seem to display "L_b-like" red-shift for the 455 and 480 cm^{-1} transitions of bare indole. A recurring theme in the unfolding drama of indole photophysics is thus: "Where (Which) is the L_a origin?" (5,7). It appears that a very appropriate approach at this stage is to supplement experimental techniques with bandshape calculations. These results of such calculations are presented in what follows.

Calculated Franck-Condon Factors

We present here the results for Franck-Condon factors calculated from the QCFFBOZE vibrational eigenvectors and equilibrium geometries. Recall that all FC factors incorporate the effects of surface displacement, frequency shifts, and Duschinsky rotation. Vibrational frequencies, displacements, and values of the Poisson model lambda parameters for these calculations were presented in Tables 15-16, and the Duschinsky rotation analysis is contained in Tables 21a and 21b.

S_1 (L_b) and S_2 (L_a) Origin Franck-Condon Factors

We now ask the following question; how large are the L_b and L_a origins calculated within the harmonic approximation and, more importantly, what are the spectral bandwidths computed for the L_b and L_a manifolds? It is here that we make the direct connection with experiment, and attempt to establish the nature of the L_a origin and to explain the observed progressions.

The absolute intensities of the computed L_b and L_a origin FC factors are contained in Table 24. For the L_b origin, we present the result obtained from the difference-density scaled QCFFBOZE vibrational eigenvectors; for L_a we present this result and the result obtained from the frozen CI calculation as well. In addition, L_a origin intensities weighted by an arbitrary L_a:L_b oscillator strength ratio of f=2.5 (3) are presented for comparison.

TABLE 24. Spectroscopic origins for L_b and L_a electronic states of indole; calculation of Franck-Condon factors incorporating surface displacements, frequency shifts, and Duschinsky rotation. Origin FC factors correspond to QCFFBOZE vibrational eigenvectors calculated with difference-density scaling (χ=1.30).

state	L_b	L_a	L_a: frozen-CI
F_{00}	0.2638	0.1382	0.0721
$f\,F_{00}$	0.3455[a]	0.1803[a]	

[a]Origin intensities for an L_a oscillator strength ratio of f~2.5

Two preliminary conclusions can be drawn on the basis of this calculation; (i) the harmonic calculation does predict an L_a origin with significant intensity relative to the L_b origin, and (ii) the L_a origin computed in the frozen CI framework for the S_2 electronic state is more commensurate with the experimental observation. We therefore conclude that the geometry changes associated with the L_a state are better represented by the frozen CI calculation.

This is, in fact, a very complex matter and contains a high degree of subtlety. The frozen CI calculation is carried out in such a way that the influence of the predicted avoided crossing on the L_a state is removed. This points to at least one complication and limitation of the theoretical method employed; since all FC factors are computed from minima on the potential surfaces, the calculation provides no mechanism for the influence of the avoided crossing except for the values of the surface displacements.

The upshot is that the normal coordinates calculated for the respective surfaces are "pure" L_b and L_a vibrations, which remain localized within the potential wells they are constructed for. In reality, however, there can be vibrations which explore regions of the conformation space of the molecule through distortion of the molecular framework

which project onto the equilibrium geometries associated with both S_1 and S_2 minima. In this way, for example, a vibration associated with L_a can "leak" into the L_b potential well and could then overlap with the ground vibrational state from both the L_b and L_a wells, resulting in a non-zero FC overlap integral and an observable transition intensity.

In the event that this mixed-surface "Gedankenexperiment" really does occur, there is one issue of critical importance to understanding the spectrum observed for indole and that is this; is the character of such a "mixed" vibration L_b, L_a, or (more likely) a mixture of both? That is, what polarization ratio might be measured in a PTPFE experiment?

The answer depends intimately on the time scale of the fluorescence which is observed. For short times following the excitation -- i.e. after the initial preparation of the excited state at time zero -- the fluorescence polarization provides a unique signature of the initially prepared state. At long times, however, molecular rotation will lead to isotropic fluorescence and the information about the initially prepared state is obscured. In order to properly study the excited state dynamics it is necessary to measure the time evolution of molecular fluorescence; an extremely difficult proposition. It is therefore difficult to discern on the basis of polarization ratios "where" measured intensity comes from, i.e. whether measured L_b (L_a) character is from a state which was initially prepared as L_b (L_a), or whether the intensity may be produced through a coupling mechanism (e.g. Herzberg-Teller) which operates on the intially prepared state.

L_b Franck-Condon Progressions

We consider next the FC factors computed for the S_2 (L_b) surface, in effort to corroborate the partial vibrational assignment of Bickel, et al. (12). Due to the rapid loss of quantum yield from >1600 cm^{-1} in the indole excitation spectrum, we shall be primarily concerned with transitions from the L_b origin to ~1600 cm^{-1} above the origin.

The higher energy transitions can contribute to the overall bandwidth, but their individual intensities are anticipated (and observed, when possible) to be small.

In our vibrational assignment calculations, all FC factors with values within 0.01% of the L_b origin intensity were written to a file and assigned by number of quanta in each mode. In this way, overall intensity is accumulated and can be summed to determine how much calculated intensity is missing. In order to "converge" the spectrum, there are two possible options; (i) the intensity cut-off for FC factors which are written to disk and saved (typically within 10^{-4} of the origin intensity) and (ii) the energy cut-off. These two factors must be balanced between the demands of disk storage space and the high-energy intensity required to predict a reasonably accurate bandwidth. In practice, saving all FC factors within 10^{-4} of the origin and to ~12,000 cm^{-1} in excess of the origin provides ~98% of the intensity. This is more than sufficient for our purposes.

As displayed in Table 24., the L_b origin intensity for excitation from the vibrationless level of the ground state is 0.2638. This accounts for ~26% of the L_b intensity and is the largest FC factor computed for L_b excitation. The largest L_b peak outside the origin is the fundamental of mode 25, 25_0^1, for which the computed FC factor is 0.1260, which is approximately 48% (nearly half) of the origin intensity. This is in reasonably good agreement with the intensity measured by Sammeth (9) for the 718.5 cm^{-1} transition which shows one-photon intensity of ~35% of the L_b origin. It is important to note that this mode, the in-plane vibration with the 25-th lowest frequency, corresponds to mode 26 of the experimental assignment (12,32). This is simply an artifact of the QCFFBOZE normal coordinates; although the frequency ordering of A' and A" modes has been done according to convention, this discrepancy simply points to the relative error in the calculated frequencies. The fact remains that the QCFFBOZE S_1 mode 25 is the most displaced normal coordinate.

There is an important point regarding this frequency error which provides some

insight into the quality of the computed spectrum. Since the calculated frequency of this mode (25) is greater than the observed value (cf. Table 18. and ref. 12), it can be argued that the agreement with experiment (~48% calculated, ~35% experimental) is in part due to the frequency overestimation of the semiempirical force field. The argument goes as follows: since the dimensionless displacement, S, of a normal coordinate is defined by

$$S = (\text{projection})/(\text{classical turning point}) = \Delta Q / (h / 2\pi\omega)^{1/2}$$

and the related parameter, lambda, is given by $(1/2)S^2$, this dimensionless displacement is proportional to the root-frequency and lambda is proportional to the frequency. Therefore, calculated frequencies which are greater than the experimental values tend to overestimate the displacement (and lambda). In this way, there is some "slack" in the interplay between the calculated normal coordinate projection, ΔQ, and the frequency. If a normal coordinate projection is smaller than that which might be derived empirically (through a Poisson model analysis of an experimental spectrum), a frequency overestimation will tend to cancel this error. Even if the value of ΔQ is in exact agreement with experiment (i.e. the limit of a perfectly harmonic molecule), computed frequencies which are greater than the experimental values will lead to overestimation of lambda and thus an overestimation of the FC factor(s) associated with the mode.

All of this is tied directly to the geometry difference vector, which is truely the central quantity in the calculation of FC factors. All of the above statements are inexorably coupled to the quality of the difference in equilibrium molecular geometries and, by extrapolation, the quality of the semiempirical force field which produces the geometries. Even in the idealized limit of a perfect force field, with an infinite basis set, doing perfect variational calculations, we would still not be able to produce FC factors which reproduced experiments in an exact fashion. The problem has its roots in both the anharmonic nature of molecules as well as the detailed couplings which produce the observed (and unobserved) transitions. For the present time, it suffices to do

approximate calculations with admittedly flawed force fields, and attempt to account for any disagreement with experiment by careful analysis.

Despite the apparent error in the FC factor for mode 25, there is one victory in this result; the calculated intensity ratio for this mode relative to the (calculated) L_b origin is in reasonably good agreement with experiment. By this is meant that the qualitative trend is captured by the QCFFBOZE normal coordinate.

We now compare the QCFFBOZE L_b vibrational assignment directly with that of the Bickel group (12). To summarize the Bickel L_b assignment, we note that they report nine (9) L_b frequencies; 5 A" modes and 4 A' modes. These are the modes for which we are able to make a comparison; the comparison with the QCFFBOZE vibrational assignment is presented in Table 25. The proposed vibrational assignment in this Table requires comment.

TABLE 25. QCFFBOZE L_b vibrational assignment.

Displacement (cm^{-1}) from origin; Bickel[a]	assignment[b]	QCFFBOZE	% 0-0[dc]
316	42(2)	0.00038	(0.14)
365	41(2)	0.00054	(0.20)
380	29(1)	0.0012	(0.45)
436	39(1)42(1)	...	
455	39(1)41(1)	0.00007	(0.03)
461	...	...	
480	28(1)	...	
526	37(1)42(1)	0.00004	(0.02)
540	27(1)	...	
548	37(1)41(1)	0.00008	(0.03)
557	39(2)	0.00075	(0.28)
718	26(1)	(0.1259)	(47.7)
720	29(1)41(1)42(1)		...
737	37(2)	0.00059	(0.22)
776	39(1)36(1)	...	

(a) ref. 9.
(b) Assignment format: mode (# quanta).
(c) QCFFBOZE assigned transitions. Values reported are FC factors.
(d) % of computed L_b origin intensity.

First, the computed FC factors which match the mode assignments of Bickel are those reported in the third column, with the exception of the computed mode 25 which is identified as the experimental mode 26. The transitions reported by Bickel at 436, 480, 540, 720, and 776 cm^{-1} were found to have no counterparts in the set of computed FC factors; these FC factors were found to have intensity less than 0.01% of the computed origin. On the other hand, this discrepancy could be due to a mode-mismatch within the QCFFBOZE normal cordinates (as is the case for the computed mode 25), as well as to errors in the coordinate displacements which result in anomolously low intensity.

The transitions at 455 and 480 cm^{-1} pose a conundrum, of sorts. Our FC factor calculations do predict a low-intensity transition corresponding to the assignment $39_0^1 41_0^1$, but the fundamental 28_0^1 proposed by Bickel is not found to have intensity within 0.01% of the origin in our calculations. Owing to the possibility of a mode discrepancy as was the case for the computed mode 25, the possibility arises that the computed mode 28 is not the same mode as identified by Bickel. The only alternatives in terms of frequency from the QCFFBOZE normal modes are modes 29, with a calculated frequency of 457 cm^{-1}, and 27 with frequency 587 cm^{-1}. If there is a mode mismatch between the computed and experimental assignment, the latter case (587 cm^{-1}) is the more probable candidate since the computed frequency is higher than the experimental value. On the other hand, since the computed mode 25 matches the experimental mode 26, it would seem more likely that mode 27 is truely vibration assigned to 28 by Bickel.

There are, however, two reasons why this reassignment of the computed mode is called into question. First is the matter of the frequency calculated for mode 27 (457 cm^{-1}) being lower than the experimental value (proposed 480 cm^{-1}) and, more importantly, the fundamental of mode 27 does not exhibit intensity within 0.01% of the origin.

There is, in addition, one more possibility, and that is that the assignment of the transition at 480 cm^{-1} by Bickel is in error. The low polarization ratio measured by

Sammeth (Table 22.) provides some compelling evidence in support of this argument, which is a much stronger argument than the one outlined above in terms of the QCFFBOZE calculation. The argument here is not one of whether the 480 cm^{-1} is the L_a origin: the central issue is to determine whether the assignment as an L_b fundamental is legitimate. The polarization ratio information and the QCFFBOZE calculation point to the possibility that the assignment as an L_b fundamental is in error.

There are at least two ways in which the assignment could be in error. First, the observed intensity could have no relationship whatsoever to an L_b fundamental vibration and be entirely localized in the L_a potential well -- i.e. it could be merely a "pure" L_a vibration which provides the intensity. This seems unlikely, however, since this would essentially require an L_a origin in isolated indole which is nearly-degenerate with the L_b origin in order that the observed intensity be at an energy "in excess" of the degenerate origin. The second possibility is that the intensity at 480 cm^{-1} is in reality a mixture of L_b and L_a, i.e. an L_b vibration which experiences Herzberg-Teller coupling to the L_a state which is responsible for the low polarization ratio.

The last possibility is that neither the fundamental assignment of Bickel nor the Herzberg-Teller argument is correct, and the 480 cm^{-1} transition is, in fact, the L_a origin or, more precisely, a component of a split L_a origin as proposed by Callis, et al.. This possibility would be conclusive if it were not for the "L_b-like" red-shift exhibited by this peak upon complexation with water. These issues taken together point very strongly to the Herzberg-Teller argument for an L_b vibration coupled to L_a.

Returning to the 455 cm^{-1} transition assigned to the L_b combination $39_0^1 41_0^1$ by Bickel, we note as before that the sum of the fundamental frequencies of these modes (39: 278 cm^{-1} and 41: 183 cm^{-1}) matches exactly the observed 461 cm^{-1} frequency transition. Interestingly, the 461 cm^{-1} is not assigned. This weak-shoulder peak is located only 6 cm^{-1} from the relatively strong transition at 455 cm^{-1} and is a much

stronger candidate for two reasons. First, the frequency match is perfect, assuming that the assignments for modes 39 and 41 (determined from their first overtone frequencies at 557 and 365 cm^{-1}) are accurate, as appears to be the case. Second, the combination of two out-of-plane modes with one quanta of vibration per mode is expected to exhibit very weak intensity (as the 461 peak does). The question which needs to be begged in this context is this: "How weak?".

Examination of the one-photon excitation spectrum of jet-cooled indole or, alternatively, the 1+1 photoionization spectrum measured by Bickel, et al., provides considerable insight. Both assigned overtone transitions 39_0^2 and 41_0^2, which gain intensity through frequency changes upon excitation, are observed to have greater relative intensity than the 461 cm^{-1} weak shoulder transition, and lower relative intensity than the 455 cm^{-1}transition. It seems counterintuitive that a combination of two out-of-plane modes would exhibit greater relative intensity (i.e. higher probability) than either of the associated overtones. This intuition is born from analogy with the situation for in-plane modes; the joint probability associated with a combination of two in-plane modes will always be lower than either of the funamentals. By analogy, for out-of-plane modes, one might anticipate the 1-1 combination to have a lower probability than either overtone.

To put this argument on a more quantitative basis, we can consider the results from the calculated FC factors. For the L_b transitions, the following FC factors were computed;

39_0^2 {0.00075}: 41_0^2 {0.00054}: $39_0^1 41_0^1$ {0.000073}.

The overtone of mode 39 is seen to have an intensity ~10 times that of the combination, while the overtone of mode 41 exhibits intensity ~7 times the combination. Whether or not intuition is correct, the calculation predicts a lower intensity for the combination than either of the overtones of the modes comprising the combination.

This situation requires extreme caution. Since the calculated overtones depend sensitively on the frequency changes upon excitation, an error in the frequency change can lead to erroneous results. It is necessary to compare the calculated FC factors with those predicted from the experimentally determined frequency changes for the A" modes. This can be accomplished directly by using the approximate expression for the overtone FC factors, which can be shown to be of the form (51,52)

$$F_{02} = \{ (\omega'' \omega')^{1/2} / (\omega'' + \omega') \} [\Delta\omega / (\omega'' + \omega')]^2,$$

from which it is seen that it is only the frequency difference which is of importance; the single and double primes are not necessary to specify which frequency corresponds to ground or excited state. We present below the comparison of first overtones computed from this expression for the QCFFBOZE L_b out-of-plane modes and those reported by Bickel.

TABLE 26. First overtones predicted from frequency changes upon excitation.

	QCFFBOZE			experimental[a]		
mode	ω''/cm^{-1}	ω'/cm^{-1}	F_{02}	ω''/cm^{-1}	ω'/cm^{-1}	F_{02}
36	747	665	0.0017	602	498	0.0044
37	693	602	0.0025	570	369	0.0224
38	527	473	0.0015	...	...	...
39	520	448	0.0028	420	278	0.0203
40	412	359	0.0024	...	...	...
41	255	225	0.0019	241	183	0.0092
42	211	190	0.0014	208	158	0.0092

(a) ref 12.

The agreement between the first overtones for the computed frequencies and those obtained from the experimental frequencies is generally quite poor, which is simply a reflection of the quality of the computed frequencies for out-of-planes modes. For QCFFBOZE modes 39 and 41, the frequency difference expression predicts F_{02} to be

higher than the exact values presented above; this difference is attributed to Duschinsky rotation of these modes, as evidenced by the form of the normal coordinates presented in Table 21a;

$$Q_{39} = 0.57\, Q''_{38} + 0.80\, Q''_{39},$$

and Q_{41} (which is not contained in Table 21a.) is given by

$$Q_{41} = -0.9966\, Q''_{41} + \text{(smaller contributions } <0.10).$$

The full Duschinsky expansion for mode 39 incorporating the smaller terms is

$$Q_{39} = 0.1245\, Q''_{37} + 0.5669\, Q''_{38} + 0.8015\, Q''_{39} - 0.1357\, Q''_{40}.$$

This mode is seen to exhibit extensive mixing, but is nonetheless still dominated by a contribution from the corresponding ground state mode. Mode 41, on the other hand, is an example of nearly "parallel mode" character, with very little discernable mixing. This is surprising, since the agreement between F_{02} computed from the frequency distortion model and the exact calculation (including Duschinsky rotation) is actually better for mode 39, in which there is more mode-mixing. This discrepancy is simply an artifact of the extent of the frequency shift encountered by these modes; mode 41 exhibits less frequency change than mode 39, resulting in an anomolously low FC factor for the first overtone.

The more important message is that provided by the experimental values. Comparison of F_{02} for the experimental frequencies of modes 39 and 41 point to a critcal issue for the assignment of the transition at 461 cm^{-1}. Neglecting the effects of Duschinsky rotation, the combination $39_0^1 41_0^1$ is effectivly "bracketed" by the first overtone intensities of the two modes comprising the two-quanta 1-1 combination. If there is no mixing between modes 39 and 41 (as is the case for the QCFFBOZE modes), and little overall mixing for the individual modes, it is highly likely that the first overtone intensity for mode 41 (0.0092) provides an upper bound for the $39_0^1 41_0^1$ combination. It would require an extensive amount of Duschinsky rotation in order to couple intensity

into this combination, and all evidence suggests that the extent of mode-mixing is very limited. The conclusion, then, is that the weak shoulder peak at 461 cm^{-1} which is not assigned by Bickel, et al., is in reality the $39_0^1 41_0^1$ combination. Bickel, et al., do not report SVLF out of the 461 cm^{-1} excitation; it is probably too weak to provide a false origin for the fluorescence.

This assignment unfortunately does not solve the more compelling issue of the 455 and 480 cm^{-1} transitions, but it does serve to show what the 455 cm^{-1} transition is not -- i.e. the $39_0^1 41_0^1$ combination. It should be emphasized that this does not refute the SVLF assignments for the 455 cm^{-1} excitation; it does, however, make necessary a reassignment of the 455 cm^{-1} false origin.

L_a Franck-Condon Progressions

As outlined previously, barring an assignment for the L_a origin(s), it is not possible to rigorously assign L_a vibrations. On the other hand, however, it most certainly is possible to perform a bandshape calculation for L_a and compare this directly with experiment. The focus, of course, is on determining the location of the L_a origin. Since there is not yet available an experimental vibrational assignment for L_a, we turn now to the bandshape calculations with the following complimentary goals; (1) fitting the experimental bandwidths for the L_b-L_a manifold, and (2) fitting the experimental oscillator strength ratios and L_a origin shift relative to the L_b origin.

Indole: Spectral Bandshape Calculations

The calculation of spectral bandshapes can be briefly summarized as a fitting procedure in which computed Franck-Condon factors are adjusted to match experimental spectra. In the case of indole, this process is complicated to some extent by the near-degeneracy of the L_b and L_a electronic states in that these bands overlap, possess

different oscillator strengths, and the assignment of the L_a origin remains elusive. These problems are diminished significantly if we adopt the approach of fitting the oscillator strength ratio and L_a origin shift, and treat these as adjustable input parameters for the calculation of the spectral bandshapes. This approach is consistent with the questions we are trying to answer and provides a straightforward way to fit the bandshapes without having to resort to an empirical adjustment of the normal coordinate displacements.

Qualitatively, the vapor phase L_b and L_a bandshapes differ in appearance in a very dramatic way. The L_b bandshape can be characterized as sharp, with a majority of the intensity localized in the origin. The L_a bandshape, in contrast, is characterized as broad, with the band maximum occurring ~3200 cm^{-1} above (to the blue) the L_b origin. The basic difference, then, is that the L_a geometry is more displaced with respect to the ground state than is the L_b geometry. It is this geometry difference which leads to the characteristic "sharp" L_b and "broad" L_a, as well as the relative locations of the band maxima for the two electronic states.

We present here the results of calculated spectral bandshapes for indole, based on our Franck-Condon factors computed by the DMM method. The bandshapes are computed as follows;

(i) The QCFFBOZE geometries and normal coordinates are used to compute FC factors as described previously (Figs. 7-8).

(ii) The L_b-L_a origin shift is input as a parameter, Δ_{00}, and the energies of the L_a transitions are defined relative to the L_b origin as $\omega_{La} = \Delta_{00} + \omega_{vib}$.

(iii) The oscillator strength ratio is input as a parameter, f_{ab}, and the L_a FC factors are modified in order to provide absolute intensities, i.e. $I_{if}(L_a) = f_{ab} F_{if}(L_a)$.

(iv) Gaussian broadening factors (FWHM, Γ) are applied to provide phenomenological inhomogeneous broadening of the FC factors.

(v) The "synthesized" spectrum is constructed and compared to experiment (Figs. 9-10).

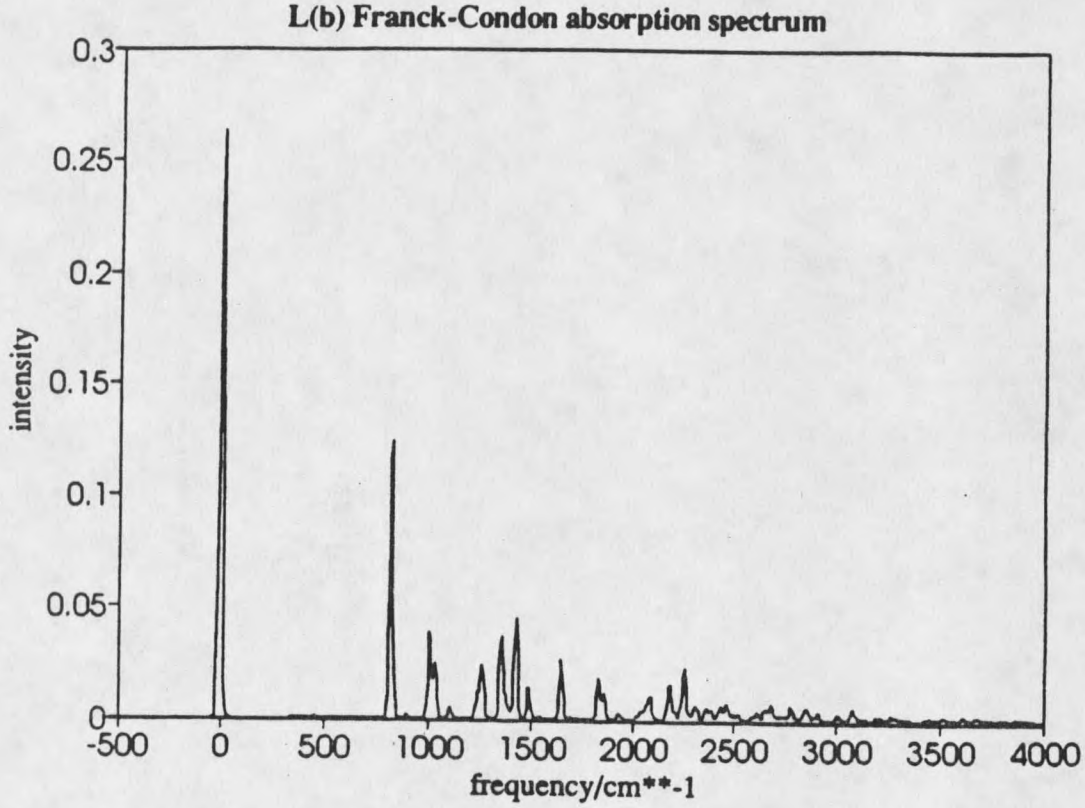

Figure 7. Indole L_b Franck-Condon absorption spectrum computed from QCFFBOZE with a nominal Gaussian broadening of FWHM 20 cm^{-1}. Note the relatively sharp appearance of the spectrum, with most of the intensity localized in the origin and fundamental of mode 26.

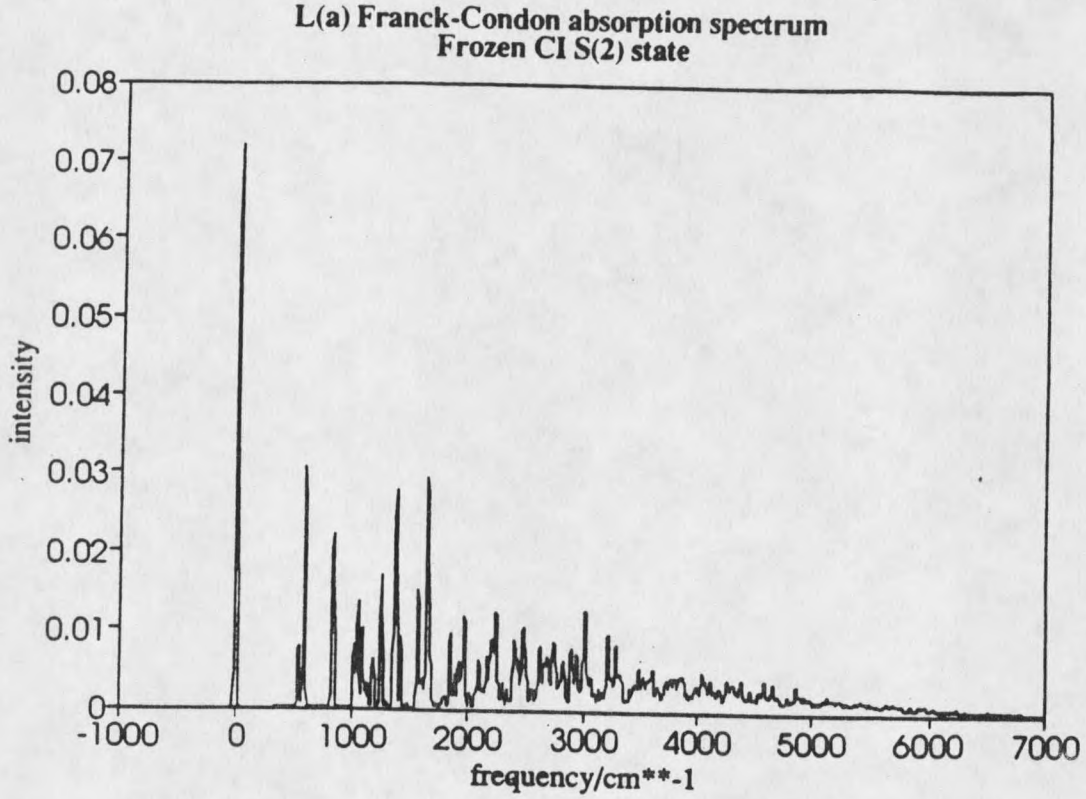

Figure 8. Indole L_a Franck-Condon absorption spectrum computed from QCFFBOZE with "Frozen configuration interaction" and a nominal Gaussian broadening of FWHM 20 cm^{-1}. Note the relatively broad appearance of the spectrum, with considerable intensity extending to ~3000 cm^{-1} above the L_a origin.

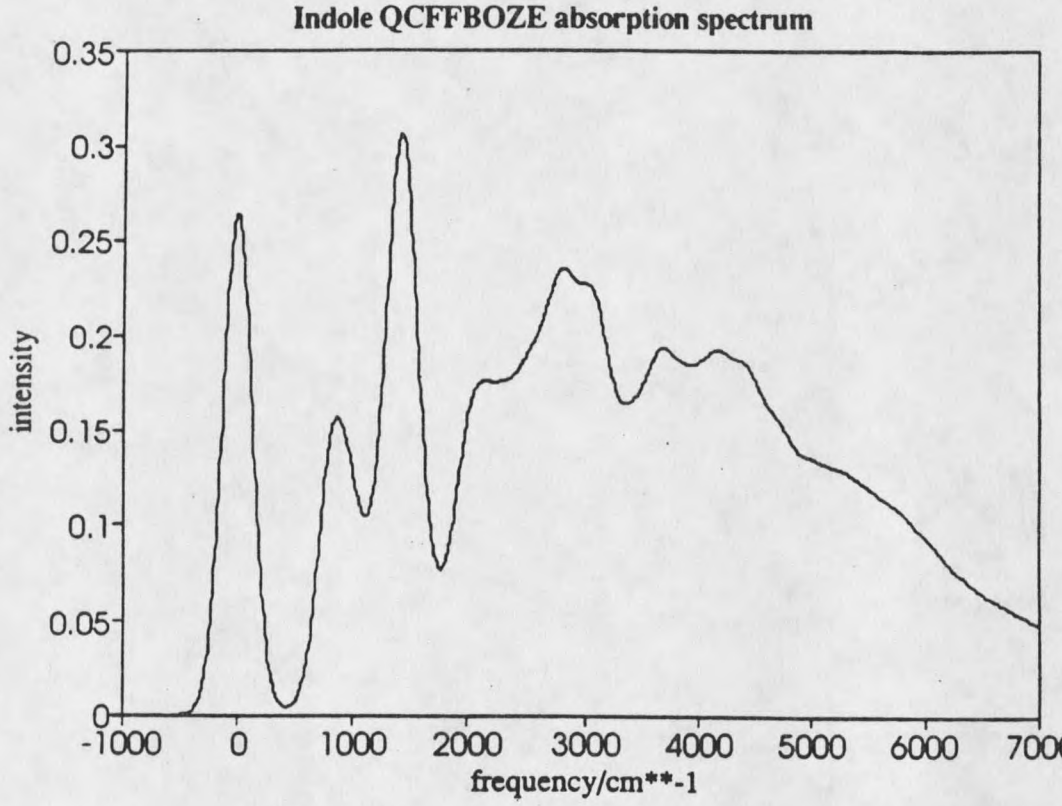

Figure 9. Indole QCFFBOZE absorption spectrum synthesized from the Franck-Condon spectra of Figures 7 and 8.. The L_a origin is shifted ~1450 cm^{-1} above the L_b origin, absolute intensities are provided by an oscillator strength ratio f=2.5, and all transitions are broadened with Gaussians FWHM 300 cm^{-1}. Note the "sharp" L_b origin and the broad L_a progression intensity with band maximum exhibited at ~3000 cm^{-1} above the L_b origin.

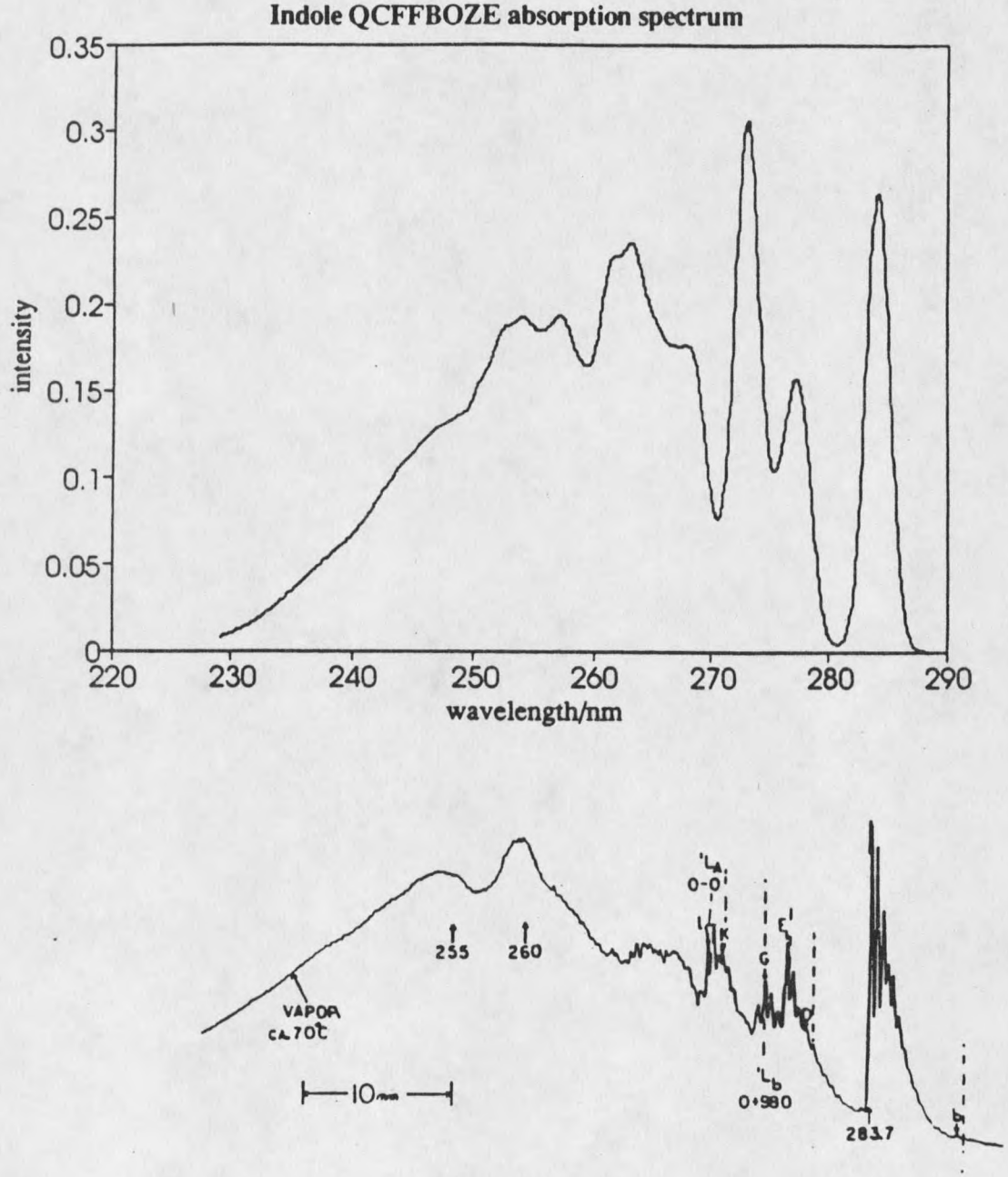

Figure 10. Indole QCFFBOZE absorption spectrum; same as Figure 9., with the energy scale in wavelength (nm) for comparison with the experimental vapor absorption spectrum of Strickland, et al. (ref. 18) which is displayed below.

In this way, there are three adjustable parameters in the calculation of the spectral bandshapes; Δ_{00}, f_{ab}, and Γ. In practice, the experimental values provide a very good guide for these parameters and the values required to fit a bandshape are in reasonable agreement with experiment and within the experimental uncertainty.

Figures 9-10 show the spectral bandshape computed using the L_a origin shift assigned by Strickland, et al. (18) of Δ_{00}~1450 cm^{-1}, an oscillator strength ratio of f_{ab}=2.5 (3), and Gaussian broadening for L_b and L_a FC factors with Γ=300 cm^{-1}. The vapor phase absorption spectrum (ca. 70 ^{0}C) of Stickland, et al., is inset for comparison.

There are several striking similarities between the computed spectral bandshape and the experimental absorption spectrum. From a qualitative perspective, the number of broad spectral features is in quite good agreement, the basic pattern being a sharp L_b origin at ~284 nm, and a broad L_a region extending beyond 250 nm, with a band maximum at ~260 nm. The sharp peak at ~278 nm in the computed spectrum, corresponding to the fundamental of mode 26, exhibits an intensity of ~60% of the L_b origin (comparing the intensity at the maximum of the bands); in the experimental spectrum this feature displays ~76% of the band origin intensity. This agreement, although qualitative, is a direct consequence of the previously noted agreement for the ratio of this fundamental to the L_b origin.

On the other hand, however, the agreement between the computed bandshape and the vapor spectrum is far from perfect. On a coarse-grained level, there are disagreements between observed and calculated frequencies (wavelengths) for the band maxima, which is a direct result of the error in the QCFFBOZE vibrational frequencies. More important are the relative intensities, although it should be noted that these effects are not entirely separate since we've performed a convolution integral for the Gaussian broadening and there is some "smearing" of the intensity which creates the long shoulder extending beyond ~250 nm.

The intensity of the computed L_a origin is predicted to be much higher than that observed for the origin proposed by Strickland, et al.. In fact, after application of the oscillator strength ratio (2.5), the L_a 0-0 is just slightly higher than the L_b 0-0. Further, the L_a band maximum at ~260 nm in the experimental absorption spectrum is not nearly as intense in the computed spectrum. In terms of the fitting procedure, there is a compromise involved; a higher oscillator strength ratio (e.g. f~3) would produce a slightly better fit for the L_a band maximum, but this would also increase the L_a 0-0 intensity. The problem associated with adjusting the oscillator strength ratio is that the differing intensities of the origin and the band maximum are not due to this feature of the bandshape calculation. Both the origin and the band maximum or, more accurately, their intensities relative to one another, are due to the geometry shift upon excitation. Thus, the disagreement between the computed and experimental bandshapes is not primarily an issue of oscillator strength -- it is a product of an incorrect geometry difference vector between the ground and L_a potential minima.

Despite these problems associated with the L_a band, there are a few features which are captured in the computed spectrum that have counterparts in the experimental spectrum. Noteworthy is the relatively lower shoulder at ~255 nm which matches reasonably well in terms of intensity relative to the band maximum at ~260 nm (~263 nm in the computed spectrum).

There is considerably more structure in the experimental spectrum, the most obvious example being the ~55 cm^{-1} spacing of sequence bands, which are attributed to excitation of vibrations which possess energy in excess of the zero-point in the ground state (18). We are not able to capture these sequence bands due to the restriction of the FC factor calculations to cold, vibrationless initial states, but a straightforward extension of the DMM method to incorporate these transitions is possible. The alternative to computing hot-term FC factors would be to apply a log-normal convolution integral

rather than Gaussians in performing the phenomenological broadening. However, since we are primarily concerned at this level with capturing the main features of the spectrum, these calculations are not really necessary.

In addition, it is well worth asking whether inclusion of hot-terms, Boltzmann factors, log-normal inhomogeneous broadening, etc., are really the proper approach at all for calculating the correct spectral bandshapes. From the perspective of a fitting procedure, these modifications to our calculations could provide some minor improvements to the overall appearance to the final bandshapes. In fact, it is likely that they would improve the appearance, but this is really an a-priori guess. On the other hand, these potential "improvements" might have little or no effect or, at worst, obscure the main features which have already been captured in the calculations to this point.

From an entirely different perspective, it is worth emphasizing that these potential variations of the fitting procedure run counter to the basic approach of this work, which is to perform a bandshape calculation at a modest level of theory, with a minimum of adjustable parameters and nominal empirical input in efforts to interpret (though not necessarily reproduce) the experimentally observed features. To that end, the correct place to perform further modifications would be at the level of theory, and not in terms of the fitting procedure or by further empirical input parameters. Those modifications which seem relevant and appropriate to extend this work are outlined in the Summary chapter of this thesis.

There are essentially two problems associated with the computed bandshape, both of which are tied to the geometry difference for the L_a state; the origin has too much intensity, and the band maximum is too low. In other words, the computed L_a geometry is not sufficiently displaced. The geometry on which the L_a FC factor calculations are based is obtained from the "frozen CI" calculation for the S_2 state (recall that the standard QCFFBOZE calculation results in a significantly larger L_a origin intensity).

Despite these persisting problems for the L_a geometry, one fact is born out by the bandshape calculation; QCFFBOZE performs much better in predicting the L_b bandshape than it does for L_a. This fact seems to contain a degree of generality and is, in many respects, a conclusion.

This conclusion, as such, contains a caveat; it is made within the context of the difference-density scaling procedure and is therefore a statement about the transferability of the difference-density scale factor from benzene to indole. It is important to recall and understand that the difference-density scale factor was introduced and defined in order to fit the correct C-C bond length change for the B_{2u}<--A_{1g} excitation in benzene. The transferability to indole is an assumption underlying the method and is vulnerable to at least two issues;

(1) Indole is not benzene. On a theoretical level, this difference manifests itself in terms of the symmetries of these molecules and by extrapolation in terms of their MO's and bond orders.

(2) The difference-density scale factor as defined for benzene is in terms of an L_b state. The extension to other molecules (i.e. indole) and/or different electronic states (e.g. L_a) is not necessarily inherent to the method.

All of this points to one very compelling problem which is best summarized in terms of a question; since the "frozen CI" calculations correspond to diabatic potential surfaces, what is the magnitude of the surface separation and, further, is it possible to rationalize the observed experimental results in terms of a diabatic picture? In order to answer this, we are required to examine the detailed nature of the L_b and L_a potential surfaces.

Indole Excited State Potential Energy Surfaces

All of the results presented to this point -- geometries, normal modes, Franck-Condon factors, spectral bandshapes, etc. -- are the currency of the Born-Oppenheimer potential energy surfaces computed within the framework of the QCFFBOZE suite. The exception to this is the frozen CI calculation introduced for the S_2 (L_a) state of indole which is designed to mimic the appropriate diabatic behavior of the S_2 PES. While this adjustment of the CI calculation does not provide a rigorous diabatic PES, it does assist in removing the influence of the avoided crossing of the L_b and L_a potential surfaces on the L_a equilibrium molecular geometry.

We present here the results for the Born-Oppenheimer adiabatic potential energy surfaces computed within the framework of QCFFBOZE, i.e.

$$V(\mathbf{x}) = V_{\sigma}(\mathbf{x}) + V_{\pi}^{0}(\mathbf{x}) + \Delta V_{N}^{\pi}(\mathbf{x}),$$

which are explicit functions of the 3N Cartesian coordinates ($\mathbf{x}$) of the molecule. To briefly review the PES calculation method, we note that the above form for the PES can be recast in the form

$$V(\mathbf{x}) = V^{(0)}(\mathbf{x}) + \Delta V_{N}^{\pi}(\mathbf{x}),$$

which is seen to be the sum of a ground state PES and the CI excitation energy appropriate to the N-th electronic state. In this way, we simply append the N-th root of the CI to the ground state potential to obtain the excited state potentials computed from QCFFBOZE.

For the purpose of the PES calculations, it is convenient to define the reference state of energy as zero and measure all energies relative to this. We adopt throughout the convention that the minimum of the indole ground state potential surface is the reference, and report all energies relative to this value. The total molecular energy of the indole ground state is computed by QCFF to be -1494.78 kcal-mol^{-1}, and this defines the effective "zero" of the energy scale.

The QCFFBOZE potential energy surfaces for the L_b and L_a states are presented in Figures 11-12. The coordinate along which these potential energy profiles are computed corresponds to the geometry difference vector (in Cartesian coordinates) between the L_b and L_a potential minima; the energy is plotted as a function of the C_2-C_3 bond length (Å). For reference, it should be noted that the 2-3 bond length is ~1.4274 Å for the L_b state, and ~1.4599 Å for the L_a state. The ground state 2-3 bond length is 1.3787 Å. Note that these surfaces are computed with the standard difference-density scaling procedure applied to both excited states.

There is one immediately obvious feature of these surfaces which provides one of the most significant results of this thesis: the existence of an avoided crossing of the L_b and L_a PES curves. The avoided crossing is evidenced by the discernible indentation of the lower (L_b) curve in the region around ~1.5 Å of the 2-3 bond. This avoided crossing, which was evidenced to a significant degree in the earlier results for oscillator strengths and the FC factor for the band origin of the L_a state can now be discussed from a quantitative point of view. Further, this calculation in some respects opens up a new avenue for discussion of the excited states of indole and closes the avenue of speculation in terms of the "cartoon" surfaces which have proliferated to this point.

There are three issues which must be addressed at this stage. First, we must address the question, "What are the implications and experimental consequences of the avoided crossing in indole?" Next, it is necessary to formulate a framework in which to interpret the indole experimental results in terms of the avoided crossing and understand what is actually observed. In particular, the L_a origin requires reexamination in light of the avoided crossing result. Lastly, as is commensurate with formulating theory, we need to attempt to extend these results to try and understand conceptually the results for 3-methylindole.

To put the calculated avoided crossing in perspective, it is crucial to note that this

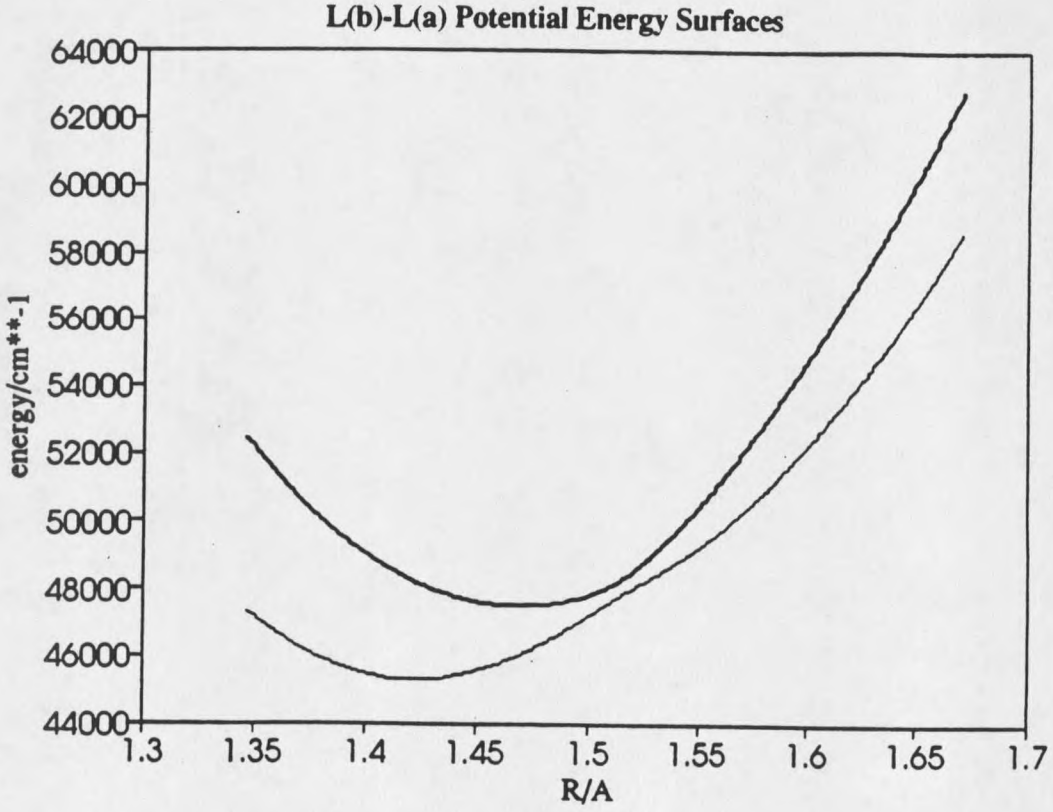

Figure 11. L_b and L_a excited state potential energy surfaces along the L_b-L_a equilibrium molecular geometry difference vector. All energies in cm^{-1} relative to the ground state minimum energy. Energies are plotted as a function of the C_2-C_3 bond length (Å). An avoided crossing region (ACR) is evidenced in the area near the L_a potential minimum (R~1.5 Å).

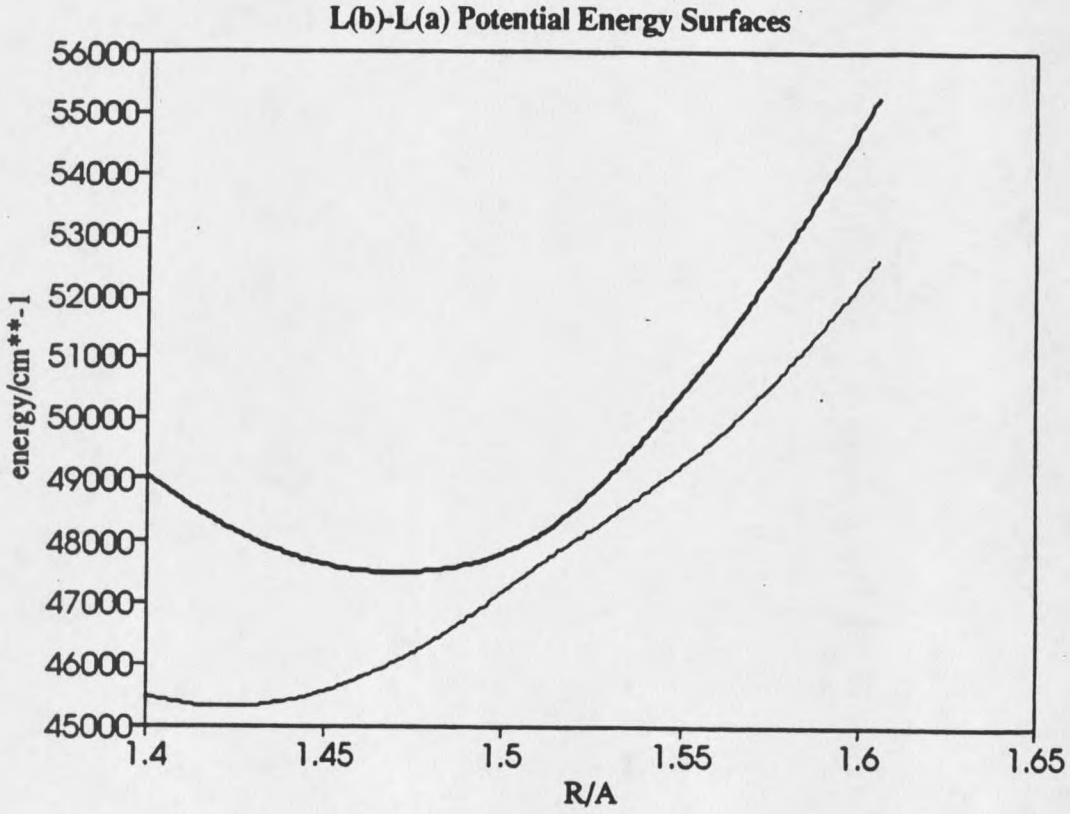

Figure 12. Expanded view of the L_b and L_a potential energy surfaces in the avoided crossing region (ACR).

result is exactly what experiments on jet-cooled indole (5,9) and the methyl-indoles (7) have pointed to and that a volume of excitation spectra have been interpreted in terms of a proposed avoided crossing in recent years (5,7,33). In particular, in the polarized two-photon fluorescence excitation (PTPFE) spectrum of jet-cooled indole, a Herzberg-Teller vibronic coupling mechanism was proposed (5) in order to provide an assignment of the 455 and 480 cm^{-1} transitions as the "split" L_a origin. While this HT mechanism is not in and of itself an avoided crossing, it is a possible result of an avoided crossing. The HT mechanism corresponds to the situation in which the transition dipole moment between initial (ground) and final (L_b, L_a) states depends explicitly on the nuclear coordinates, i.e. to breakdown of the Condon approximation. Failure of the Condon approximation would be extreme at an avoided crossing, since at this region of the potential surfaces there is strong mixing of the two states. This is seen more clearly in terms of the HT expansion of the transition dipole,

$$\mathbf{M}_{if}(\mathbf{Q}) = \mathbf{M}(\mathbf{Q}_0) \int \psi_i(\mathbf{Q})\, \psi_f(\mathbf{Q})\, d\mathbf{Q} + \Sigma_k \left(\partial \mathbf{M}(\mathbf{Q})/\partial Q_k \right)_0 \int \psi_i(\mathbf{Q})\, Q_k \psi_f(\mathbf{Q})\, d\mathbf{Q}$$
$$+ (1/2)\, \Sigma_k \Sigma_m \left(\partial^2 \mathbf{M}(\mathbf{Q})/\partial Q_k\, \partial Q_m \right)_0 \int \psi_i(\mathbf{Q})\, Q_k\, Q_m \psi_f(\mathbf{Q})\, d\mathbf{Q} + \ldots,$$

the first term of which is recognized as the familiar Franck-Condon integral. Consistent with this expansion and more fundamental are the corresponding electron-nuclear wavefunctions, which can be written to first-order (Rayleigh-Schrödinger perturbation theory) as

$$\Psi_m(\mathbf{q},\mathbf{Q}) = \Psi_m(\mathbf{q},\mathbf{Q}_0) + \Sigma_{k \neq m}\, a_{km}(\mathbf{Q})\, \Psi_k(\mathbf{q},\mathbf{Q}_0)$$

in which the expansion coefficients are dependent on the nuclear coordinates and are given by familiar "energy-denominator" forms which are prevasive in secular perturbation theory;

$$a_{km}(\mathbf{Q}) \sim \{ \text{ coupling matrix element } \} / \{ E_k(\mathbf{Q}_0) - E_m(\mathbf{Q}_0) \} + \text{(higher terms)}.$$

This heuristic form for the expansion coefficients is sufficient for the purposes of this discussion. The important point is that when we invoke the term "Herzberg-Teller"

coupling, by this we mean a transition dipole which depends upon the vibrational coordinates and a wavefunction which incorporates mixing. The extent of mixing is governed by the competing effects of the coupling matrix elements and the energy denominator(s). Notice that for exact degeneracy, $E_k(Q_0) = E_m(Q_0)$, the denominator is zero and the expansion coefficient tends to infinity; the closer the states approach in the crossing region, the larger the mixing terms.

In Callis's work on the MO theory of the excited states of indole (33), it was pointed out that in terms of INDO/S calculations the important displacement for the L_b-L_a manifold appears to be primarily lengthening of the 2-3 bond, as dictated by changes in the INDO/S bond orders to wit; "It seems likely that only along the 2-3 bond stretching mode can the two surfaces cross". It is primarily for this reason that we have chosen to present the surfaces as a function of the 2-3 bond length.

Returning to Figure 12., it appears that the distance of closest approach of the L_b and L_a surfaces occurs at ~1.5 Å for the 2-3 bond length. The bond length increment in the PES calculation (~0.01 Å) is relatively large, but this does not present any accuracy problems in the PES calculation since the calculation is not carried out with a Newton-Raphson minimization procedure (the excited state minima have been computed prior to the PES calculation). Nonetheless, since the PES calculation is designed to "sweep" through the minimum -- the L_b equilibrium geometry is the initial geometry for the calculation -- this region of the surface is explored during the course of calculating the PES along the difference geometry vector. The L_a minimum is also approached in the corresponding calculation for this surface. Again, this is no accident, since the geometry is distorted from a configuration away from the L_b minimum geometry, through the L_b minimum, and out towards the L_a minimum along the coordinate representing the equilibrium geometry difference for these two states. A more complete picture of the surface energy differences is presented in Figure 13.

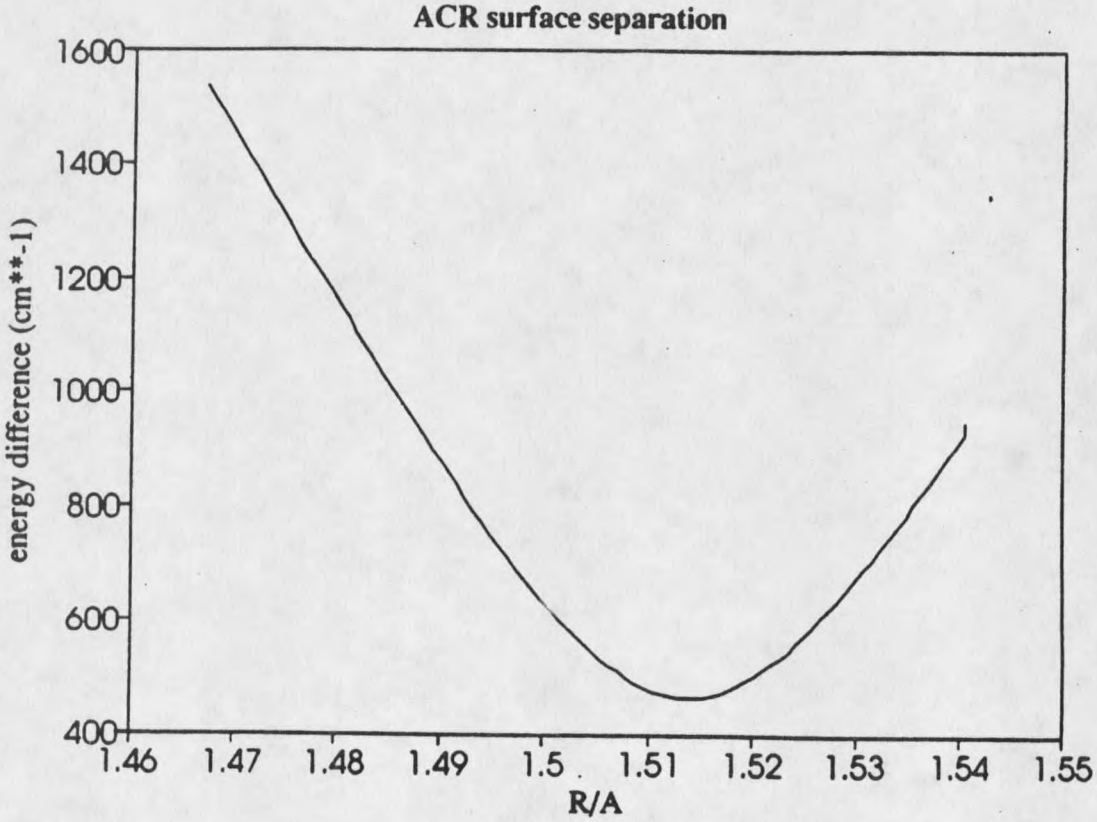

Figure 13. L_b-L_a potential surface separation energy (cm^{-1}) in the avoided crossing region. The avoided crossing is clearly evidenced in the region R~(1.51-1.52 Å) along the difference geometry.

Qualitatively, this avoided crossing should be termed "strong coupling" (108), since the avoided crossing zone occurs very close to the L_a (S_2) minimum. In fact, the more correct statement might be a variation on this -- it seems more correct to say that the S_2 minimum occurs in the avoided crossing region (ACR), and not the other way around. This location of the S_2 minimum in the ACR has a pronounced effect on the normal modes of vibration, in particular, in that the potential wells for each coordinate are compressed relative to those potentials which would occur if the surfaces crossed. The net result of the ACR on the normal modes is that the narrower S_2 potentials imply higher vibrational frequencies.

The effect on the vibrational frequencies is not a serious issue in terms of the spectral bandshapes, but the influence of the ACR on the geometry is critical. Simplistically, the ACR can be viewed as "pushing" the equilibrium molecular geometry for the S_2 state into a minimum which is less displaced than would be the case if the surfaces did cross. This lower displacement (with respect to the ground state) results in a higher value for the L_a origin, a smaller spectral bandwidth, and a more "L_b-like" S_2 state.

This "L_b-like" character is reflected in the CI eigenvectors, as presented previously, and the oscillator strength ratio approaching unity in the ACR. The situation is such that for a molecular configuration which corresponds to the ACR, the S_1 and S_2 labelling is more appropriate than L_b and L_a. In fact, beyond the crossing (i.e. beyond the S_2 minimum), the "upper" (S_2) surface is characterized as L_b, and the "lower" (S_1) surface is primarily L_a.

These points can be made more quantitative by directly examining the oscillator strength along the surfaces. Figure 14 displays the oscillator strength variations for the S_1 and S_2 states along the equilibrium geometry difference vector. As expected, at the avoided crossing, the oscillator strengths do "cross" (become identical), reflecting the mixing of the S_1 and S_2 states. This equality of the oscillator strengths corresponds to a

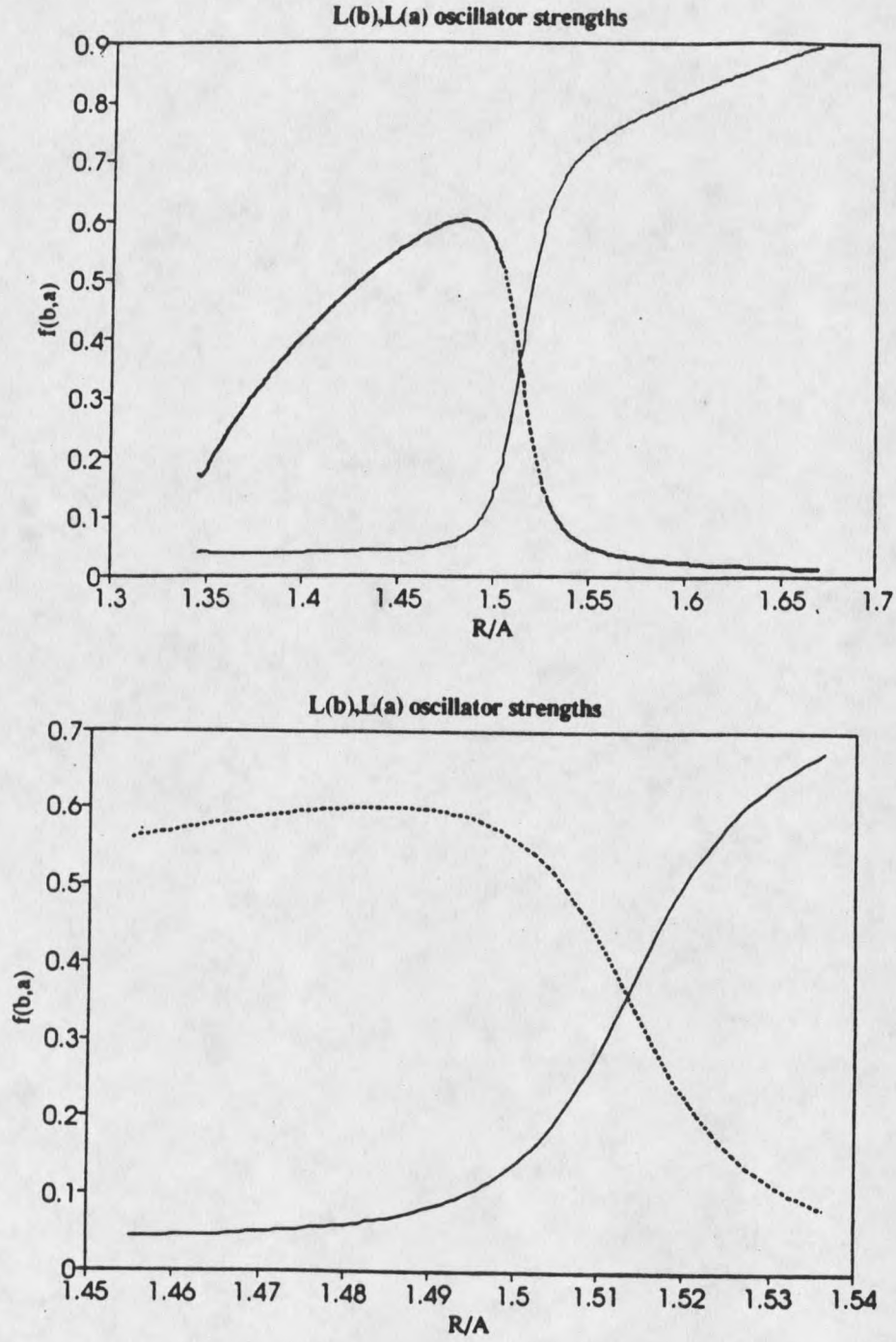

Figure 14. QCFFBOZE oscillator strengths, $f_{b,a}$ along the potential energy surfaces for the L_b, L_a electronic states. The avoided crossing is evidenced by the crossing of the oscillator strengths along the difference geometry; the S_1 and S_2 states exchange character on going through the ACR.

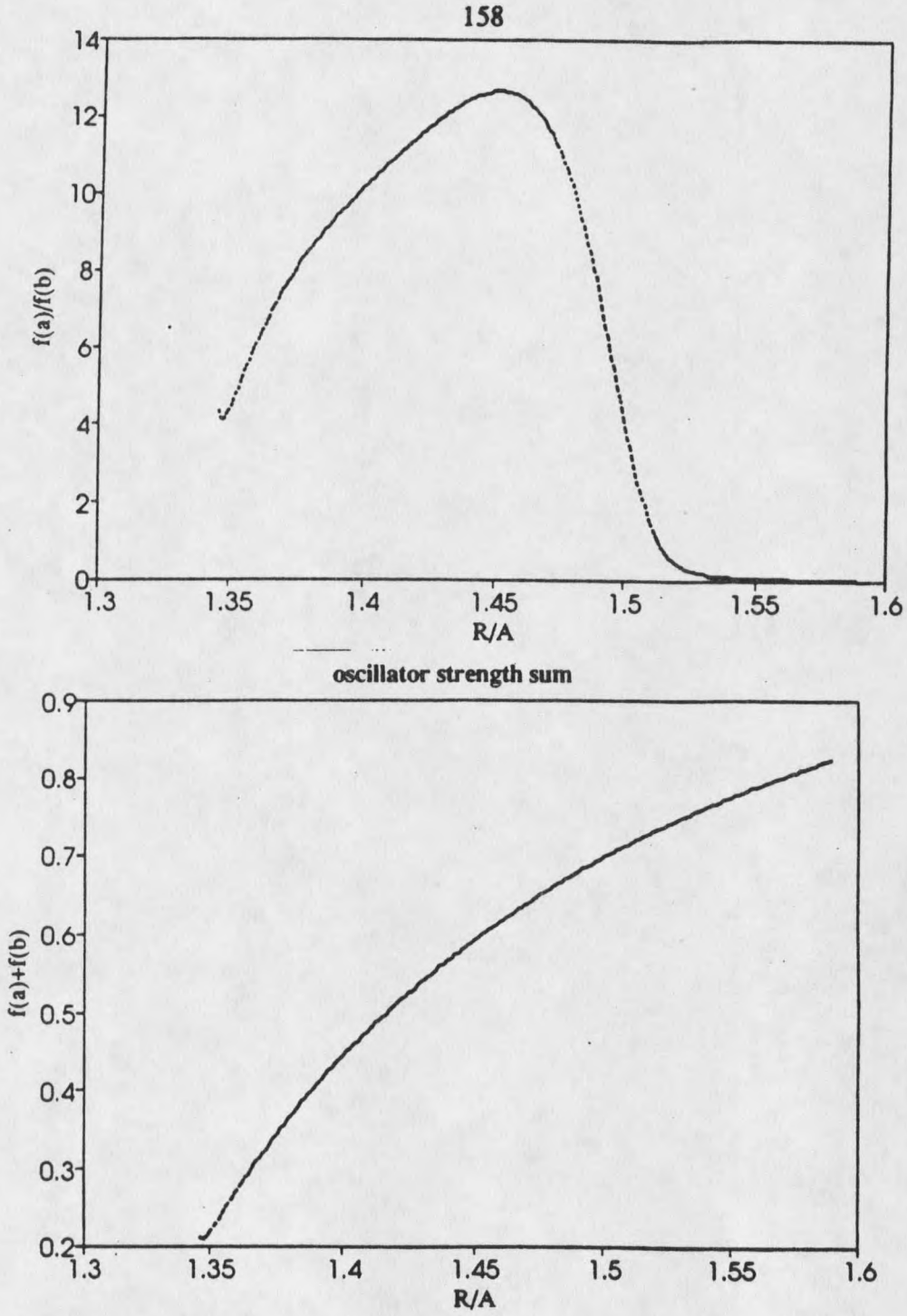

Figure 15. Oscillator strength ratio (f_a/f_b) and sum (f_a+f_b) along the potential energy surfaces. The ratio exhibits a maximum outside the ACR, then approaches zero upon passing through the ACR, reflecting the dramatically larger f for the S_1 state on approaching the S_2 (L_a) geometry. The oscillator strength sum (lower figure) is seen to increase along the geometry difference vector, indicating mixing with higher electronic states ($B_{b,a}$).

"50-50" mixing of the two states.

Figure 15 displays the oscillator strength ratio (f_a/f_b) and sum (f_a+f_b) along this coordinate. Again, at the crossing the ratio is seen to be unity, but it is perhaps more important to note that the oscillator strength sum for the S_1 and S_2 states is not constant. This means, of course, that these two electronic states are not truely isolated -- there is a fair amount of mixing with a higher state ($B_{b,a}$) through which both the S_1 and S_2 states gain oscillator strength. This could be an artifact of the CI singles approach to the excited states calculations, but in any case it should be noted that this phenomenon is observed when computing oscillator strengths with QCFFBOZE. It is at least at this stage not a problem in terms of our bandshape calculations, since in this work we have fitted bandshapes using experimental oscillator strength ratios. Nonetheless -- and this is not a trivial point -- it should be emphasized that the CI singles calculations in general overestimate the oscillator strength ratio for the S_1 and S_2 states and that this is an area which probably warrants further work in the future.

Simple Model for Curve-Crossing

Lastly, we ask one very relevant question regarding the avoided crossing region: What is the probability of crossing from the S_2 (L_a) surface to the S_1 (L_b) surface for a wavepacket prepared on the S_2 surface by vertical excitation from the vibrationless level of the ground state? We attempt to answer this from a qualitative perspective by adopting a very simple model for the curve crossing. Our interest here is not in a detailed treatment of the dynamics -- the primary concern is a rough estimate of the crossing within the limit of a single pass (104) along the surface.

We adopt a Landau-Zener (LZ) model (102-105) for the crossing dynamics, in which the probability for crossing is given by the LZ formula (102);

$$P_{LZ} = \exp\{-(2\pi)(\varepsilon_{12})^2 / [(h/2\pi)[\partial(\varepsilon_1 - \varepsilon_2)/\partial t]]\}$$

in which ε_{12} is the surface coupling (one-half the surface separation) at the point of crossing for diabatic potentials, ε_1 and ε_2 are the potentials for the "upper" and "lower" state in the crossing region, and the time-derivative can thus be interpreted as an effective {force x velocity} at the crossing zone.

We further assume harmonic potentials with identical force constants (k) and frequencies (ω) for the two states. It can then be shown that for these approximations, the velocity term is given by

$$[\partial(\varepsilon_1 - \varepsilon_2)/\partial t] = k\, d\, \Delta\, \omega,$$

in which d represents the displacement (in normal coordinate space) of the crossing from the equilibrium position of the lower well, and Δ is the displacement of the initially excited (Gaussian) wavepacket above the minimum of the upper well. If we take the approximate value for the L_b-L_a surface separation in the ACR, ~400 cm^{-1} (ε_{12}~200 cm^{-1}), for an initial excitation ~1000 cm^{-1} above the L_a minimum, i.e.

$$(1/2)\, k\, \Delta^2 \sim 1000\ cm^{-1}$$

and for a typical vibrational frequency of ~1000 cm^{-1} (e.g. an in-plane skeletal mode), we obtain from the LZ probability expression

$$P_{LZ} \sim 0.88,$$

that is, a curve-crossing probability of ~88% for a wavepacket starting on the upper surface at time t=0. Thus, this model predicts extreme Born-Oppenheimer breakdown for the L_b-L_a ACR, and the appropriate picture appears to be closer to a diabatic one than it is to Born-Oppenheimer adiabatic and serves to justify the frozen CI approach.

Certainly, this result must be viewed with some skepticism. The model is an extremely simplified one, it involves a classical-path approximation for the trajectory of the nuclei, and ignores the details of the surfaces. On the other hand, however, for a "single pass" along the surface, the LZ probability of crossing is quite high. If one were

to perform calculations which incorporate multiple-passes through the minimum of the well, i.e. an ensemble of trajectories, the classical calculation will result in probablility being transferred onto the lower surface at each pass. Quantum mechanically, however, there will be interference as the wavepacket splits and this can be a problem in trying to interpret the classical result. In addition, the result depends intimately on how far the crossing zone is from any classical turning points -- the LZ model assumes, implicitly, a "localized" crossing region.

And, perhaps more importantly, this model depends upon the representation we have chosen for the surfaces in that the problem of making transitions on adiabatic surfaces is formally the same problem as not making transitions on diabatic surfaces. This is missed in the oversimplified LZ model, and more detailed calculations incorporating the diabatic coupling are required to make precise statements about the crossing probability.

Nonetheless, it seems reasonably accurate to state that certainly some L_a-->L_b probability amplitude transfer does occur in reality in that this picture is consistent with only L_b emission being observed in SVLF experiments (12). Probably not as much probability transfer occurs as that predicted by the single-pass LZ model, but possibly enough to allow observable "communication" between L_b and L_a wells. That is not so much a conjecture as it is a suggestion for further work on this problem -- utilizing the potential energy surfaces developed in this study.

CHAPTER FIVE

SUMMARY

General Results

In this thesis results for normal coordinates, Franck-Condon factors, vibronic bandshapes and potential energy surfaces of indole were presented. These calculations, carried out in the framework of the Quantum Consistent Force Field (QCFF) semiempirical method, constitute what appears to be the first comprehensive theoretical treatment of the L_b-L_a electronic manifold of indole in which bandshapes and potential energy surfaces are obtained from the theoretical model.

Although the calculations presented in this work were carried out at the level of Born-Oppenheimer, harmonic, and Condon approximations, a reasonably useful and semi-quantitative picture of the photophysics of the L_b-L_a electronic manifold is achieved. The final result for the indole vibronic bandshape captures the major features of the experimental absorption spectrum, and the avoided crossing which has been employed previously to interpret fluorescence excitation experiments on jet-cooled indoles (5,7,9) has been predicted through this work.

In addition, this body of work contains a new and potentially powerful method for fitting spectral bandshapes -- the difference-density scaling procedure -- which represents an improvement over the more common empirical fitting procedures (70,87) which are restricted to adjusting normal mode displacements based on experimental transition intensities. The advantage of this procedure and, indeed, a unique feature to it, is that it is systematic and does not involve the inherent uncertainty in the sign of normal mode displacements which other methods are vulnerable to (70,87).

Specific Results

The Franck-Condon factors and spectral bandshape calculations presented in this work appear to be the first such calculations performed for indole and, in a much broader sense, one of the few calculations of this type to be performed for any molecule which incorporates the combined effects of surface displacements, frequency shifts, and Duschinsky rotation (70, 84, 85, 87). In this sense, the computational methods provided in this work represent a prototype for bandshape calculations.

One of the most compelling results of this work is the prediction of an avoided crossing of the L_b and L_a potential energy surfaces in the region of the L_a equilibrium molecular geometry. This avoided crossing region (ACR), which has been pointed to previously in order to explain experimental results (5,7,9), does well to explain some of the seemingly bizarre behavior observed for indole under jet-cooled conditions. Most notably, the magnitude of the avoided crossing -- i.e. the surface coupling -- is found to be only a few hundred wavenumbers. This result is significant in that it predicts the avoided crossing to be relatively weak and locates the L_a surface minimum very close to the L_b surface.

Although we do predict an L_a band origin through this work, it is not possible through the calculated L_b-L_a origin separations to verify which jet-cooled transitions are the L_a origin. Nonetheless, from the fitted spectral bandshape with an L_a origin displacement of ~1450 cm^{-1} above the L_b origin, the agreement with experiment seems quite convincing.

Nonetheless, this work fails to predict L_a transitions with significant intensity which closely match the 455-480 cm^{-1} pair observed and assigned as a "split" L_a origin. This points to a conjecture regarding the nature of these peaks which will probably require further experimental efforts to corroborate: The 455+480 cm^{-1} pair are not features associated with vertical transitions between Born-Oppenheimer potential surfaces.

Whether they gain intensity from Herzberg-Teller vibronic coupling, Fermi resonance, or a curve-crossing mechanism, it is increasingly obvious that the complete story regarding these peaks will require both additional experimental efforts and a theoretical method which goes beyond the Born-Oppenheimer and Condon approximations.

Finally, in order to provide some insight into the dynamics following excitation to the L_a surface, we have briefly investigated a semiclassical model for the curve crossing phenomenon. At the level of a simple one-dimensional Landau-Zener model, we are able to obtain an estimate of the curve-crossing probability for wave packets initially prepared on the L_a potential energy surface. This provides a very rough estimate of the effect of nuclear kinetic energy coupling on the potential surfaces and indicates that the crossing probability is probably quite high (~80-90%).

Suggestions for Further Investigation

Several points in this work give rise to questions which probably cannot be answered within the framework of the Born-Oppenheimer, harmonic, and Condon approximations. In addition, there are certain features of this work which probably warrant extension, modifications, or development of new techniques to gain further insight into the photophysics and dynamics associated with the L_b-L_a electronic manifold of indole. We briefly outline here some of the potential and possibilities for further work which arose during the course of this investigation.

(i) The extension of the difference density scaling procedure and associated bandshape calculations presented in this work to other molecules -- in particular, to naphthalene and styrene (109) -- is probably necessary to establish the general validity of the method and transferability between molecules.

(ii) Extending the Franck-Condon factor calculations, utilizing the Doktorov recursion relations, to include hot terms would be reasonably straightforward and provide a

route to incorporation of sequence bands into the bandshape calculations.

(iii) Explicit vibronic-coupling calculations involving the indole vibrational modes would be laborious but might provide further insight into the magnitude of Born-Oppenheimer breakdown which is evidenced by this work and experiments on indole.

(iv) Inclusion of CI-doubles excitations into the QCFF-QCFFBOZE routines may ultimately prove necessary to provide more accurate oscillator strength values, as well as the more fundamental issue of CI eigenvectors.

(v) The dynamics within the L_b-L_a manifold remains, for the most part, an open area for very exciting work. Once accurate potential energy surfaces for these states are available, the dynamics should be explored.

Concluding Remarks

This work constitutes a reasonably comprehensive theoretical treatment of the first two excited singlet states of indole. As such, it represents only an intermediate stage in the development of our understanding of the unusual and interesting photophysics of this extremely important biological chromophore. From a theoretical perspective, indole remains a challenging and compelling system for investigation. It is hoped that the results contained in this thesis provide some insight into the on-going work in this area, that ultimately this study motivates further theoretical treatments, and that a comprehensive vibrational assignment of the L_a state will soon be possible.

REFERENCES CITED

REFERENCES CITED

1. J.R. Platt, J. Chem. Phys. **17**, 484 (1949).
2. B.E. Anderson, R.D. Jones, A.A. Rehms, P. Ilich, and P.R. Callis, Chem. Phys. Lett. **125**, 106 (1986).
3. B. Valeur and G. Weber, Photochem. Photobiol. **25**, 441 (1977).
4. A.A. Rehms and P.R. Callis, Chem. Phys. Lett. **140**, 83 (1987).
5. D.M. Sammeth, S. Yan, L.H. Spangler, and P.R. Callis, J. Phys. Chem. **94**, 7340 (1990).
6. D.M. Sammeth, S.S. Siewert, P.R. Callis, and L.H. Spangler, J. Chem. Phys. **96**, 5771 (1992).
7. D.M. Sammeth, S.S. Siewert, L.H. Spangler, and P.R. Callis, Chem. Phys. Lett. **193**, 532 (1992).
8. L.A. Philips and D.H. Levy, J. Chem. Phys. **85**, 1327 (1986).
9. David M. Sammeth, Ph.D. thesis, Montana State University (1992).
10. R. Bersohn, U. Even, and J. Jortner, J. Chem. Phys. **80**, 1050 (1983).
11. J.R. Cable, J. Chem. Phys. **92**, 1627 (1990).
12. G.A. Bickel, D.R. Demmer, E.A. Outhouse, and S. C. Wallace, J. Chem. Phys. **91**, 6013 (1989).
13. G.A. Bickel, et al., J. Chem. Phys. **91**, 6014 (1989), PAPS JCPSA-91-6013-51.
14. B. Albinsson and B. Norden, J. Phys. Chem. **96**, 6204 (1992).
15. H. Lami and N. Glasser, J. Chem. Phys. **84**, 597 (1986).
16. A.P. Demchenko and A.S. Ladokhin, Eur. Biophys. J. **15**, 369 (1988).
17. T. Montoro, M. Chabbert, J. Tyrzyk, H. Lami, J. Chem. Phys. **89**, 2712 (1988).
18. E.H. Stickland, J. Horwitz, and C. Billups, Biochem. **9**, 4914 (1970).
19. P. Muiño and P.R. Callis, unpublished results.
20. P. Muiño, unpublished results.
21. J.B. Foresman, M. Head-Gordon, J.A. Pople, and M.J. Frisch, J. Phys. Chem. **96**, 135 (1992).
22. M.P. Fülscher, K. Andersson, and B.O. Roos, J. Phys. Chem. **96**, 9204 (1992).

23. C.F. Chabalowski, D.R Garmer, J.O. Jensen, and M. Krauss, J. Phys. Chem. **97**, 1608 (1993).

24. J.D. Westbrook, R.M. Levy, and K. Krough-Jespersen, J. Comp. Chem. **13**, 979 (1992).

25. T.L.O. Barstis, L.I. Grace, T.M. Dunn, and D.M. Lubman, J. Phys. Chem., **97**, 5820 (1993).

26. M. Majoube and G. Vergoten, J. Raman Spec. **23**, 431 (1992).

27. L. Slater, unpublished results.

28. E.J. Heller, J. Chem. Phys. **62**, 1544 (1974).

29. E.J. Heller, Accts. Chem. Res. **14**, 368 (1981).

30. J.R. Reimers, K.R. Wilson, and E.J. Heller, **79**, 4749 (1983).

31. R.D. Coalson and J.L. Kinsey, J. Chem. Phys. **85**, 4322 (1986).

32. H. Takeuchi and I. Harada, Spectrochimica. Acta. **42A**, 1069 (1986).

33. P.R. Callis, J. Chem. Phys. **95**, 4230 (1991).

34. A. Warshel and M. Karplus, J. Am. Chem. Soc. **94**, 5612 (1972).

35. A. Warshel, in *Semiempirical Methods of Electronic Structure Calculation*, Mod. Theo. Chem. A, vol. 7, edited by G.A. Segal (Plenum, New York, 1977).

36. B. Honig, A. Warshel, and M. Karplus, Acc. Chem. Res. **8**, 92 (1975).

37. A. Warshel and A. Lappicirella, J. Am. Chem. Soc., **103**, 4664 (1981).

38. A.C. Lasaga, R.J. Aerni, and M. Karplus, J. Chem. Phys. **73**, 5230 (1980).

39. E.V. Doktorov, I.A. Malkin, and V.I. Man'ko, J. Mol. Spect. **56**, 1 (1975).

40. E.V. Doktorov, I.A. Malkin, and V.I. Man'ko, J. Mol. Spect. **64**, 302 (1977).

41. F. Duschinskii, Acta. Physiochem. (URSS) **7**, 551 (1937).

42. M. Born and J.R. Oppenheimer, Ann. Physik **84**, 457 (1927).

43. G.C. Schatz and M.A. Ratner, *Quantum Mechanics in Chemistry* (Prentice Hall, Englewood Cliffs, NJ, 1993).

44. E.B. Wilson, Jr., J.C. Decius, and P.C. Cross, *Molecular Vibrations* (Dover, New York, 1980).

45. F. L. Pilar, *Elementary Quantum Chemistry* (McGraw-Hill, New York, 1990).

46. P. Jørgensen and J. Simons, *Second Quantization-Based Methods in Quantum Chemistry* (Academic Press, New York, 1981).

47. L. Salem, *The Molecular Orbital Theory of Conjugated Systems* (W.A. Benjamin, Inc., New York, 1966).

48. J.A. Pople and D.L. Beveridge, *Approximate Molecular Orbital Theory* (McGraw-Hill, New York, 1970).

49. R. Moccia, Theor. Chim. Acta. **8**, 8 (1967).

50. H. Margenau and G.M. Murphy, *The Mathematics of Physics and Chemistry* (Van Nostrand, New York, 1943).

51. W. Siebrand, J. Chem. Phys. **46**, 440 (1967).

52. W. Siebrand, in *Dynamics of Molecular Collisions*, edited by W.H. Miller (Plenum, New York, 1976), Part A.

53. T.E. Sharp and H.M. Rosenstock, J. Chem. Phys. **41**, 3453 (1964).

54. E. Hutchisson, Phys. Rev. **36**, 410 (1930).

55. C. Manneback, Physica **17**, 1001 (1951).

56. J.B. Coon, R.E. DeWames, and C.M. Loyd, J. Mol. Spect. **8**, 285 (1962).

57. J.R. Henderson, M. Muramato, and R.A. Willett, J. Chem. Phys.

58. L.S. Cederbaum and W. Domcke, J. Chem. Phys. **64**, 603 (1976).

59. H. Kupka and O.E. Polansky, J. Chem. Phys. **80**, 3153 (1984).

60. H. Kupka and G. Olbrich, J. Chem. Phys. **80**, 3163 (1984).

61. H. Kupka and G. Olbrich, J. Chem. Phys. **82**, 3975 (1985).

62. H. Kupka and P.H. Cribb, J. Chem. Phys. **85**, 1303 (1986).

63. T.R. Faulkner and F.S. Richardson, J. Chem. Phys. **70**, 1201 (1979).

64. M. Roche, Chem. Phys. Lett. **168**, 556 (1990).

65. Y.J. Yan and S. Mukamel, J. Chem. Phys. **85**, 5908 (1986).

66. E.J. Heller, *Wavepacket Dynamics and Quantum Chaology*, N.A.T.O. Les Houches Lecture Notes, North-Holland (1990).

67. Go. Torres-Vega and J.H. Frederick, J. Chem. Phys. **98**, 3103 (1993)

68. D. Gruner and P. Brumer, Chem. Phys. Lett. **138**, 310 (1987).

69. D. Gruner and P. Brumer, J. Chem. Phys. **94**, 2848 (1991).

70. D. Gruner and P. Brumer, J. Chem. Phys. **94**, 2862 (1991).

71. J.B. Hopkins, D.E. Powers, and R.E. Smalley, J. Chem. Phys. **72**, 5039 (1980).

72. J.B. Hopkins, D.E. Powers, and R.E. Smalley, J. Chem. Phys. **72**, 5049 (1980).

73. J.B. Hopkins, D.E. Powers, and R.E. Smalley, J. Chem. Phys. **72**, 5721 (1980).

74. J.B. Hopkins, D.E. Powers, and R.E. Smalley, J. Chem. Phys. **73**, 683 (1980).

75. Quantum Chemistry Program Exchange, Indiana University. Program #534.

76. B.T. Smith, et al., *Matrix Eigensystems Routines - EISPACK Guide*, 2nd ed., vol. 6 of Lecture Notes in Computer Science (Springer-Verlag, New York, 1976).

77. P.R. Callis, Int. J. Quantum Chem. Symp. **18**, 579 (1984).

78. R.S. Berry, S.A. Rice, and J. Ross, *Physical Chemistry*, Part One (John Wiley & Sons, New York, 1980).

79. K. Miller and J.N. Murrell, Theoret. chim. Acta **3**, 18 (1965).

80. C.S. Parmenter, K.Y. Tang, and W.R. Ware, Chem. Phys. **17**, 359 (1976).

81. W.R. Ware, A.M. Garcia, C.S. Parmenter, M.D. Schuh, and K.Y. Tang, Chem. Phys. **17**, 377 (1976).

82. A. Hiraya and K. Shobatake, J. Chem. Phys. **94**, 7700 (1991).

83. G. Fischer, Chem. Phys. Lett. **56**, 186 (1978).

84. G. Fischer, *Vibronic Coupling: The Interaction between the Electronic and Nuclear Motions* (Academic Press, New York, 1984).

85. F. Metz, M.J. Robey, E.W. Schlag, and F. Dörr, Chem. Phys. Lett. **51**, 8 (1977).

86. G. Fischer, S. Jakobson, and R. Naaman, Chem. Phys. Lett. **49**, 427 (1977).

87. R.J. Hemley, D.G. Leopold, V. Vaida, and M. Karplus, J. Chem. Phys. **82**, 5379 (1985).

88. W.H. Press, B.P. Flannery, S.A. Teukolsky, and W.T. Vetterling, *Numerical Recipes: The Art of Scientific Computing* (Cambridge University Press, Cambridge, 1986).

89. VAX-VMS FORTRAN *Language Reference Manual* (AA-DO34C-TE) (Digital Equipment Corporation, Maynard, MA 1982).

90. J.I. Steinfeld, *Molecules and Radiation: An Introduction to Molecular Spectroscopy* (M.I.T. Press, Cambridge, MA, 1974).

91. I. von Neumann and E. Wigner, Physik. Z. **30**, 467 (1929).

92. J.E. Hadder and J.H. Frederick, J. Chem. Phys. **97**, 3500 (1992).

93. S. Kato, J. Chem. Phys. **88**, 3045 (1988).

94. T.W. Scott, B.F. Campbell, R.L. Cone, and J.M. Friedman, Chem. Phys. **131**, 63 (1989).

95. D.R. Demmer, G.W. Leach, E.A. Outhouse, J.W. Hager, and S.C. Wallace, J. Phys. Chem. **95**, 582 (1991)

96. M.J. Tubergen and D.H. Levy, J. Phys Chem. **95**, 2175 (1991).

97. L. Spangler, personal communication.

98. A. Lautie, M.F. Lautie, A. Gruger, and S.A. Fakhri, Spectrochim. Acta **36A**, 85 (1980).

99. A. Suwaiyan and R. Zwarich, Spectrochim. Acta **42A**, 1017 (1986).

100. W.B. Collier, J. Chem. Phys. **88**, 7295 (1988).

101. P.R. Callis, et al., unpublished results.

102. C. Zener, Proc. Roy. Soc. London Ser. A **137**, 692 (1932).

103. D.W. Noid, M.L. Koszykowski, and R.A. Marcus, J. Chem. Phys. **78**, 4018 (1983).

104. D.J. Nesbitt and J.T. Hynes, J. Chem. Phys. **84**, 1544 (1986).

105. E.J. Heller, J. Chem. Phys. **92**, 1718 (1990).

106. J.H. Callomon, T.M. Dunn and I.M. Mills, Phil. Trans. Roy. Soc. (London) **A259**, 499 (1966).

107. J.H. Callomon, unpublished results.

108. J. Jortner and R.D. Levine, Adv. Chem. Phys. **47**, 1 (1980).

109. J. Vivian and P.R. Callis, work in progress.

APPENDICES

Appendix 1: Execution Times Report for the QCFFBOZE Suite

Machine; VAX 6520, Montana State University (TREX).

Molecule; Indole, 3n=48, 3n-6=42 vibrational modes, ground and L_b electronic states.

DCL Command File Sequence

@INDLB

L_b electronic state	55. sec.
ground electronic state	60. sec.
total time	128 sec.

@FCPREPLBIND (symmetry assignments)

total time	14. sec.

@FC (Franck-Condon factor calculations); 8 quanta overtone maximum.

total time	37. sec.

{calculation and sorting of ca. 1.5×10^6 for ground-->L_b absorption}

Total Execution Time; 179. sec. (~3. min.)

Time per Franck-Condon factor; ~2.5×10^{-5} sec.

Time per vibrational mode (QCFF); ~1.43 sec.

Time per vibrational mode (FCF's); ~0.88 sec.

APPENDIX 2. FORTRAN program "PSURF".

```
************************************************************************
************************************************************************
************************************************************************
cc
cc   Subroutine to construct QCFF potential energy surfaces for ground
cc   and excited states.  The PES is computed along a specified coordinate
cc   without energy minimization.  SCF+CI is performed @ each molecular
cc   geometry.
cc
cc    Bozeman, MT.  March-April, 1993.
cc    James T. Vivian;  Callis Group.
cc
      subroutine psurf
cc
cc
cc
      character*1 at,piat
      parameter( cw=8066. , ck=349.755 , cev=23.119 )
      dimension dv(99),delta(99),xzero(99)
      dimension dsx(12,90),p(99)
      dimension eground(300),rootm(99)
      common/flag/dflag
      common/modes/xvector(99,99),qground(99,99),qex(99,99)
      common/hh/h(32,32),f(32,32),r(32,32),p1(32,32),p2(32,32),
     1 p3(32,32),pc(32,32),v1(32,32),e1(32),ec(32),z(32),ps(64)
      common/intern/b(80),th(100),phi(180)
      common/type/npa,at(15),npi,piat(8),no(15,15),cg2(20),sqrtm(15)
      common/code/wb(80),wt(100),wnb(80),wp(180),icg(80),iac(80),nc(50)
      common/enstor/ith,ens(200),steps(200)
      common/final/nat3,dd(11325),d(200),x(200)
      common/contro/natom,nbond,ntheta,nphi,nof,nap,nao,nex,newton,idsx
      common/energy/eb,et,ep,enb,er,edcor
      common/ij/ici(20),jci(20),inci,ia
      common/nbonru/ nrangl,iblo(100)
      common/polr/ipolr1
      common/scratc/c1(200),c2(200),c3(200),c4(200),c5(200),c6(200)
      equivalence(dd(1),dsx(1))

      integer wb,wt,wp,wnb                                    --
cc
cc
cc
      read(9,*)isurf
      if(isurf.eq.666) goto 300
      close(6)
      rewind(67)
      do i=1,nat3
      read(67,*)rootm(i)
      enddo
      newton=1
      idsx=1
      open(6,file='qcffboze.out',status='new')
      read(9,*)npts
      read(9,*)nmax
      read(9,*)icoord
      read(9,*)e0kcal
      e0=-e0kcal*ck
      read(9,*)mode
cc
      open(78,file='distort.dat',      status='old')
      open(79,file='pes.dat' ,         status='new')
      open(80,file='geometry.dat',     status='new')
      open(81,file='excitation.dat',   status='new')
      rewind(78)
cc
```

Figure 16. Subroutine PSURF, written in VAX FORTRAN 77, for calculation of potential energy surfaces from the QCFFBOZE semiempirical method.

```
cc
      write(80,*)' initial geometry '
      write(6,*) ' initial geometry '
      do i=1,nat3,3
         write(80,55)x(i),x(i+1),x(i+2)
55       format(5x,f8.4,3x,f8.4,3x,f8.4)
      enddo
      call intero(nbond,ntheta,nphi,wb,wt,wp,iac,b,th,phi,at)
      write(80,*) ' distortion coordinate '
      do i=1,nat3,3
         j=i+1
         k=j+1
         read(78,*)dv(i),dv(j),dv(k)
         read(9,*)xzero(i),xzero(j),xzero(k)
           delta(i)=dv(i)/npts
           delta(j)=dv(j)/npts
           delta(k)=dv(k)/npts
           write(80,55)delta(i),delta(j),delta(k)
      enddo
cc
```

```
           x(k)=xzero(k)-dv(k)
           enddo
           write(80,*)' starting geometry '
           write(6,*) ' starting geometry '
           do k=1,nat3,3
           write(80,55)x(k),x(k+1),x(k+2)
           enddo
      cc
      cc
           call intero(nbond,ntheta,nphi,wb,wt,wp,iac,b,th,phi,at)
           write(80,*)' intermediate geometry '
           write(6,*) ' intermediate geometry '
           call molecu(1,1,x,d,e)
      cc
      cc
      cc      Compute the potential energy surface...

              "This ain't no manky cartoon surface...."


           np=nmax*npts
           if(isurf.gt.0)then
           open(82,file='gsurf.dat',status='old')
           rewind(82)
           do i=1,np
           read(82,*)n,q,eground(n)
           enddo
           else
           open(82,file='gsurf.dat',status='new')
           endif
           call molecu(1,1,x,d,e)
           dflag=1.0
           do 200 k=1,np
              call molecu(1,1,x,d,e)
              if(k.eq.npts)then
              do i=1,nat3,3
              write(80,55)x(i),x(i+1),x(i+2)
              enddo
              call intero(nbond,ntheta,nphi,wb,wt,wp,iac,b,th,phi,at)
              write(80,*)
              write(80,*)
              write(80,*)
              endif
              if(isurf.eq.0)esurf=e*ck-e0
              if(isurf.gt.0)esurf=eground(k)+ec(isurf)*cw
              if(isurf.gt.0)de=esurf-eground(k)
              write(*,*) k,b(icoord),esurf,ec(isurf)*cw
              write(79,*)k,b(icoord),esurf,de
              write(81,*)k,b(icoord),ec(isurf)*cw,de
              if(isurf.eq.0)write(82,*)k,b(icoord),esurf

              do i=1,nat3
              x(i)=x(i)+delta(i)
              enddo

      200   continue

      cc
```

```
cc
cc
      write(80,*)' final geometry '
      write(6,*) ' final geometry '
      do i=1,nat3,3
      write(80,55)x(i),x(i+1),x(i+2)
      enddo
      call intero(nbond,ntheta,nphi,wb,wt,wp,iac,b,th,phi,at)
cc
      call molecu(1,1,xzero,d,e)
cc
cc
30    continue
      if(mode.gt.0) then
      do i=1,nat3,3
      j=i+1
      k=j+1
      dv(i)=dv(i)/rootm(i)
      dv(j)=dv(j)/rootm(j)
      dv(k)=dv(k)/rootm(k)
      delta(i)=dv(i)/npts
      delta(j)=dv(j)/npts
      delta(k)=dv(k)/npts
      enddo
      freq=p(mode)


      cc
      cc
            close(6)
            close(78)
            close(79)
            close(80)
            close(81)
            close(82)
      cc
      cc
      00    continue
            return
            end

      ********************************************************************************
      ********************************************************************************
      ********************************************************************************
      ********************************************************************************
      ********************************************************************************
```